Electrochemical Generation of Reactive Species and their Application as Chemotherapeutics

by

Jordache Boudreau

A Thesis
presented to
The University of Guelph

In partial fulfilment of requirements
for the degree of
Master of Science
in
Chemistry and Toxicology

Guelph, Ontario, Canada

© Jordache Boudreau, April, 2012

ABSTRACT

ELECTROCHEMICAL GENERATION OF REACTIVE SPECIES AND THEIR APPLICATION AS CHEMOTHERAPEUTICS

Jordache Boudreau
University of Guelph, 2012

Advisor:
Professor N. J. Bunce

A major limitation in developing a successful cancer treatment is the need for a distinction between normal and cancerous tissue. For solid tumors, this distinction can be made on a spatial basis, and successful treatments have been developed accordingly; however, many of these treatments cause pathologies in healthy tissue, much to the detriment of patient health. To address this issue for solid tumours, a conceptual approach would be to administer the chemotherapeutic drug locally, such that the intra-tumour concentration was high, while the systemic exposure to the drug remained low, thus, minimizing side effects. The present research focuses on providing proof-of-concept for the electrochemical generation of a toxicant from a prodrug, and subsequent use to elicit cytotoxicity in cancer cells, in attempts to electrochemically mimic monooxygenase-catalyzed bioactivation. Electro-oxidation of acetaminophen and cyclophosphamide substrates at graphite and Ti/RuO_2 anodes was successful in generating their respective toxicants; however, the graphite anode was superior with respect to current efficiency and toxicant yield. Electrolyses conducted in batch and flow reactors produced effluents which reduced EMT-6 cell viability to the IC_{99} level. This thesis provides proof-of-concept for electrochemical prodrug activation as a viable area for further cancer research.

For myself, my family, my friends, and those who will benefit from the knowledge within.

Acknowledgements

I would like to thank my advisor, Dr. Nigel Bunce, for the mentorship, patience, and guidance offered during this project. I am especially grateful for his willingness, encouragement, and commitment, in undertaking this novel thesis topic with me.

For their advice, training, and critical reviews, I would like to thank my advisory committee of Dr. David Josephy, Dr. Jacek Lipkowski, Dr. Richard Manderville, and Dr. Alicia Viloria-Petit. A special thanks to Dr. Alicia Viloria-Petit for providing technical training in cell culture, and to Dr. David Josephy for the use of his cell culture equipment.

Thank you to the Natural Sciences and Engineering Research Council of Canada for providing funding for the research project, and to Dr. Julie De Merchant for providing access to a 96-well plate reader.

I would like to thank Dr. Dorin Bejan for providing his piercing criticisms, helpful suggestions, and clarity, in both scientific and congenial discussions. Your friendship and assistance are greatly valued, and I hope they continue long into the future.

Finally, I would take the time to acknowledge the support and love of my family and friends. To those who endured my existential crises, tilting at windmills, and expletive frustrations, I am profoundly, and deeply, grateful.

Table of Contents

Title Page	*i*
Abstract	*ii*
Dedication	*iii*
Acknowledgements	*iv*
Table of Contents	*v*
List of Abbreviations	viii
List of Tables	*x*
List of Figures	*xi*
Preface	1
Chapter 1: Hypothesis Introduction	2
1.1 Standard of Care for Solid Tumors	2
1.2 Localized Chemotherapy	3
1.3 Drug Activation	6
1.4 Electrochemical Drug Activation	9
1.5 Summary	11
Chapter 2: General Knowledge for Experimentation	12
2.1 Basics of Electrolysis	12
2.2 Biomimetic Electrochemistry	15
2.3 Analysis and Quantitation	18
2.4 EMT-6 Cell Line	21
2.5 Summary	22
Chapter 3: Model Compounds	23
3.1 Cyclophosphamide	23
3.2 Acetaminophen	26
3.3 Summary	34
Chapter 4: Materials and Methods	35
4.1 Materials	35

4.1.1 Chemicals and Other Reagents 35
4.1.2 Batch Cell Electrolysis 35
4.1.3 HPLC 36
4.1.4 Flow Cell Electrolysis 36
4.1.5 Cell Culture 37
4.2 Methods 37
4.2.1 Batch Cell Electrolysis 37
4.2.2 Batch Cell Electrolysis - Buffers 38
4.2.3 HPLC Method 38
4.2.4 Synthesis of N-Acetyl-*p*-quinonimine 39
4.2.5 Cell Culture 39
4.2.5.1 Thawing Cells from Liquid Nitrogen 39
4.2.5.2 Cell Passage 40
4.2.5.3 Plating Cells for Assay 40
4.2.6 MTS Viability assay 41
4.2.7 Statistical Analysis 42
4.2.8 Probit Analysis 42
4.2.9 Electrolysis Cytotoxicity 42
4.2.10 Flow Cell Construction and Characterization 43
Chapter 5: Results and Discussion 44
5.1 Introduction 44
5.2 NAPQI Synthesis 44
5.3 Benzoquinone Calibration Curve 45
5.4 Preliminary Experimentation 46
5.4.1 Electrolysis of Buffered Solutions 46
5.4.2 MTS Assay Calibration 48
5.4.3 Chemical Reactivity of the MTS Reagent 51
5.4.4 Model Compound Dose-Response Curves 52
5.5 The Electrolysis of Cyclophosphamide 56

5.6 The Electrolysis of Acetaminophen 62
5.6.1 Potentiostatic Electrolyses 62
5.6.2 Amperostatic Electrolyses 66
5.6.3 The Absence of NAPQI 73
5.7 Toxicity of Electrolyzed Solutions 73
5.8 Flow Cell: Design and Construction 77
5.9 Toxicity of Electrolyzed Flow Cell Effluent 80
5.10 Limitations of Designed Flow Cell 82
Chapter 6: Conclusions 85
References 89

List of Abbreviations

4–OH–CP – 4-Hydroxycyclophosphamide

AM404 – *N*-(4-Hydroxyphenyl)-arachidonoylethanolamide

AOP – Advanced oxidation process

AP – Acetaminophen

BDD – Boron doped diamond

BQ – 1,4-Benzoquinone

CB – Cannabinoid receptor

COX2 – Cyclooxygenase 2

CP – Cyclophosphamide

d.f. – Degrees of freedom

DDTC – Dithiodiethylcarbamate

DET – Direct electron transfer dinucleotide phosphate

DMEM – Dulbecco's Modified Eagle's medium

EMT – Epithelial-mesenchymal transition

ER – Endoplasmic reticulum

FAAH – Fatty acid amide hydrolase

FBS – Fetal bovine serum

GSH – Glutathione

HQ – Hydroquinone

IC – Inhibitory concentration

IFF – Ifosfamide

ILI – Isolated limb infusion

ILP – Isolated limb perfusion

ITI – Intratumor injection

LC – Lethal concentration

LD – Lethal dose

MEC – Microencapsulated cells

MTS – [3–(4,5–Dimethylthiazol–2–yl)–5–(3–carboxymethoxyphenyl)–2–(4–sulfophenyl)–2H–tetrazolium, inner salt]

NADH – Nicotinamide adenine dinucleotide

NADPH – Nicotinamide adenine

NAPQI – N-Acetyl-*p*-benzoquinonimine

PBS – Phosphate buffered saline

PDT – Photodynamic therapy

PM – Phosphoramide mustard

POM – Post-oxidation modification

PUFA – Polyunsaturated fatty acid

SAM – Standard assay medium

SCE – Standard calomel electrode

SGM – Stock growth medium

TA – Tetrazolium

TFF – Trofosfamide

TFG-β – Transforming growth factor beta

TRIS – TRIS (2–amino–2–hydroxymethyl–propane–1,3–diol)

TRPA1 – Transient receptor potential A1 cation channels

TRPV1 – Transient receptor potential vanilloid 1 cation channels

List of Tables

Table 1.	Amperostatic electrolysis efficiency as a measure of benzoquinone yield	71
Table 2.	Anode surface area and current density in flow and batch systems	80

List of Figures

Figure 1	The pro-drug cyclophosphamide and its toxicant species, the phosphoramide mustard	8
Figure 2	An electrochemical cell; batch reactor.	12
Figure 3	Mechanism of water oxidation at chemically inactive and chemically active anodes.	16
Figure 4	Cytochrome P450 catalytic cycle.	17
Figure 5	Reduction of MTS dye to its formazan product	19
Figure 6	Dose-response data transformations.	20
Figure 7	Oxazaphosphorine alkylating agents	23
Figure 8	Metabolism of cyclophosphamide	24
Figure 9	Stabilizing effects of chloride ions on the reactivity of the phosphoramide mustard	25
Figure 10	Endogenous cannabinoid receptor agonist anandamide and the analogous acetaminophen metabolite, AM404	27
Figure 11	Metabolic fates of acetaminophen.	29
Figure 12	Acetaminophen redox chemistry.	30
Figure 13	General mechanism of lipid peroxidation	32
Figure 14	Hemocytometer Grid.	41
Figure 15	Reversed phase HPLC chromatogram of a mixture of purified acetaminophen, benzoquinone and NAPQI.	45
Figure 16	Benzoquinone calibration curve.	46
Figure 17	Effect of cell density on MTS response.	50
Figure 18	Chemical reaction of model compounds with MTS reagent in cell-free growth media.	52
Figure 19	Dose-response curve of EMT-6 cells treated with cyclophosphamide.	53
Figure 20	Dose-response curve of EMT-6 cells treated with acetaminophen.	54

Figure 21	Dose-response curve of EMT-6 cells treated with benzoquinone and probit transformation of data (insert)	55
Figure 22	Reversed phase HPLC chromatograph of 0.5 mM cyclophosphamide electrolyzed at 5 mA with a Ti/RuO_2 anode.	58
Figure 23	Reversed phase HPLC chromatograph of 0.5 mM cyclophosphamide electrolyzed at 5 mA with a graphite anode.	59
Figure 24	Reversed phase HPLC chromatograph of 0.5 mM cyclophosphamide electrolyzed at 20 mA with a Ti/RuO_2 anode.	60
Figure 25	Reversed phase HPLC chromatograph of 0.5 mM CP electrolyzed at 20 mA with a graphite anode.	61
Figure 26	Linear sweep voltammograms for 1 mM acetaminophen at Ti/RuO_2 and graphite anodes vs. SCE.	63
Figure 27	Potentiostatic electrolysis of 1 mM acetaminophen at graphite and Ti/RuO_2.	65
Figure 28	Amperostatic electrolysis of 1 mM acetaminophen at Ti/RuO_2.	67
Figure 29	Amperostatic electrolysis of 1 mM acetaminophen at graphite.	69
Figure 30	Amperostatic electrolysis of 5 mM acetaminophen at Ti/RuO_2.	72
Figure 31	Response of EMT-6 cells treated with 1 or 5 mM solutions of electrolyzed acetaminophen and cyclophosphamide.	74
Figure 32	Comparison of EMT-6 cell response to electrolyzed solutions of acetaminophen and benzoquinone probit plot.	76
Figure 33	Diagram of the constructed flow cell.	78
Figure 34	Photograph of the constructed flow cell.	79

Figure 35	Response of EMT-6 cells treated with 1 or 5 mM solutions of acetaminophen or cyclophosphamide electrolyzed in the constructed flow cell.	82
Figure 36	Generation of erratic flow by anodic oxygen production.	84

Preface

The standard of care for cancer patients with localized tumors is surgical excision. However, disease that is confirmed to have advanced locally (stage II) still requires treatment with radiation and or chemotherapy. These techniques have one intrinsic problem: dosages used in both radiation and chemotherapy are limited because collateral toxicities significantly affect patient health, often at therapeutic levels. This problem arises because these techniques are not very selective in their mechanism of toxicity. While ionizing radiation is focused on specific areas, the energy must still pass through healthy tissue; chemotherapy fares worse, as agents are systemically delivered. By targeting actively dividing cells, a serious problem occurs when healthy tissue is exposed to these cytotoxic agents. Often, the chemotherapeutic agents used to fight cancer are, themselves, carcinogenic, and their use incurs the risks of developing *de novo* cancers. Multiple rounds of toxicant exposure are required because cancerous cells not actively dividing at the time of exposure evade treatment, increasing the chances of a cancer developing resistance to the drug. In short, these factors contribute to disease progression. Now, envision a scenario in which it is possible to deliver high concentrations of cytotoxic agents to a tumor with minimal collateral toxicities.

This thesis uses principles from the fields of toxicology and electrochemistry to show that practical concentrations of a toxicant can be generated electrochemically from non-toxic precursors, and, that said compounds can be used as chemotherapeutics. Although the long term goals of this research would be to develop a clinical treatment, this thesis is directed towards proof-of-concept, and has been confined to the use of *in vitro* techniques.

Chapter One: Hypothesis Introduction

1.1 Standard of Care for Solid Tumors

Breast, prostate, colon, and lung, are some of the most common forms of cancer that manifest as solid tumors. The highest recovery rates and two year life expectancies are found in those patients diagnosed with pre- or locally invasive disease (Canadian Cancer Society, 2011). Provided the tissue in question is surgically accessible, resection is the primary form of treatment. It must be emphasized that individual treatment regimens are based on several factors: disease progression, anatomical location, patient choice, etc., and that it is the decision of the health care team to choose a treatment suited for a particular cancer. But in general, in cases of disease staged II or later, surgery alone has an increased rate of recurrence compared to surgery and chemotherapy; in colorectal cancer, even carcinoma *in situ* (stage 0) has a 1% recurrence rate with just surgery (National Cancer Institute, 2011). Post-excision, there is still a need for radiation and chemotherapy as a safeguard against any latent cancerous cells. However, in situations where a tumor is inoperable, a radiation and chemotherapy combination regime is the primary mode of treatment (Canadian Cancer Society, 2011). Therefore, most people diagnosed with cancer will need to undergo some form of chemo- or radiation therapy, even though the primary tumor is amenable to resection.

Despite being successful tumor-shrinking techniques, radiation and chemotherapy subject the patient to toxic levels of their respective agents. Arguably, a treatment must be aggressive for the abatement and elimination of a neoplastic growth. Yet, because of such aggression, overall patient health and quality of life suffers because of one reason: there is poor discrimination between healthy and cancerous cells. In the case of radiation, varying beam trajectory and intensity through different segments of healthy tissue can better manage any collateral damage that may occur (Veldeman *et al.,* 2008; Videtic *et al.,* 2010). In chemotherapy, compounds are selected for use because they disrupt some aspect of cellular replication; the tumour cannot grow, if the cells cannot

replicate. Traditionally, these compounds targeted aspects of DNA replication, but other processes involved in cell division, such as microtubule or hormonal signalling disruption, have become increasingly common in the clinic. Actively dividing cells such as those which maintain hair, blood, and the intestinal tract, are especially susceptible to radiation and chemotherapeutic drugs. Gastrointestinal pain, diarrhea, alopecia, anemia, weight loss, etc., are the hallmark pathologies associated with patients undergoing chemotherapy (Shapiro and Recht, 2001). These unintended toxicities arise solely from the exposure of normally dividing cells to a systemically circulating toxicant. By eliminating the systemic aspect of chemotherapy, these secondary pathologies can be entirely prevented.

1.2 Localized Chemotherapy

Intratumor injection (ITI) obviously cannot be used in advanced metastatic disease, nor is it intended to do so. However, ITI can provide three distinct advantages over conventional chemical and irradiative therapies:

1. the ability to use drug concentrations that would otherwise be systemically lethal, while simultaneously using smaller amounts of said drug,
2. the mitigation of collateral pathologies caused by systemic administration, and
3. the option to use a wider variety of cytotoxic compounds; i.e., not targeting aspects of cell division.

ITI effectively eradicates the pharmacokinetics of absorption and distribution, although interstitial diffusion would still factor into the success of a treatment (Pulen *et al.,* 2001). Using the same principles as ITI, isolated limb perfusion (ILP) and infusion (ILI) techniques have been developed to deliver high concentrations while mitigating systemic damage. These techniques are successful in treating solitary tumors and local metastases, with curative treatment in 50-80% of patients (Eggermont *et al.,* 2001). As their name suggests, these techniques are limited to use in the extremities. Essentially, a

tourniquet is applied to a cancer-containing limb while chemo drugs are infused into the limb's circulatory system. In isolating the limb from the rest of the circulation, a higher concentration of drug can be attained as compared to systemic chemotherapy (Eggermont *et al.,* 2001). This relationship is elaborated upon in the following example:

> A hypothetical patient has an inoperable tumor with a size of 50 g. To treat this tumor using standard chemotherapy dosages, a one-time dose of 15 mg/kg body weight cyclophosphamide is administered intravenously (BC Cancer Agency Breast Tumor Group, 2001). If the patient weighs 70 kg, then the amount of drug given is 1.05 g; for simplicity's sake a one compartment model is assumed. The amount of drug that is available to treat the tumor is therefore 0.75 mg, or 0.07% of the initial 1.05 g used.

Of the total dose administered, the amount available to kill the cancerous cells is three orders of magnitude smaller than what was given. Not only is this scenario inefficient, it provides selection pressure for resistant cells to replicate, as not all cancer cells are killed during the initial exposure. However, in an ITI scenario the full amount of 1.05 g is administered to the tumor, meaning a dosage of 21 mg/g tumour (i.e., 21,000 mg/kg) – a lethal dosage in any other context. However, the full 1.05 g dose should not be administered, a dose proportional to the volume to be treated should be instead. This would ensure toxicity to the tumour while safeguarding against a scenario where all the injected drug diffuses out into the body, where the systemic concentration would remain well below a toxic concentration. However, to minimize this diffusion, a compound would have to exhibit certain characteristics regarding its reactivity. It must be reactive enough to be cytotoxic, but not so reactive that it is destroyed before it can enter the cell; this type of reactivity would limit the molecule's diffusion beyond the site of administration (Pulen *et al.,* 2001). With these two criteria satisfied, the probability of the drug producing collateral toxicities would be reduced.

In using higher concentrations of drug, the probability of all tumor cells dying increases. This is an important consideration because a tumour is, in actuality, a complex microenvironment comprised of an assortment of cells of cancerous,

immunological, vascular, and stromal origin. Inefficient vascularization within the tumour is a significant impediment to intravenous drug delivery, resulting in non-uniform distribution of cytotoxic agents (i.e., not all cells within the tumour will be exposed to cytotoxic concentrations); this sub-lethal exposure is what drives the development of cancer resistance (Dunst *et al.*, 2003). However, by surgically injecting cytotoxic agents directly into areas of poor vascularization, the problem of intratumour distribution can is avoided and a new, cytotoxic microenvironment is created. This carries an implication that rates of recurrence would also be expected to decrease. In other words: the greater the dosage used, the greater the probability all cells exposed will be killed. This is an important benefit of localized chemotherapy techniques because very few cancer cells are required to (re-)establish a tumor.

Radiation and chemotherapy drugs are often carcinogenic themselves because they interfere with aspects of mitosis, or more accurately, because they failed to elicit cytotoxicity and the cell survived. Regardless of the specific mechanism of action of a particular agent, the underlying paradigm in cancer therapy is to interrupt cell division; this is primarily achieved through the prevention of DNA replication and repair. Recently it has been hypothesized that cancer cells exhibiting stem cell phenotypes (i.e., cancer stem cells) are responsible for tumorigenesis (Al-Hajj *et al.,* 2003). These cells circumvent treatments through asymmetrical DNA replication and the expression of drug efflux pumps (Pine *et al.,* 2010). Therefore, these features make certain cancer cells particularly robust. By using compounds that disrupt pathways of cell metabolism or disrupt cellular membranes, the chances of killing these cancer cells would be increased, as non-specific cell damage would be produced. The probability of a *de novo* cancer developing post-treatment would also be reduced, as the drug would not have to interfere with DNA replication. The use of metabolic toxicants intravenously would be disastrous to patient health because most metabolic pathways are identical in both healthy and cancerous cells (DeBerardinis *et al.,* 2008). Yet, through local administration, only the cells in the vicinity of the application site would be affected.

The reliance on accurate medical imaging techniques would also be essential to the success of ITI. Medical technologies such as magnetic resonance imaging and positron emission tomography are routinely used to construct detailed 3-D images of tumors *in situ* prior to surgery (Langley and Liang, 2002). These techniques are frequently used in brachytherapy to treat patients with prostate cancer. Traditional prostate brachytherapy involves the distributed implantation of radioisotope 'seeds' directly into the prostate gland. This might appear to be an ideal solution to other forms of non-metastatic cancer; however, it is the typically slow progression and confined nature of prostate cancer that allows this therapy to be used (McNeal *et al.,* 1986). A recent, and successful, modification of this technique replaces the radioisotopes with a laser beam, in a process which is called photothermal laser ablation therapy (PLAT). By heating the tumour to the point of cytotoxicity, PLAT has shown success in treating early-stage, low volume prostate tumours (Lindner *et al.*, 2009; Raz *et al.*, 2010). Importantly, PLAT exemplifies the principles discussed regarding successful localized treatments, and provides a working clinical framework for a similar chemotherapeutic approach. Another variation on the same theme, using ultrasound to kill cancerous tissue, has been shown to be successful in treating localized prostate tumours (Siddiqui *et al.*, 2010). In using implantation techniques developed for focal treatments, intratumor injection of a cytotoxic agent could be used instead of radioisotopes, ultrasound, or laser beams.

1.3 Drug Activation

Minimizing the systemic toxicities of cytotoxic drugs is one area of research that has produced highly innovative results. In the last 25 years, there have been several techniques developed which limit the drawbacks of intravenous chemotherapy, all making use of the same basic principle: the local activation of a chemical into a more reactive form. By generating a toxic compound *in situ,* a greater level of treatment control and toxicity reduction can be achieved. One technique in particular has had a significant level of success: photodynamic therapy (PDT). Photodynamic therapy is a

treatment in which infrared radiation causes localized, electronic excitation of certain porphyrins. Subsequent transfer of energy promotes molecular oxygen into an activated state, known as singlet oxygen (O'Conner *et al.,* 2009). The use of a fibre optic probe allows the surgeon to direct the radiation beam directly into the tumor, and treatment effectiveness is based on this localization (Vrouenraets *et al.,* 2008). The histological type and location of a tumor dictates which specific sensitizer is used, but in general, the main concern is the absorption characteristics of the compound; a clinically favourable sensitizing agent will be preferentially taken up into a tumor, compared to normal tissue. This characteristic limits the severity of side-effects and enhances success of the therapy; however, such an ideal agent has yet to be discovered. The major limitation to PDT is that the probe's light can only penetrate approximately 1 cm into tissue. Therefore, the main application of this technique is for dermal tumours, or those which lie on the surfaces of organs; the sensitizer can be given in a topical or systemic fashion, respectively. One of the most significant side-effects of PDT occurs when sensitizing agents are inadvertently activated by sunlight, whose broad spectrum of wavelengths can activate many different types of photosensitizers used (O'Conner *et al.,* 2009). When sensitizers in sunlight-exposed skin become activated, the pathological outcome is similar to a severe sunburn: reddening, pain, blistering, and the eventual sloughing of dermal layers (Vrouenraets *et al.,* 2008). This 'sunburn' can occur in conditions of low-intensity sunlight and short exposure duration; however, photodynamic therapy is a successful clinical technique, one that uses intra-tumor chemical activation.

Exploiting a cell's biochemistry to activate compounds has been a clinically successful method of cancer treatment since the early 1960s. One of the most successful anti-neoplastic drugs, cyclophosphamide, was conceived on the principle of biochemically activating a pro-drug *in situ* to minimize the toxicity of nitrogen mustards, the active toxicants (see section 3.1; Brock, 1998). Bioactivation is frequently an oxidative process catalyzed by cytochrome P450s, which are monooxygenase enzymes (Ding and Kaminsky, 2003; Yap *et al.,* 2008). By adding a functional group to a molecule, reactivity is temporarily increased so that water-soluble groups can be conjugated,

allowing the substrate to be more easily excreted. Some functional groups introduced are nucleophilic (e.g., alcohols), which make the molecule reactive towards conjugating agents. Other functional groups, such as epoxides and mustards, are electrophilic, and can exert toxicity by covalently binding to nucleophilic sites on cellular macromolecules (e.g., amine or thiol groups in proteins). Toxicity arises when an activated compound overwhelms the cell's excretory ability and the molecule begins to react with cellular components. Given sufficient amounts of such a chemical, the damage done to the cell can overwhelm its ability to function, and the cell dies. Therapeutic biochemical activation is exemplified in the case of cyclophosphamide, which is only cytotoxic once it has been activated by cytochrome P450s in the liver (Sladek, 1973). Cyclophosphamide toxicity involves the addition of a hydroxyl group by hepatic P450 enzymes; a systemically circulating species (to reach the tumor); and an intra-cellular decomposition step to yield the toxicant species, the phosphoramide mustard (figure 1; see Chapter 3.1). The requirement for bioactivation significantly reduces the toxicity of circulating cyclophosphamide compared to nitrogen mustards. However, the systemic circulation of an 'active' species leads to the cytotoxicity of healthy cells. Lohr *et al.* have undertaken work attempting to address this systemic component from therapeutic bioactivation.

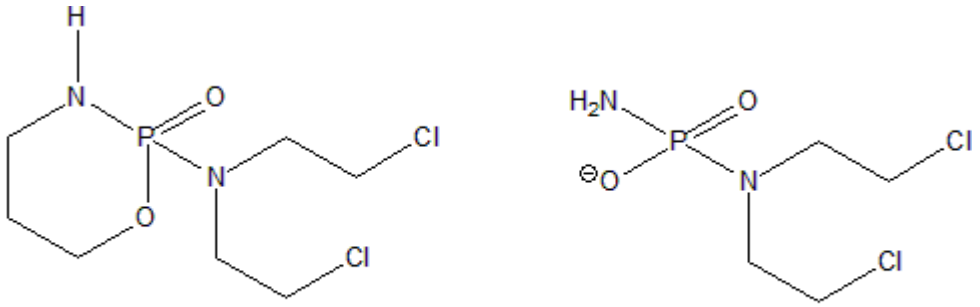

Cyclophosphamide **Phosphoramide mustard**

Figure 1. The pro-drug cyclophosphamide and its toxicant species, the phosphoramide mustard.

Attempts have been made by Lorh *et al.* (1998) to develop a clinical technique which combines several of the previously seen principles discussed in chapters 1.2,

localized chemotherapy, and 1.3, drug activation. Cells were encapsulated to prevent an immune response and genetically modified to express high levels of specific P450 enzymes (Lorh *et al.,* 1998; Samel *et al.,* 2006). These cells were then implanted in the vicinity of locally metastasized tumours. This was done so that the chosen prodrug, ifosfamide, an analogue of cyclophosphamide, would become activated in higher concentrations where the implanted cells reside. Animal models have shown significant benefit from microencapsulated cells (MEC) plus ifosfamide over other forms of treatment; response rate, tumor volume, and survivability were significantly improved over ifosfamide and radiation treatments alone in inoperable pancreatic cancer (Lohr *et al.,* 1998). Pancreatic cancer is a highly aggressive and fatal disease that first presents with extensive localized tumors (Canadian Cancer Society, 2011). Combination therapy of localized MEC, ifosfamide, and radiation, provided the best outcomes overall. From phase I and II clinical trials, this technique boasts a doubling of the median survival (44 weeks), and a 100% tumor response in patients (Lohr *et al.,* 2002). However, as with all of the previously discussed anti-cancer techniques, the work by Lorh *et al.* uses a systemically administered prodrug. Because the specific form of P450 used is also expressed in relatively high amounts in the liver, toxicities were observed there as well (Lohr *et al.,* 1998). There are still systemic toxicities associated with this treatment, albeit, with a far better profile than with conventional chemotherapy of the same drug (Lohr *et al.,* 1998, 2002). Lorh *et al*.'s work manages to embody many of the principles on which this thesis is based, in a successful therapy.

1.4 Electrochemical Drug Activation

In order to better understand P450 oxidation *in vivo,* much work has been done on the electrochemical generation of P450 metabolites, as the two processes can mechanistically parallel each other (see Section 2.2; Lohmann and Karst, 2008; Madsen *et al.,* 2007). Of the compounds which are oxidized by P450 reactions, electrochemical oxidation can generate a majority of the primary products observed *in vivo*. Sometimes, additional oxidation products can be observed electrochemically that are not seen

biologically (Madsen *et al.,* 2007). *In vivo,* substrate specificity of the enzyme determines which oxidation products can be formed; however, electrochemical oxidation is comparatively less selective, and additional products can often be observed. Despite additional products, there is evidence supporting electrochemical oxidation as a good predictor of primary metabolites of P450 oxidation; i.e., there is a high degree of biological relevance (Baumann *et al.,* 2009; Jurva *et al.,* 2003, 2008; Madsen *et al.,* 2007, 2008). Products of electrochemical oxidation are influenced by the choice of electrode material, one must be selected that preferentially gives the same oxidation products as the enzymatic oxidation (see Section 2.2). It must be noted that the majority of research in this area involves *in situ* oxidations that have been analyzed by electrochemical-mass spectrometry. As such, the higher potentials required for aromatic hydroxylation reactions are deliberately not used, so as to avoid water oxidation and oxygen evolution (see Section 2.2). Electrochemically-generated mimics of P450 oxidation have been documented, specifically: the dehydrogenation of acetaminophen (Madsen *et al,.* 2007), the hydroxylation of diclofenac (Madsen *et al.,* 2008), the N-dealkylation of imipramine and lidocaine (Shono *et al.,* 1982; Nouri-Nigjeh *et al.,* 2011), and the phosphothionate oxidation of parathione (Jurva *et al.,* 2003). Because many of these primary metabolites are highly electrophilic molecules, the absence of biological nucleophiles in an electrochemical system is a distinct advantage over other *in vitro* techniques, which use cell homogenates or cultures to study P450 catalysis. However, inorganic nucleophiles, such as water or electrolyte anions, are present in electrochemical systems. By using electrochemical oxidation as a means of prodrug activation, in combination with intratumor injection, many of the limitations associated with the aforementioned cancer treatments can be significantly mitigated. Hillard et al. (2008) have discussed some of the electrochemical requirements for designing redox-selective drugs; here they emphasize the use of quinoid compounds such as benzoquinone. Surprisingly though, no cancer treatment currently exists which uses electrochemical oxidation to generate cytotoxic agents.

1.5 Summary

By electrochemically activating a prodrug through oxidation, and subsequently injecting said toxicant directly into a tumor, dosages can be attained that are otherwise unrealistic through via systemic administration. Targeting the tumour directly allows for the use of toxicants that do not target cellular replication. In the next chapter, subject material will focus on the general, technical knowledge required for successful proof of concept.

Chapter Two: Practical Knowledge

2.1 The Basics of Electrolysis

In the general sense, electrolysis is a simple idea: pass a current through a solution so that electrons can be used for chemical work. An electrolytic reactor requires three basic components: a power supply, an interface, and a conductive solution (figure 2). An electron source can be as simple as a battery, but the amount of control offered by a potentiostat has made it the standard apparatus in electrolysis. The potentiostat allows one to vary such parameters as the direction of electron flow and either the voltage or current being applied across the interface. Two electrodes, the anode and cathode, serve as electron exchange interfaces between the power supply and the solution being electrolysed. The cathode is negatively polarized (reduction) and the anode is positively polarized (oxidation). Finally, an ionic solution is used to complete the electrical circuit between the cathode and anode, as without a supporting electrolyte, the cell is non-conductive.

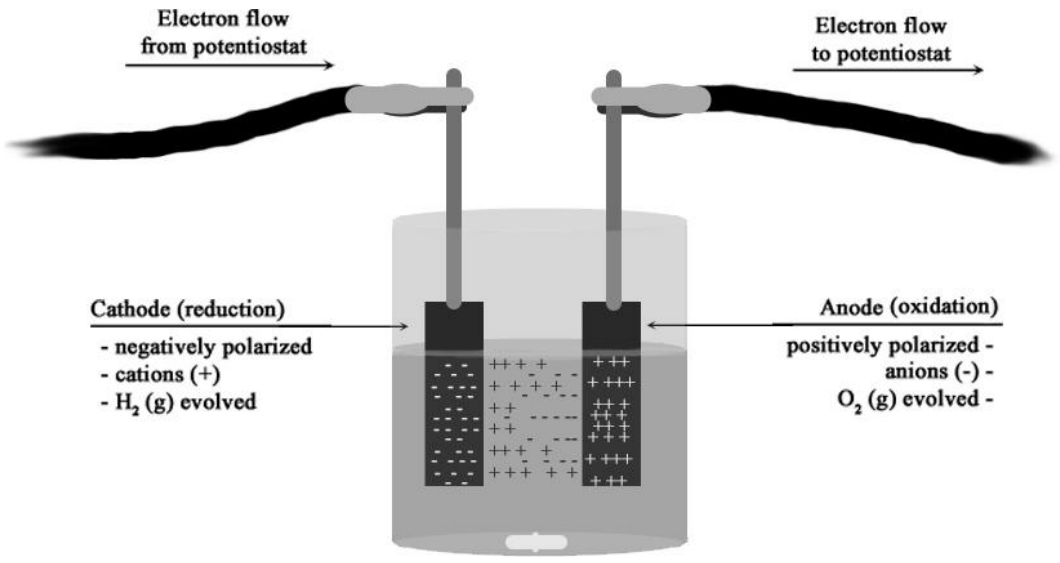

Figure 2. An electrochemical cell; batch reactor

Amperostatic and potentiostatic electrolyses are two ways in which the potentiostat can apply a potential between the anode and cathode. In the former mode, the current, or flow of electrons, is held at a constant rate allowing the electrical potential, or voltage, to change. This voltage change is in accordance to Ohm's law (voltage = current x resistance) and is dependent on the resistance generated, in part, by the anode material; the substrate being oxidized; and electrolytes in solution. During potentiostatic electrolyses, the potential is held constant and the current (i.e., the rate of oxidation) becomes dependent on the concentration of substrate.

Similar in concept to activation energy, overpotential is the excess potential above a thermodynamic value required for an electrochemical reaction to occur. In this thesis, overpotential will be used when discussing water oxidation and the production of oxygen at the anode. While both substrate and water oxidation can occur simultaneously at an anode, it is not always the case; once again, anode material plays a crucial role in determining mechanism of substrate oxidation. Easily polarizable anodes such as ruthenium dioxide, oxidize water at very low potentials; meaning that substrates and water oxidation are almost inseparable (Boudreau *et al.,* 2010 B). Anode materials which are more difficult to polarize, such as boron-doped diamond (BDD) and graphite, have higher potentials for water oxidation. At potentials which are lower than that required to oxidize water, direct electron transfer oxidations take place (Boudreau *et al.,* 2010 B). As its name suggests, direct electron transfer (DET), occurs when a substrate gives up electrons directly to the anode's surface; this type of electron transfer is typically observed with metals dipped into ionic solutions, e.g., $Cu^{+2}(aq)$ + Fe(*s*) => $Fe^{+2}(aq)$ + Cu(*s*). Above the overpotential, substrates are predominantly oxidized by the advanced oxidation processes that will be discussed in detail in Section 2.2.

The design of an electrochemical cell is just as important as the selection of anode material. There are two general cell designs for an electrochemical reactor, flow or batch circulation. Flow reactors involve a continuous flow of solution through the reactor and, for this thesis, can be considered as a 'one pass' design; the solution is exposed to the electrodes only once before exiting the reactor. The amount of oxidation

products formed is dependent on residency time within the reactor and the amount of charge passing through the cell (Polocaro *et al.,* 2008). The residency time of a substrate in the reactor is dependent on reactor volume and the solution's flow rate. Effluent must be monitored for an efficient steady-state formation of products; for this project, monitoring is most easily done by HPLC. Contrary to flow designs, batch reactors are closed systems in which the electrolysed solution is circulated within a single chamber. Substrates are continuously exposed to the electrodes, meaning products can undergo several rounds of oxidation (i.e., become fully oxidized). The advantages of using a batch cell lies mainly in the work of reaction characterization and optimization. Following prodrug activation as a function of concentration, current, and time, allows one to conveniently optimize conditions for the more intricate flow reactor. Product yield per charge passed is a measure of current efficiency, and optimizing this value in a batch cell allows one to easily define efficient operating conditions in a flow reactor.

During electrolysis, some substrates inter-convert between their oxidized and reduced forms. Known as redox cycling, this occurs when a molecule is initially oxidized at the anode, diffuses into the solution, and is then reduced back to the original form at the cathode, or *vice versa*. While redox cycling is a reversible substrate modification, its presence during electrolysis only serves to decrease overall efficiency. Redox cycling is a form of reversible post-oxidation modifications (POMs). In the case of a substrate that undergoes irreversible oxidation, POMs are more detrimental, the activated compound cannot be reduced back to its original form; from an efficiency standpoint, both charge and substrate are wasted. Post-oxidation modifications are a substantial problem when one oxidation step is desired, as is the case when attempting to mimic bioactivation. To avoid this problem, the reactor can be divided using an ion-permeable membrane. While dividing an electrolytic cell prevents redox cycling, doing so creates another problem: the two compartments begin to drift away from neutral pH. This is caused by the accumulation of hydroxide and hydronium ions at the cathode (1) and anode (2) and can be described by the following half-reactions:

Cathode: $2H_2O\ (l) + 2e^- \rightarrow H_2\ (g) + 2OH^-\ (aq)$ (1)

Anode: $2H_2O\ (l) \rightarrow O_2\ (g) + 4H^+(aq) + 4e^-$ (2)

In an undivided cell, the basic (OH^-) and acidic (H^+) ions that are produced are able to diffuse into solution and neutralize each other, resulting in a solution whose pH is almost constant during electrolysis; in the divided cell this neutralization is prevented and the ions accumulate. The resulting pH imbalance is undesirable from a chemical standpoint as the electrochemical reaction may be pH dependent, or, the desired compound is only stable at a specific pH; in any case, a buffered solution can be used to control pH.

While it is standard practice to use saline solutions to formulate drug suspensions, during water oxidation, the chloride ion is readily oxidized electrochemically to hypochlorite (bleach), which is both a potent oxidizing and chlorinating agent; any toxicant produced would react with this compound. Yet, within the scope of this thesis, the use of hypochlorite as an electrochemically generated toxicant is still applicable because hypochlorite is a potent cytotoxic agent (e.g., its use as a disinfectant). The use of sodium sulfate or sodium perchlorate, two fully oxidized anions, is therefore recommended.

2.2 Biomimetic Electrochemistry

Substrate oxidation mechanisms between electrochemical prodrug activation and P450 bioactivation are paralleled by the formation of transient metal oxides. In the absence of water oxidation, only direct electron transfer occurs (see Section 2.1). When potentials are large enough to oxidize water, substrates are oxidized by one of two advanced oxidation processes (AOP; figure 3). Which mechanism of substrate oxidation that occurs is dependent on anode material.

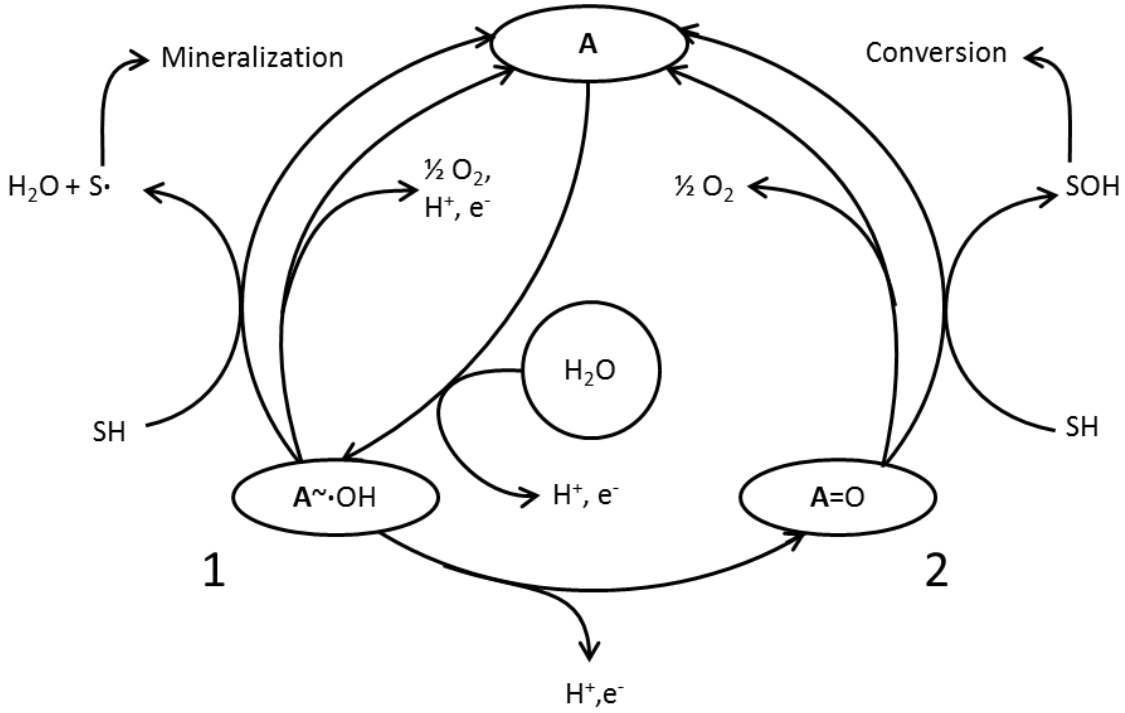

Figure 3. Mechanism of water oxidation at chemically inactive (1) and chemically active (1, 2) anodes; A: anode surface; S: substrate (figure courtesy of Dr. Dorin Bejan, Chemistry Department, University of Guelph).

Chemically inactive anodes, such as β-PbO_2 and boron-doped diamond (BDD), oxidize water via a one-electron transfer mechanism and do not chemically alter their surface (figure 2-1). When water oxidation occurs, these anodes physically adsorb hydroxyl radicals to their surface (A~•OH) antecedent to the oxidization of substrates in solution (Kapalka *et al.,* 2007). Substrate oxidation, in the presence of water oxidation, at inactive anodes, leads to a process known as mineralization, a phenomenon to avoid when attempting to activate prodrugs. The reactive oxygen species produced at inactive anodes repeatedly, and indiscriminately, oxidize organic substrates until only inorganic components remain (CO_2, H_2O, NO_x^{-y}, SO_x^{-y}, etc.) (Kapalka *et al.*, 2007; Boudreau *et al.,* 2010 A, B). Additionally, because of the one-electron transfer mechanism of inactive anodes, certain compounds will form polymeric films on the anode's surface, fouling the electrode. Anilines and phenols are well known for this behaviour, and are found in

many drugs (Bao *et al.,* 2010; Boudreau *et al.,* 2010 A). Consequently, inactive anodes are not candidates for prodrug activation.

The other mechanism of AOP occurs at dimensionally stable, or chemically active anodes. These anodes chemically alter their surface to a higher oxide, i.e., AO_x becomes AO_{x+1}, through a two-electron transfer mechanism (figure 3-1, 2). This oxygen-transfer reaction is parallel to the process whereby Fe^{+2} becomes $(Fe=O)^{+3}$ during P450 catalysis (figure 4; Meunier *et al.*, 2004).

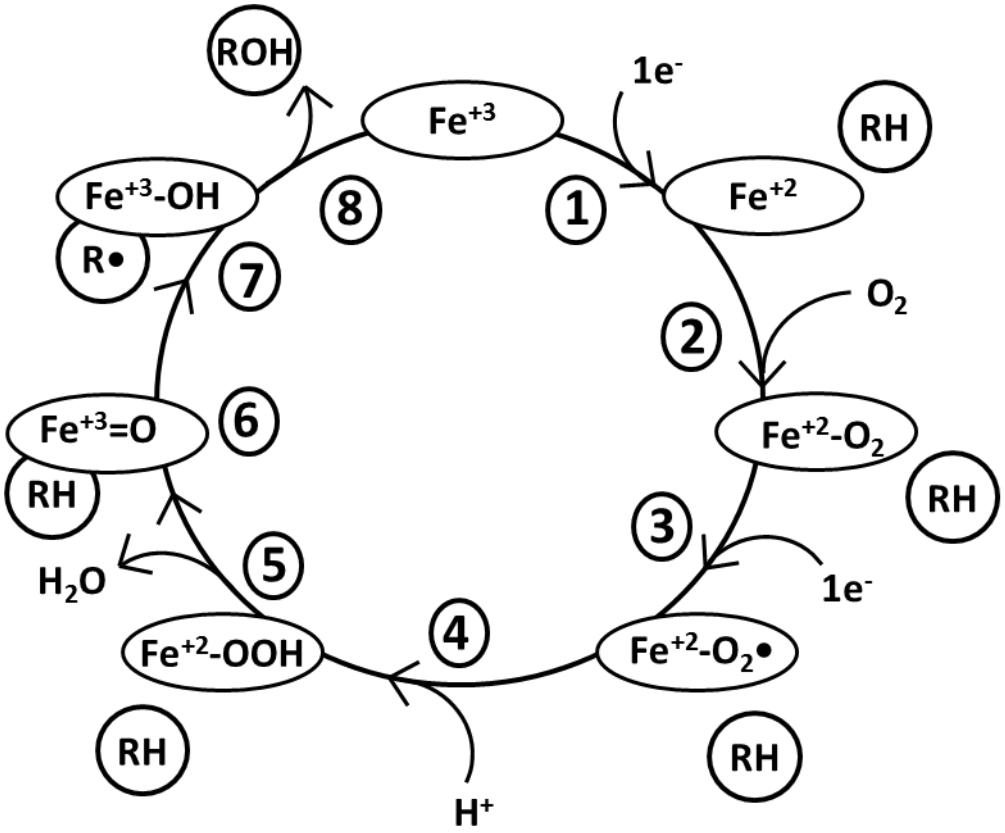

Figure 4. The P450 catalytic cycle (recreated from Meunier *et al.*, 2004).

During both electrochemical and P450 oxidation, the '+1' oxygen atom oxidizes the substrate, often resulting in an oxygen transfer reaction taking place. Chemically active anodes are commonly made from films of iridium and ruthenium dioxides on a base of titanium; as a consideration, ruthenium is below iron on the periodic table. Graphite can also be categorized as a chemically active anode, as its surface

functionalizes in the range of water oxidation; however, this surface modification is more complex than is seen at AO_x based anodes (Rueffer *et al.,* 2011). While polymerization does occur at active anodes, the extent is diminished compared to inactive anodes because of the absence of radical species. Although P450s use O_2, and chemically active anodes use H_2O to produce their respective '+1' oxides, there exists a significant overlap of oxidation products between the two mechanisms (see Section 1.4; Fierro et al., 2007; Jurva *et al.,* 2003; Madsen *et al.,* 2007). Therefore, chemically active anodes are best suited for the activation of a prodrug as they are incapable of mineralization, and are less prone to substrate polymerization (Boudreau *et al.,* 2010 A, B).

2.3 Analysis and Quantitation

In order to assess the toxicity of electrolyzed solutions, a means of quantifying cell viability is required; to this end, a tetrazolium dye-based assay was chosen. Tetrazolium (TA) dyes, in colorimetric assays, are able to quantify increases or decreases in cell viability resulting from treatment, by measuring changes in absorbance versus controls; a distinct advantage over other cell viability techniques which typically can only measure proliferation or toxicity but not both. When reduced, these dyes are converted into a coloured formazan product. Reduction of the dye occurs via intracellular electron donors, NADH and NADPH, and is indirectly dependent on mitochondrial function of viable cells. A cell must be metabolically active in order to produce a detectable formazan product. TA dyes used in cell assays require an electron coupling reagent to link the production of NAD(P)H and the reduction of the dye; the agent used in this thesis is phenazine methosulfate (Mossman, 1983). The specific dye used in this thesis is [3-(4,5-dimethylthiazol-2-yl)-5-(3-carboxymethoxyphenyl)-2-(4-sulfophenyl)-2H-tetrazolium, inner salt] or MTS (figure 5). The water-soluble formazan product is measured spectrophotometrically at 490 nm, after an incubation time of at least 1-4 hours. Because NAD(P)H is also used by bacteria, which are more prevalent than mammalian cells, sterility is essential to the accuracy of the assay (Promega MTS assay

technical bulletin, 2009). A contaminated sample will produce a greater signal response as more of the MTS dye is reduced by bacteria. A naive interpretation of this hypothetical result would mean that the treatment actually enhanced cell viability, otherwise known as a false negative; 1% penicillin-streptomycin (v/v) was added to the incubation medium to prevent this from occurring.

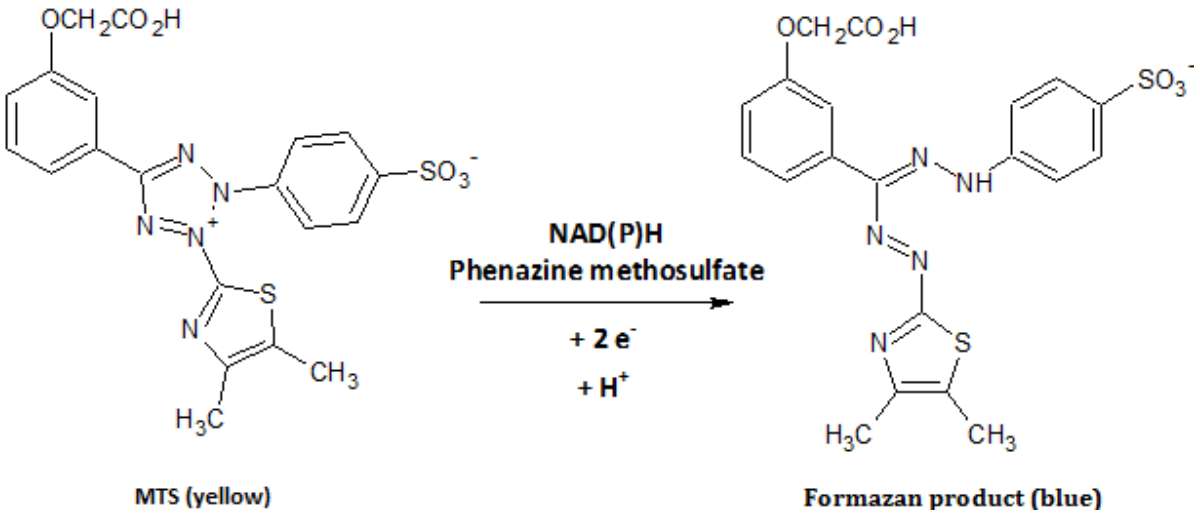

Figure 5. Reduction of MTS dye to its formazan product (Promega MTS assay technical bulletin, 2009)

Toxicological data are generated by exposing a group of cells to a toxicant and measuring the response, a percentage of cell viability. Properly constructing a dose-response curve requires the use of concentrations that span several orders of magnitude. Typically, after a wide range of concentrations is assayed, a more detailed study is conducted over the toxic range. The plot of response versus concentration is difficult to analyze at the lowest concentrations (figure 6A). Logarithmic transformation of the concentration yields a plot that is sigmoidal in nature and appears as though there is a response threshold – this interpretation is wrong (figure 6B). In order to properly analyze the data obtained from a dose-response curve, a probit plot must be constructed.

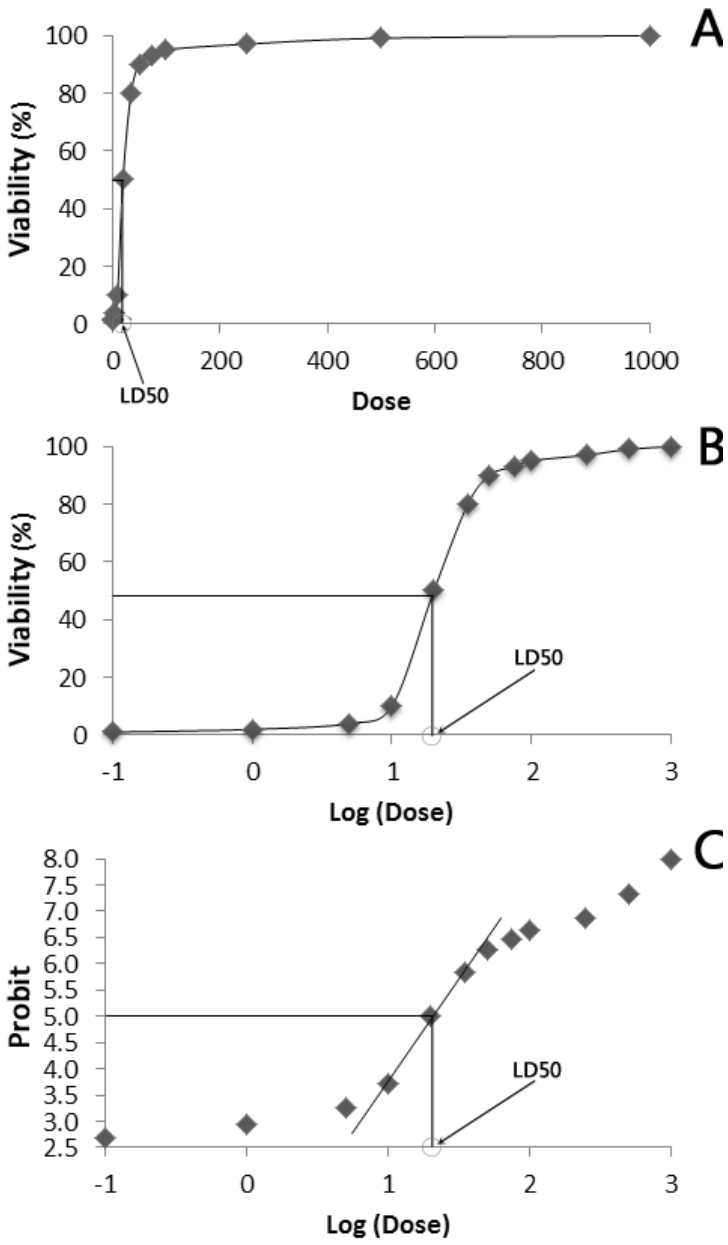

Figure 6. Transformations of dose-response data. A: dose-response plot; B: log dose-response plot; C: probit plot.

A probit is a probability unit that assigns a numerical value to percent responses ranging from 0 to 10, so that a response of 50% viability is equal to a probit of 5.00 (Hubert, 1992). A probit scale is not a linear scale, but rather, one designed to enhance statistical confidence of data nearest the mean of distribution (e.g., a probit of 5.00). Due to larger variances in the low and high percent response portion of the probit plot,

LD values in these regions must be extrapolated from data nearest the LD_{50}, as there is higher associated variance in this region. A logarithmic transformation is applied to the dosages in a probit graph in order to obtain a linear plot of probit versus log concentration (figure 6C; Hubert, 1992). All of this is done so that the dose producing a 50% response in the population has the lowest variance associated with it. Additionally, the linear line produced from the transformation better approximates the entire data set, rather than having to rely on point estimates for LC concentrations. The dosage, or concentration, which elicits a lethal response in 50% of a treatment group is known as the LD_{50} or LC_{50}, respectively. Responses measured are binary in nature and, as such, death is the typical endpoint measured; although, other metrics of toxicity can be used (e.g., teratogenicity, carcinogenicity, etc.). If there is a different number of 'n' observations per dose, a weighted probit plot can be constructed. The weighting coefficients used are designed to give the largest weight to response values closest to the mean (LD_{50}). There are several methods which are mathematically designed to estimate the LC_{50}; however, this thesis is most interested in doses which produce a high response, at least 99% mortality, meaning this dose value will need to be extrapolated from a probit plot.

2.4 EMT-6 Cell Line

EMT-6 is a mouse mammary adenocarcinoma cell line derived from glandular epithelial cells lining milk ducts (Rockwell *et al.,* 1972; Owens *et al.,* 1974). When transplanted into naive mice, EMT-6 cells readily form solid tumours. The *in vivo* progression of this cell line parallels human breast cancer, in that the cancer initially remains within the mammary organs, producing localized tumor clusters before lymph and pulmonary metastases occur (Rockwell *et al.,* 1972; 1977). EMT-6 is well characterized *in vivo* and *in vitro*, with thorough description of how it responds to chemotherapy in both models, specifically to cyclophosphamide (Chatterjee *et al.,* 1995; Twentyman, 1977; Ono and Shrieve, 1987). Therefore, the significance of any results obtained *in vitro* with this cell line can be feasibly tested *in vivo* using orthotopic (i.e.,

mammary gland) implantation of cells into a syngeneic BALB/c host, the original mouse strain from which the EMT-6 cell lines was derived (Rockwell et al., 1972). Cyclophosphamide and acetaminophen have been selected for this thesis as chemical probes for cytotoxicity and will be discussed in more detail in Chapter 3.

2.5 Summary

The use of a chemically active anode, such as Ti/RuO_2 or graphite, is best suited for the oxidation of a prodrug because the mechanism of substrate oxidation mimics enzymatic bioactivation. The mouse mammary cancer cell line, EMT-6, was chosen because of its well characterized response to chemotherapy, and its paralleled disease progression to human breast cancer. A tetrazolium dye (MTS) assay was selected for toxicological analysis due to its convenience of use, and ability to measure either proliferative or inhibitive cell growth in response to a particular treatment.

Chapter Three: Model Compounds

3.1 Cyclophosphamide

Cyclophosphamide (CP) was developed in the late-1940s in order to minimize the systemic toxicities of *nor*-N-mustard analogues in clinical use at the time (Brock, 1989). Brock and colleagues chemically deactivated the N-mustard by incorporating it into a cyclic phosphorus ester. Cyclophosphamide and its analogues, ifosfamide (IFF) and trofosfamide (TFF), which were synthesized shortly thereafter, differ from each other in the number and placement of the chloroethyl arms: RCH_2CH_2Cl; a characteristic that significantly impacts toxicity and clinical efficacy (figure 7). The difference in effectiveness between the analogues occurs because the chloroethyl arms are separated onto different nitrogens of the phosphoramide mustard. This enhances inter-strand and inter-helical cross-linking of DNA, an alkylation event which is known to trigger cell death more readily than other types of alkylation (e.g., mono-adduct or intra-strand cross-linking). Regardless of the relative toxicities, oxazaphosphorine alkylating agents require liberation of the phosphorus ester in order to elicit toxicity.

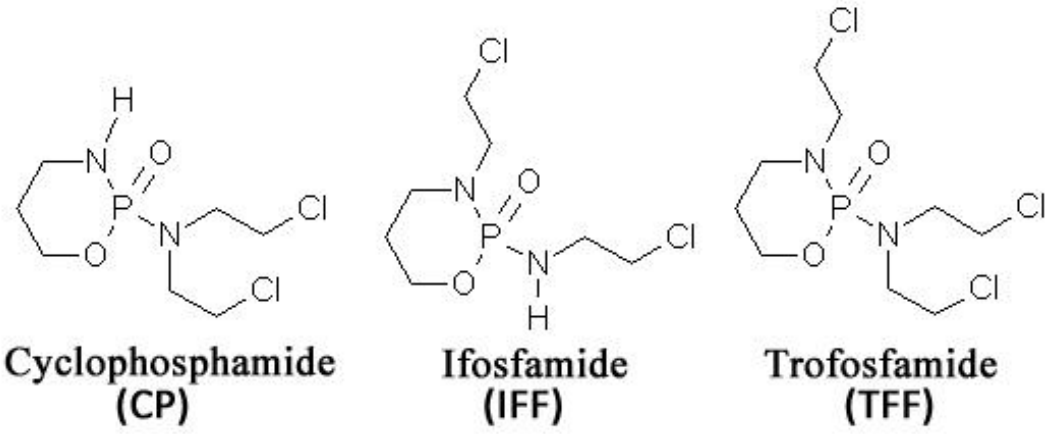

Figure 7. Oxazaphosphorine alkylating agents

Cyclophosphamide is bioactivated *in vivo* via hepatic P450 oxidation, catalyzed principally by CYP 2B6, and hydroxylated at the C-4 position (Figure 8; Chang et al., 1993). Other sites of oxidation lead to non-toxic metabolites, principally catalyzed by CYP 3A4, with CYP 2C8 and 2C9 contributing moderately to side chain oxidation

(Bohnenstengel *et al.*, 1996). This relationship is reversed in ifosfamide metabolism, where CYP 3A4 is responsible for generating the 4-OH-ifosfamide metabolite, and CYP 2B6 predominately oxidizes the mustard alkyl groups (Chang *et al.*, 1993).

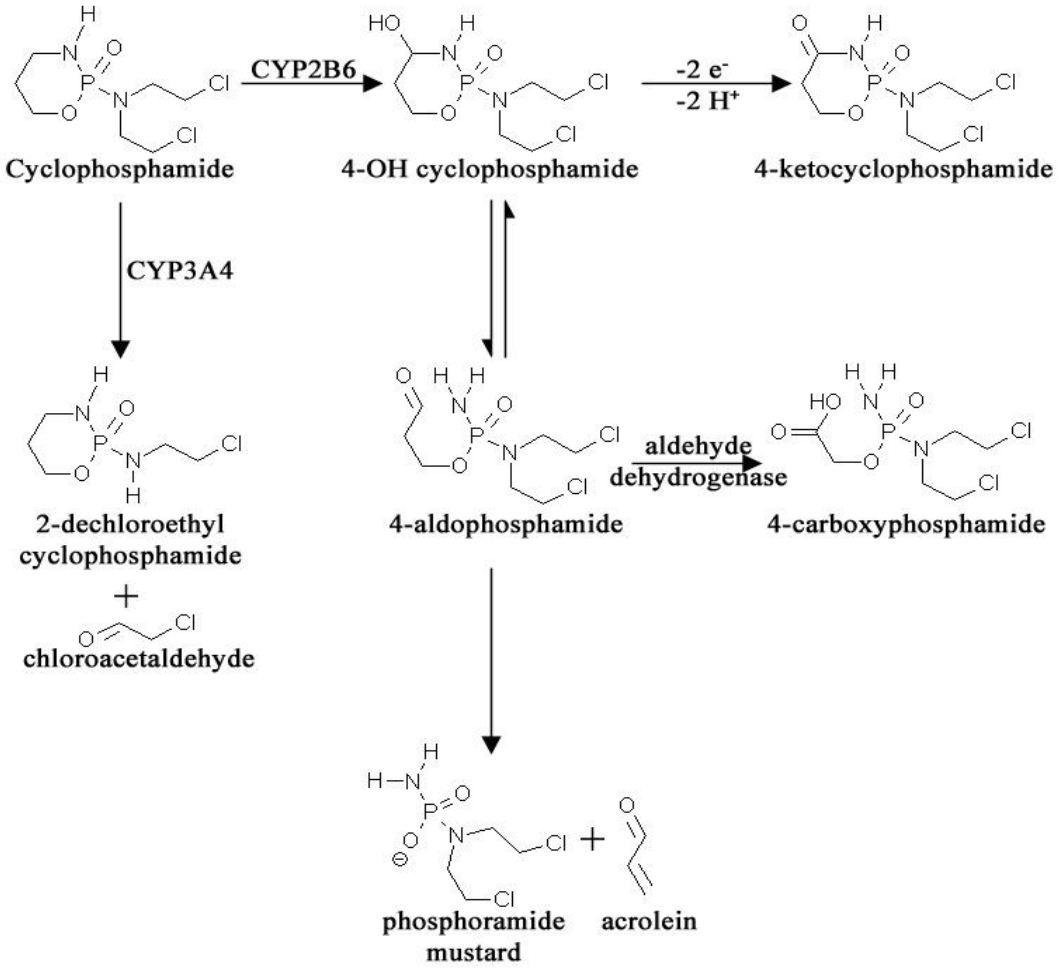

Figure 8. Metabolism of cyclophosphamide

Tautomerization of the 4-OH metabolite gives 4-aldophosphamide; the ring opens, and allows for the loss of acrolein via a reverse Michael addition, thus, liberating the PM (figure 8). In losing acrolein, the oxygen to which it was attached becomes negatively charged at physiologic pH (pKa 4.5-4.8; Zhang *et al.*, 2006). This charge not only prevents the crossing of biological membranes, it increases the nucleophilicity of the nitrogen in the mustard group, allowing it to form an aziridinium ion (figure 9).

However, two enzymatic detoxication reactions can occur following the formation of the 4-OH metabolite: further oxidation by P450s to yield 4-ketocyclophosphamide, and the production of carboxyphosphamide, from 4-aldophosphamide, by aldehyde dehydrogenases (Ren *et al.*, 1998). These two metabolites account for the majority of urinary excretion products of the respective oxazaphosphorine. The 4-OH metabolite circulates through the body, primarily via the erythrocyte fraction (58%), and not the PM (Watson *et al.*, 1985, Kerbusch *et al.*, 2001). The PM itself is quite stable however, attributed in part to the regenerating effects of chloride ions at physiologic concentrations (~100 mM). Essentially, chloride ion acts to restore the chloroethyl chain by reacting with the aziridinium ion, increasing the PM half-life; this was shown experimentally using deuterium labelled PM (Figure 9; Watson *et al.*, 1985). Toxicity of CP is typically elicited via nucleophilic attack of the PM, specifically the aziridinium ion, on the N7 position of guanosine, cross-linking DNA strands, and preventing replication enzymes from functioning. With enough CP adducts, cell death occurs by apoptosis.

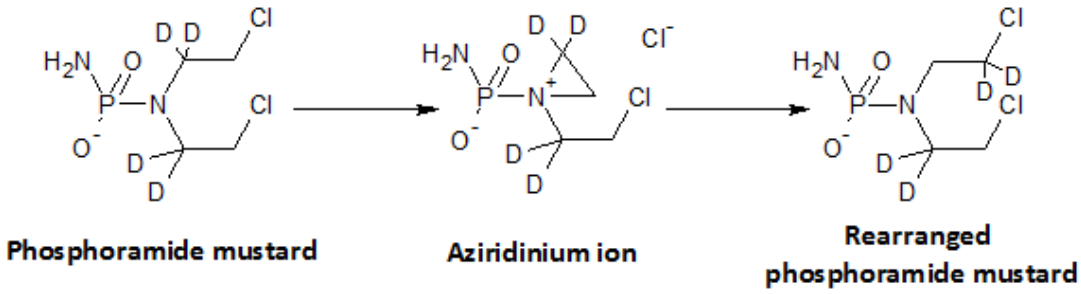

Figure 9. Stabilizing effects of chloride ions on the reactivity of the phosphoramide mustard (Watson *et al.*, 1985)

While much work has been done attempting to quantify cyclophosphamide and metabolites using electrochemical detection, there exists a dearth of information regarding its prolonged electrolysis. Only one paper could be found regarding prolonged electrolyses of cyclophosphamide. Paci *et al.* (2001) reported that both CP and IFF could be oxidized to their respective 4-MeO compounds upon electrolysis in methanol at graphite. When compared against the cytotoxicity of the respective oxazaphosphorines, a ten-fold increase in toxicity was found for the MeO compounds (IC_{50} 20 vs 200 µM); in-

line with the IC_{50}s of the 4-OH compounds (10-20 μM; Takamizawa *et al.*, 1975). Our hypothesis is that a parallel 4-hydroxylation will occur under similar conditions in aqueous solution, a trial which was not performed by Paci *et al*. If so, electrolysis could be used to mimic the P-450-catalyzed bioactivation of cyclophosphamide, consistent with the overall aim of this thesis. As discussed in Section 1.4, consideration must be given to the nature of the oxidation process at different anodes. Once again, the most appropriate anode would be a chemically active one, such as Ti/RuO_2 or graphite, the latter of which was used by Paci *et al.* (2001).

3.2 Acetaminophen

Acetaminophen, or paracetamol (AP), was first synthesized in 1887 as an attempt to decrease the toxicity of aniline-derived analgesics in use at the time. However, its widespread use did not occur until the 1950s, due in part to the dominance of aspirin and incorrect initial findings (Bertolini *et al.*, 2007). Upon initial toxicity testing, acetaminophen was believed to cause methemoglobinemia; a condition where hemoglobin fails to deliver oxygen to tissues. This result was believed to be due to an impurity of *p*-nitrophenol in the sample used for testing. In fact, a major analytical issue in acetaminophen manufacturing is measuring levels of *p*-nitrophenol. These initial findings were not followed up until the 1940s when they were disproven (Lester and Greenberg, 1947). Despite its prevalent use in society, the mechanisms of AP's analgesic and anti-pyretic effects have yet to be fully elucidated; AP's toxicological mechanisms, however, are fairly well understood. Acetaminophen is metabolized to several pharmacologically active forms including N-acetyl-*p*-benzoquinonimine (NAPQI), *p*-benzoquinone (BQ), *p*-aminophenol and *N*-(4-hydroxyphenyl)-arachidonoylethanolamide (AM404; see later).

AM404 (figure 10) is an important mediator of AP's analgesic and anti-pyretic effects, acting as an inhibitor of transient receptor potential vanilloid 1 ($TRPV_1$) cation channels, cyclooxygenase 2 (COX2), and anandamide transport. $TRPV_1$ is part of a thermoregulatory cascade that induces hypothermia upon activation (Rawls et al., 2006;

Gavva *et al.*, 2008). By binding to $TRPV_1$, AM404 stimulates this pathway, causing body temperature to drop (Rawls *et al.*, 2006; Gavva *et al.*, 2008). Fever reduction is also caused by the inhibition of prostaglandin synthesis. In the context of AP pharmacology, COX2 enzymes produce prostaglandins: a class of lipid molecules which regulate body temperature, amongst other functions. Prostaglandins are synthesized from arachidonic acid, the fatty acid used in AM404 synthesis; they positively affect body temperature regulation in the hypothalamus, i.e., more prostaglandins, higher body temperature (Lin, 1978). AM404 is synthesized in the central nervous system through a deacetylation of acetaminophen to *p*-aminophenol, followed by enzymatic conjugation with arachidonic acid by fatty acid amide hydrolase (FAAH; Hogestatt *et al.*, 2005; Hwang *et al.*, 2007). By inhibiting COX2 prostaglandin synthesis, AM404 indirectly causes body temperature to decrease, reducing fever (Hogestatt *et al.*, 2005; Hinz et al., 2008).

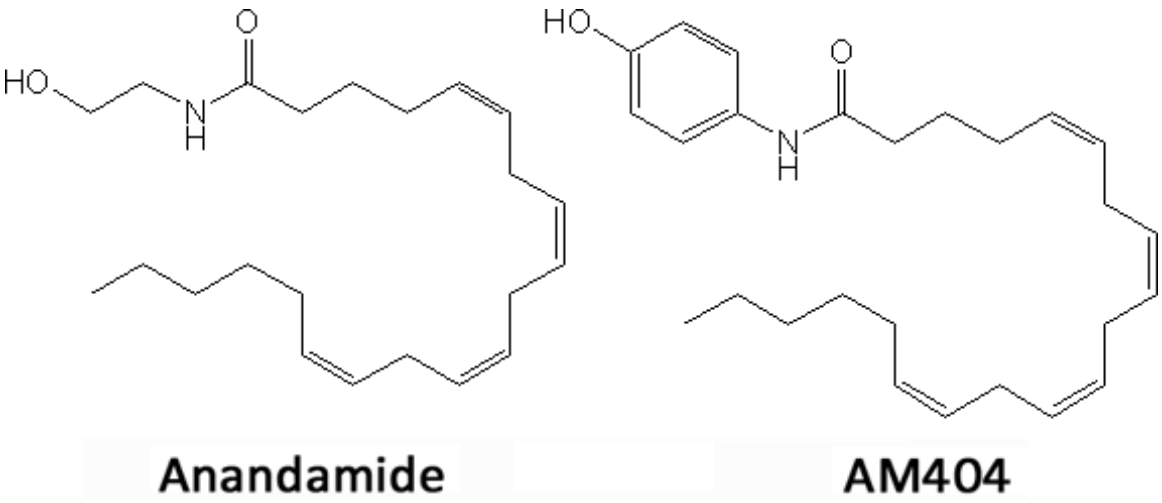

Figure 10. Endogenous cannabinoid receptor agonist anandamide and the analogous acetaminophen metabolite, AM404

In the early 1990s, advances in understanding the analgesic effects of AP came about when the endogenous cannabinoid (CB) receptor agonist anandamide was discovered (figure 10; Devane *et al.*, 1992). By activating CB1 and CB2 receptors in central nervous system synapses, anandamide suppresses the transmission of pain stimuli form peripheral nerves; it is degraded by FAAH in the neuron (Bracey *et al.*,

2002). The AP metabolite AM404 inhibits the removal of anandamide from the synaptic cleft, resulting in an increase in CB receptor activation. Transportation inhibition is the contending theory for AM404's role in analgesia; however, it is unknown, at this time, what specific transporter, if any, AM404 is inhibiting. Supporting evidence for transport inhibition has shown that neither direct activation of CB receptors or inhibition of FAAH occurs via AM404 (Ottani *et al.*, 2006; Fegley et al., 2004). What is known, is that the accumulation of anandamide in the synapse is partially responsible for the analgesic effects of acetaminophen. Only recently, Andersson *et al.* (2011) have provided evidence that the electrophilic metabolites, NAPQI and BQ, are directly capable of analgesia. This effect was found to be mediated by interaction of these compounds with transient receptor potential A1 (TRPA1) cation channels. Intrathecal administration of NAPQI and BQ produced analgesia that was not observed in TRPA1 knockout mice (Andersson *et al.*, 2011). It is not known to what extent analgesia is dependent on AM404 or TRPA1 mediated pathways. Acetaminophen's pharmacological effects are derived from its metabolites AM404, NAPQI, and BQ.

The beneficial effects of acetaminophen are exhibited in the brain and nervous system, but the toxic effects of this compound are observed at the source of its metabolism, the liver. The majority of acetaminophen absorbed in a given dose is conjugated with glucuronic acid, or sulfate, and excreted in the urine (figure 11; Gregus *et al.,* 1988). The remaining 15-20% of AP is competitively oxidized by CYP 2E1 and 1A2 into NAPQI; only a minor fraction is metabolised into AM404 (Gregus *et al.*, 1988; Anundi *et al*., 1993). The majority of NAPQI is conjugated with glutathione (GSH), although, conjugation with glucuronic acid and sulphate is known to occur; excretion occurs via the urine for all of the conjugation products mentioned (Gregus *et al.*, 1988). Acetaminophen toxicity occurs once a majority of available glutathione has been consumed by NAPQI.

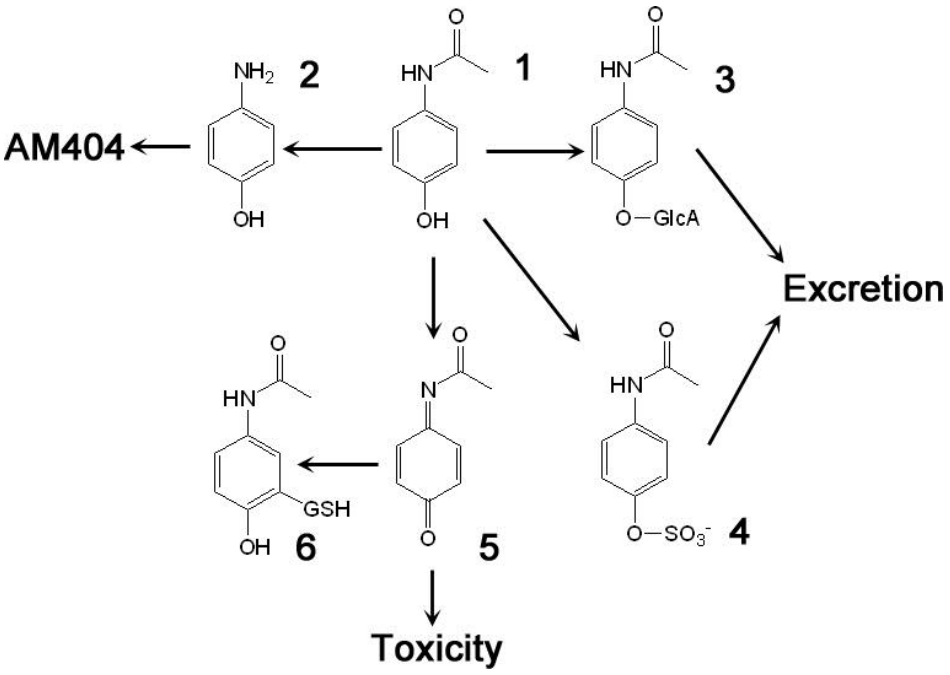

Figure 11. Metabolic fates of acetaminophen. Acetaminophen (1) can undergo deacetylation to form *p*-aminophenol (2) which is required for AM404 synthesis. Conjugation reactions with glucuronic acid (3) and sulphate (4) are responsible for producing acetaminophen's primary excretion products. P450 oxidation produces the reactive electrophile NAPQI (5), which reacts with glutathione (GSH) to yield 3-(glutathion-S-yl)acetaminophen (6) or with proteins to yield toxicity.

Glutathione (GSH) serves as a protective agent against reactive electrophiles generated normally during metabolism. By exhausting GSH levels, peptide nucleophilic sites (NH_2, OH, and SH groups) are left exposed to modification by NAPQI (or other cellular electrophiles). Covalent modification of a protein can render it non-functional, this occurs due to conformational changes brought on by the interaction of the new adducts or blockage of the active site (Bond, 2009). If the cell cannot restore GSH levels, or replace defective proteins in a timely manner, it dies via apoptotic mechanisms; although necrosis is known to occur due to lipid peroxidation (see later; Ghavam Baigi *et al.*, 2007). Although NAPQI readily hydrolyzes into benzoquinone (figure 12D), benzoquinone adducts are not typically thought of in the context of AP metabolism, despite benzoquinone being known to form adducts *in vivo* and *in vitro* (Ghavam Baigi *et*

al., 2007). The absence of benzoquinone is likely do to the hydrophobic microenvironment of the endoplasmic reticulum (ER) where P450 enzymes reside (Bond, 2009). NAPQI protein adducts that are seen can be found primarily on enzymes that reside in the ER (Bond, 2009). Thus, the high reactivity of NAPQI towards nucleophilies, their prevalence in the cell, and a hydrophobic micro environment, out-competes hydrolysis to benzoquinone.

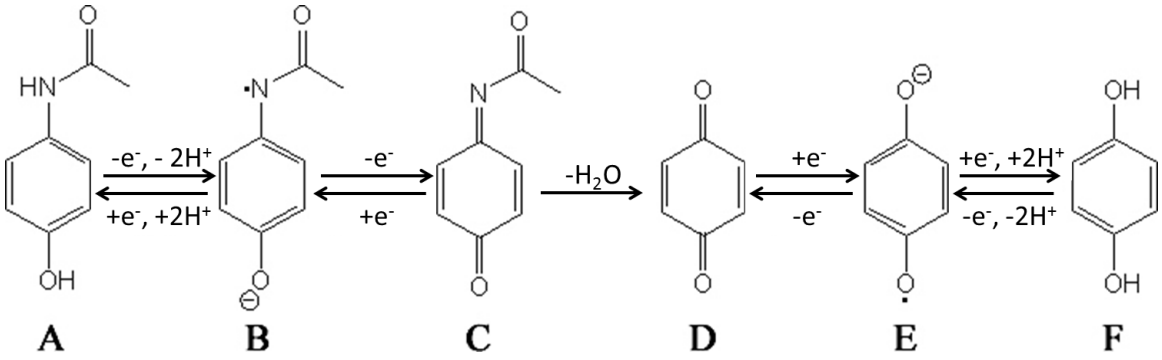

Figure 12. Acetaminophen redox chemistry. A: acetaminophen; B: N-acetyl-*p*-benzosemiquinonimine radical ($NAPQI^{-\bullet}$); C: N-acetyl-*p*-benzoquinonimine (NAPQI); D: benzoquinone (BQ); E: semi-quinone radical; F: hydroquinone

Few studies have been done using NAPQI as a direct toxicant because of its reactivity. As such, the toxicity of NAPQI outside the liver is not well documented; one of the few studies examining this, injected freshly synthesized NAPQI into mice. The authors observed widespread blood coagulation after intraperitoneal injection, and deemed it as the cause of death, i.e., widespread protein denaturation (Dahlin *et al.*, 1982). These results were in agreement with the effects seen when injecting benzoquinone (Ghavam Baigi *et al.*, 2007). A significant factor in determining AP toxicity is alcohol consumption, both in binge drinking and chronic consumption scenarios. Toxicity is potentiated by two factors: induction of CYP 2E1 levels by ethanol, and GSH depletion by poor nutrition (Schmidt *et al.*, 2002).

In addition to protein damage, lipid peroxidation is another form of cellular insult resulting from AP metabolism. Acetaminophen, NAPQI, benzoquinone, and *p*-

nitrophenol are all capable of redox cycling (figure 12). By reducing NAPQI or oxidizing AP via one electron, the semi-quinonimine radical ($NAPQI^{-\bullet}$) is generated, a minor but arguably more potent molecule (figure 12B; Yin *et al.*, 2011). Radicals cause non-specific damage by extracting hydrogen atoms or single electrons from substrates, which, in turn, makes the substrate a radical species. This chain reaction perpetuates until two radicals combine and the reaction is terminated. Lipid peroxidation is a process known to degrade biological membranes, and is known to be caused by acetaminophen metabolites (figure 13). Significant lipid peroxidation eventually leads to the loss of membrane integrity, resulting in cell death via necrosis (Yin *et al.*, 2011). The 'digestion' of polyunsaturated fatty acids in the membrane causes a loss of membrane integrity, and the cell lyses. The 3-carbon molecule, malondialdehyde, is a major product of lipid peroxidation, and is a known carcinogen and alkylating agent (figure 13-7; Marnett, 1999).

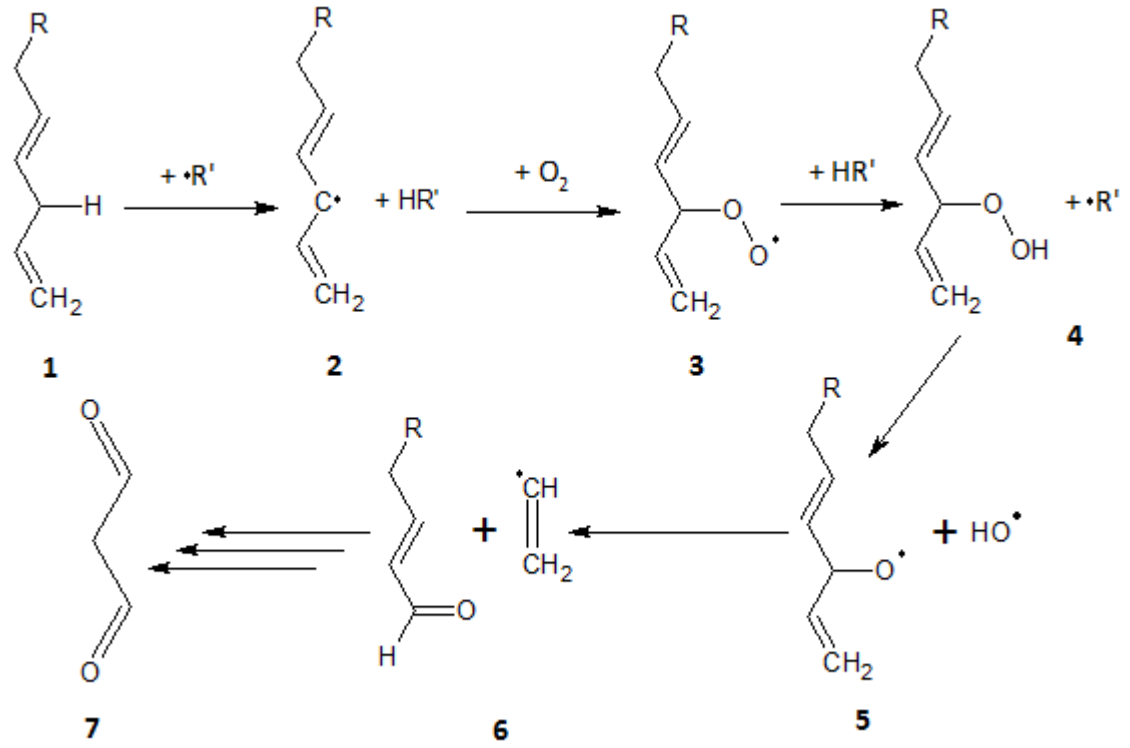

Figure 13. General mechanism of lipid peroxidation (LP). Radical initiation of polyunsaturated fatty acid (PUFA; 1-2); formation of lipid peroxide radical (2-3); formation (3-4) and decomposition (4-5) of lipid peroxide; formation of lipid aldehyde (5-6); lipid aldehydes undergo additional rounds of reaction, fragmenting, and forming malondialdehyde (6-7).

There have been many studies on the electrochemical relationship between acetaminophen and its mechanism of toxicity, the majority of which have been done with active anodes. Initially undertaken to elucidate the mechanism of AP toxicity, this work was performed by potentiostatic oxidation of AP in the presence of GSH (Miner and Kissinger, 1979). Typical experiments involved the use of graphite anodes in on-line liquid chromatography-electrochemical detection systems with amperostatic detectors. These experiments provided clear evidence of AP oxidation, and the reduction of NAPQI, independent of water oxidation (Miner and Kissinger, 1979). When GSH was present, the reduction of AP was no longer visible, indicating that AP was no longer able to redox

cycle; the GSH had reacted with NAPQI produced through oxidation, i.e., NAPQI was 'detoxified'. These products were then later characterized by mass spectrometry and correlated to *in vivo* results (Lohmann and Karst, 2006).

In the field of electrochemistry, acetaminophen is a favourite compound for study because of its ease of use and consistent results amongst various anodes. It is often used as a model compound when investigating novel anode materials; nanoparticle and metal composite, or metal oxide-based electrodes are currently of particular research interest (Razmi *et al.*, 2010; Alothman *et al.*, 2010; Ghoreishi *et al.*, 2010). In addition to using acetaminophen as an electrochemical standard, a more practical use of the compound is in the development of biological sensors. Acetaminophen overdose is the leading cause of acute liver failure, and is the most common drug used in suicide attempts in developed nations (Larson *et al.*, 2005). In a concept akin to glucose blood monitors, there is a great deal of research into the development of electrochemical probes which can detect circulating acetaminophen in cases of overdose (Manjunatha *et al.*, 2011). Being able to quantify the extent of the dose *in situ* can help medical professionals administer treatment, a precursor to GSH known as N-acetyl-cysteine. Additional work in AP research has been in the synthesis of non-toxic analogues which retain analgesic and antipyretic properties (Vaccarino *et al.*, 2007).

The majority of mechanistic work on AP electrochemistry does not involve long electrolysis times as the short-lived NAPQI quickly converts into other products, primarily benzoquinone (Dahlin and Nelson, 1982; Neamtollahi *et al.*, 2009). As the hydrolysis product of NAPQI, BQ shares the same basic mechanisms of toxicity, as both are oxidizing agents as well as reactive electrophiles (Monks and Jones, 2002). While NAPQI is most stable at physiologic pHs (6.5-7.5), dimerization is most prevalent in this pH range *in vitro*; hydroxylation is favoured in basic conditions; and hydrolysis in acidic ones (Neamtollahi *et al.*, 2009). By using anodic oxidation and a divided cell, the production of benzoquinone is expected to be favoured. With this in mind, practical yields of NAPQI may not be attainable through electrolytic means. Even though NAPQI

hydrolysis is rapid, electrolysed solutions of acetaminophen are expected to retain toxicity because of the presence of benzoquinone.

3.3 Summary

Model compounds, cyclophosphamide and acetaminophen, were selected because they are both well studied cases of oxidatively bioactivated toxicants, with documented electrochemical oxidations. Cyclophosphamide is an example of a chemotherapeutic agent that interferes with DNA replication, whereas acetaminophen has been chosen to represent a toxicant which does not target mitosis as a mechanism of action.

Chapter Four: Materials and Methods

4.1 Materials

4.1.1 Chemicals and Other Reagents

All chemicals listed are of at least 99% purity. Acetaminophen (N-(4-hydroxyphenyl)ethanamide), 1,4-benzoquinone, cyclophosphamide (*N*,*N*-bis(2-chloroethyl)-1,3,2-oxazaphosphinan-2-amine-2-oxide), dithiodiethylcarbamate (sodium (diethylcarbamothioyl)sulfanide), silver (I) oxide, sodium sulfate, sodium perchlorate, ammonium acetate, trypan blue dye and grade 60 silica gel were supplied by Sigma-Aldrich (St Louis, MO). Monobasic sodium phosphate, sodium hydroxide, ethanol, HPLC grade methanol, acetone, methylene dichloride, hydrochloric acid, sodium citrate, ethyl ether, chloroform, trypsin (1X, 0.25%), Dulbecco's modified Eagle's medium, TRIS (2-amino-2-hydroxymethyl-propane-1,3-diol), fetal bovine serum, and alumina-silicate molecular sieves (4 Å) were supplied by Fisher Scientific (Fair Lawn, NJ). Penicillin/streptomycin (100X) and phosphate buffered saline solutions (1X, pH 7.4) were obtained from Invitrogen (Grand Island, NY). CellTiter 96® AQ_{ueous} One Solution Cell Proliferation Assay (MTS assay) was obtained from Promega (Madison, WI). HPLC grade acetonitrile was purchased from Caledon Laboratories (Georgetown, ON). ''Ultra'' bleach (6%) was purchased from No-Frills (Guelph, ON), a subsidiary of Loblaws Inc., (Toronto, ON). Activated carbon was obtained from Calgon Carbon Corporation (Pittsburgh, PA). All solutions were prepared using a Millipore Milli-Q Reagent Water System with water having resistivity of approximately 18.2 MΩ cm. EMT-6 cells (passage: 13) were a gift from Dr. Alicia Viloria-Petit, Department of Biomedical Sciences, University of Guelph (Guelph, ON).

4.1.2 Batch Cell Electrolysis

A 1.5 x 5.0 cm boron-doped diamond (Si/BDD) anode and BDD MDA5–150/106 microelectrode array was obtained from the Swiss Center for Electronics and Microtechnology Inc., (Neuchatel, Switzerland). A 1.0 mm diameter titanium wire served

as the cathode (Chemistry Department machine shop, University of Guelph). The Ti/RuO_2 (1.5 x 5.0 cm) and graphite (d = 1.5 cm) anodes were purchased from De Nora Tech., (Painsville, OH) and Fisher (St Louis, MO), respectively. A saturated calomel reference (SCE) electrode was purchased from Fisher (Toronto, ON). Solutions were stirred during electrolysis using a Thermix stirrer (Fisher Scientific Model 120 MR). Voltage, electrode potential, and current were monitored using either a Wavetek DM5XL Voltmeter or Mastercraft 052–0060–2 multimeter. Power to the electrochemical reactor was supplied by an EG&G Model 363 potentiostat/galvanostat. Cyclic voltammetric data were obtained using an EG&G Model 273 potentiostat/galvanostat controlled using Power Suite software (version 2.12.1); a fixed sweep rate of 50 mV s^{-1} was used. A 100 ml Pyrex beaker served as a batch cell and was obtained from Fisher Scientific (Fair Lawn, NJ).

4.1.3 HPLC

Electrolyses were followed by HPLC using a Waters 600E pump system equipped with a Waters 2487 dual λ absorbance detector with a silica pre-column guard. Samples were manually injected into the 20 µl sample loop of a Rheodyne injector. Acetaminophen-based experiments used a reversed phase Inertsil Sulfa C_{18} column (150 x 4.6 mm; 5 µm particle size; GL Sciences, Inc.). Experiments concerning cyclophosphamide employed a Waters reverse phase C_{18} µBondapack column (300 x 3.9 mm; 10µm particle size). Chromatographic analysis was performed with Millenium[32] Chromatography Manager software from Waters (Milford, MA). Concentrations of acetaminophen are presented as a percentage relative to the starting concentration for solutions under 1 mM; i.e., 50% of the absorbance value equals 0.5 mM in a 1 mM solution.

4.1.4 Flow Cell Electrolysis

Plexiglas used in the construction of the flow cell was obtained from the chemistry department machine shop (University of Guelph). The flow cell was divided using a 1.0 ml Spectra/Por® Float-A-Lyzer® G2 (0.1-0.5 kDa) dialysis membrane from Spectrum

Laboratories (Rancho Dominguez, CA); the dialysis membrane consists of a proprietary cellulose ester. A 10.0 ml Luer-lok™ syringe and 26 G needle from Becton Dickson and Company (Franklin Lanes, NJ) were also used in the construction of the flow cell. The graphite anode used in the flow cell was machined down from a diameter of 1.5 cm to 0.4 cm. The Ti/RuO_2 anode used in the flow cell was cut from a larger 1.5 x 5.0 cm anode to a dimension of 0.4 x 5.0 cm. Unelectrolyzed solution was provided to the flow cell by a Masterflex C/L peristaltic pump with adjustable flow.

4.1.5 Cell culture

Sterile 100 x 15 mm polystyrene Petri dishes used for cell culture were obtained from Fisher Scientific (Fair Lawn, NJ). 96 well polystyrene tissue culture plates and 15 ml centrifuge tubes were obtained from Celltreat Scientific Products (Shirley, MA). Cytotoxicity experiments were analyzed using a Bio-Tek µQuant 96-well plate analyzer.

4.2 Methods

4.2.1 Batch Cell Electrolyses

Batch cell electrolyses were carried out in a clean 100 ml Pyrex beaker with a solution volume of 50 ml. The cell was divided with a porous ceramic frit fitted inside a glass tube. A titanium wire served as the cathode. The anode consisted of either a Ti/RuO_2 or graphite anode with submerged areas of 3.75 cm^2 and approximately 6.13 cm^2, respectively. Each solution was prepared fresh before each experiment in a 50 ml volumetric flask with mQ water, 25 mM sodium sulfate, and 1.0 or 5.0 mM of either acetaminophen or cyclophosphamide. A solution of 25 mM sodium sulfate served as electrolyte to the cathodic compartment of the cell. Potentiostatic electrolyses used a saturated calomel reference electrode in the anodic compartment of the cell, and a multimeter was used to monitor anodic potential at 1.00 V vs SCE. Cell potential was not monitored during amperostatic electrolyses. Cyclophosphamide experiments were carried out for 90 minutes with samples collected at 30 minute intervals. Cyclophosphamide samples were taken as 1 ml aliquots to which 100 µL of 1.0 mg/ml

dithiodiethylcarbamate (DDTC) was immediately added; 1 dram glass vials were used. The sample was lightly agitated by vortex, and placed in a 70 ^{o}C water bath for 30 minutes, after which the sample was cooled in a room temperature water bath for 10 minutes and injected into the HPLC. Time zero samples were prepared in this manner, but not subjected to electrolysis. Materials or solutions which came into contact with cyclophosphamide were exposed to 6% hypochlorite to destroy the compound prior to disposal; materials were then washed in deionized water (Hansel *et al.*, 1997). After each experiment anodes were visually inspected for polymeric deposition and cleaned with either ethanol or acetone.

4.2.2 Batch Cell Electrolyses - Buffers

Monobasic sodium phosphate, phosphate buffered saline, sodium citrate, and 2-amino-2-hydroxymethyl-propane-1,3-diol (TRIS) buffers were made to pH 7.0-7.4 at ionic strength of 100 mM. These solutions were then electrolyzed at 20 mA in a divided batch cell and changes in pH were measured by pH meter. The experiment was then repeated with buffered 1 mM acetaminophen and monitored by HPLC. 25 mM sodium sulfate was added as a supporting electrolyte where needed for conductivity purposes. Culture media was electrolyzed in fashion, and subsequently checked for sterility by plating cells according to Section 4.2.5.2 protocol.

4.2.3 HPLC Method

The HPLC method for acetaminophen-based experiments consisted of an isocratic mobile phase of 30:70 acetonitrile-water, at a flow rate of 1.0 ml/min; absorbance was read at 254 nm. A modified gradient-elution HPLC method by Cummings *et al.* (1991) was employed as the mobile phase. Solvent A consisted of 100% acetonitrile and solvent B consisted of mQ water; the gradient at time zero was 30:70 A:B and remained constant for 5 minutes. A linear increase to 100% solvent A by 10 minutes was followed by a decrease of A by 15 min to the original 30%; a full run lasted 30 min. Flow rate was also 1.0 ml/min and absorbance was read at 275 nm.

4.2.4 Synthesis of N-Acetyl-p-benzoquinonimine

N-Acetyl-*p*-benzoquinonimine (NAPQI) synthesis was conducted according to Dahlin and Nelson (1984). Solvents used were dried with 1 g of flame activated molecular sieves (4 Å) which were added to 250 ml of solvent. 1.0 g of acetaminophen was added to 50 ml of dried chloroform containing 1.10 g of silver (I) oxide. The mixture was stirred and the reaction was allowed to proceed at room temperature for 45 min. in a covered 100 ml beaker shielded from light. Approximately 1.0 g of activated carbon was then added and the mixture was filtered through a funnel fitted with a ceramic frit into a flask containing 0.5 mg of sodium citrate as a radical scavenger. The funnel was then rinsed with 2 ml of unused chloroform. The filtrate was then concentrated to a final volume of approximately 2-5 ml via rotary evaporation and purified by flash chromatography. The flash chromatography column (3.6 x 15 cm) was constructed with dried silica gel and anhydrous ethyl ether; the silica gel was dried at 102 ^{o}C for 24 hours before use. The crude NAQPI solution was eluted through the column with anhydrous ethyl ether and effluent was collected in 1 ml fractions. Fractions containing NAPQI were identified by HPLC, pooled and stored for up to 3 days under ether at 4 ^{o}C.

4.2.5 Cell Culture

NB: All solutions mentioned in this section regarding cell culture were stored at 4^{o} C and were only used once warmed to room temperature.

4.2.5.1 Thawing Cells from Liquid Nitrogen

EMT-6 cell cultures were maintained in a stock growth medium (SGM) containing 10% v/v fetal bovine serum (FBS), 1% v/v penicillin-streptomycin (100x) and 89% v/v Dulbecco's modified Eagle's Medium (DMEM). Cells were recovered from liquid nitrogen storage by placing them on dry ice for 15-20 min; during this time a culture dish was prepared with 19.0 ml SGM plus 1.0 ml FBS (15% FBS total). The still frozen vial of cells was then quickly warmed under hot running water and immediately introduced into the

culture dish as soon as thawed. The media was gently swirled to ensure even distribution of the cells, and then incubated for 24 hours at 37 ^{o}C and 5% atmospheric CO_2 in a humidified incubator.. The cells were then rinsed with 5.0 ml phosphate buffered saline (PBS) and 10.0 ml fresh SGM was introduced followed by an additional 24 hour incubation.

4.2.5.2 Cell Passage

Once cells reached confluency (approximately 48 hours) the SGM was aspirated and plated cells were rinsed with 5.0 ml PBS. Next, 1.0 ml typsin (0.25%) was added and cells were incubated for 5 minutes; an additional 1.0 ml trypsin was added if required. Cell disaggregation was facilitated with gentle agitation from a 1000 µl pipette if required. During this time, a new culture dish was labeled and prepared by incubating 10.0 ml SGM. The trypsinized cells were then transferred to a 15.0 ml centrifuge tube and the culture dish was rinsed twice with 3.0 ml SGM; which was also added to the centrifuge tube. Cells were centrifuged for 5 minutes at room temperature, the supernatant was discarded, and the pellet was re-suspended in 10.0 ml supplemented assay medium (SAM): SGM with 1% v/v FBS instead of 10%. Finally, a 1.0 ml aliquot was plated into a newculture dish to maintain a colony.

4.2.5.3 Plating Cells for Assay

From the 10.0 ml SAM suspension, a 50.0 µl aliquot was combined in a 1:1 ratio with trypan blue dye. A 10.0 µl aliquot of the cell-dye suspension was then placed onto a Neubauer hemocytometer, and cells with intact membranes (i.e., which excluded the trypan blue dye) were counted. Only cell suspensions with 95% or higher cell viability, as shown by trypan blue exclusion, were used for subsequent assay. Cells were tallied in four different 100 nl sized grids and then averaged (figure 14). After correcting for the initial dilution, this average represents the number of cells x 10^4 ml^{-1}; all of the cells contained in an aggregate were counted. An aliquot of the 10.0 ml SAM suspension was then taken and diluted to 10.0 ml with fresh SAM, so that a 100.0 µl aliquot of the diluted

suspension would contain 5000 cells. This diluted suspension was then plated into a 96-well plate and the cells were left to incubate overnight. Cells were visually (i.e., microscopically) inspected for uniform distribution as well as viability.

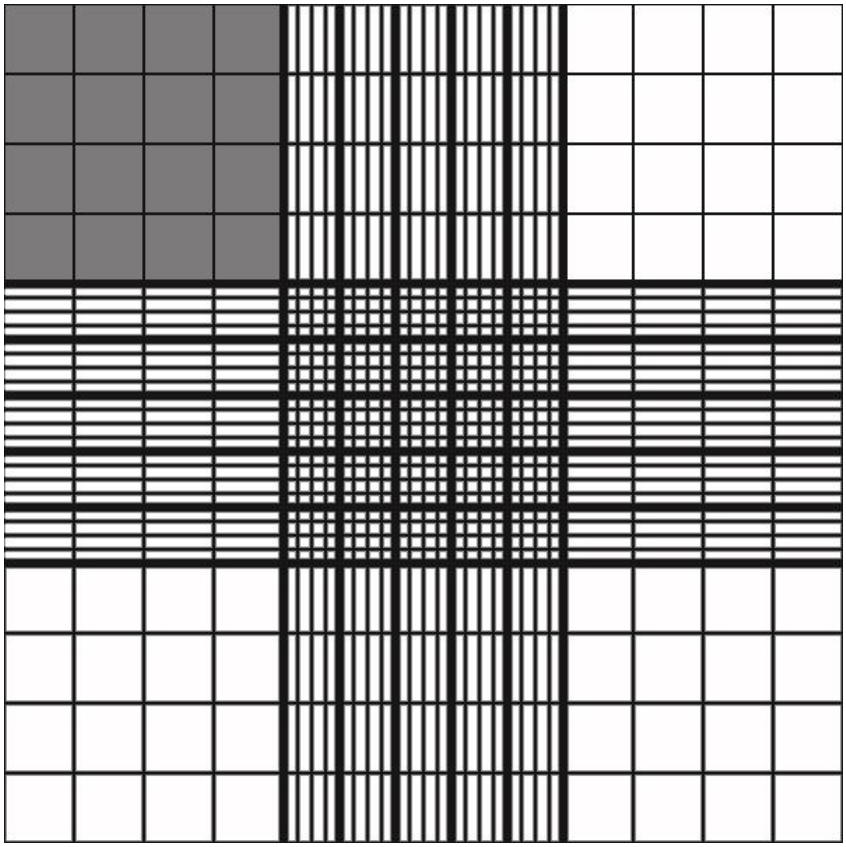

Figure 14. Hemocytometer Grid. At a depth of 0.1 mm the highlighted area corresponds to a volume of 100 nl.

4.2.6 MTS Viability Assay

The toxicity of a solution was assessed by introducing 50.0 µl of solution to a well containing 5000 cells and incubating for 24 hours; 50.0 µl mQ water served as the control treatment in all toxicity experiments. 20.0 µl MTS reagent was added to each well of the 96-well plate and incubated at 37 ^{o}C for 2 hours; absorbance was then read at 490 nm using a 96-well plate reader. All treatments and controls were performed in triplicate.

4.2.7 Statistical Analysis

Statistical analysis of batch and flow cell toxicity assays were performed using a Student's t-test. Analysis was done by assessing homogeneity of the data as an average of non-toxic results (across experiments) versus the individual toxic response (equation 1).

$$T_{value} = \frac{|\text{average non-toxic responses across treatments} - \text{toxic response}|\ \sqrt{n}}{\text{Standard deviation of non-toxic responses}} \quad (1)$$

Where n = number of data points included in the average. If $T_{value} > T_{0.95}$ ($T_{0.95}$ = 2.447 for 6 degrees of freedom (d.f.), where d.f. = n-1) then the null hypothesis of non-significance was rejected, and the toxic response is statistically significantly at 95% confidence.

4.2.8 Probit Analysis

Toxicity data obtained were expressed as a percentage of viability relative to naive controls (50.0 µl mQ water), and probit curves were subsequently constructed from these data where applicable. To construct the probit curve, the percent response of treated cells were transformed into a probit by using the "=NORMINV()" function in Microsoft Excel 2010. This function returns the inverse of the normal distribution of a probability for a specified mean and standard deviation, for which 5 is the value of the mean and 1 is the value of the standard deviation (i.e., a probit). For example, a probability of 0.50 or 50% response of cell viability would correspond to a probit value of 5.00. Calculated probit values were then plotted against their respective log transformed concentrations and lethal concentrations were calculated from the slope of the regression line.

4.2.9 Electrolysis Cytotoxicity

To investigate the toxicity of electrolyzed solutions, the same experimental conditions used in the electrochemical experiments were employed (see Section 4.2.1). After a set amount of electrolysis time had passed, a 1.0 ml aliquot was taken from the batch cell

and used to dose EMT-6 cells according to procedures previously outlined for cytotoxicity (see Section 4.2.6). Solutions of electrolyzed and non-electrolyzed 25 mM sodium sulfate were included as controls. There was no derivatization step for solutions containing cyclophosphamide.

4.2.10 Flow Cell Construction and Characterization

The flow cell used in experiments was modified from a design by Miner and Kissinger (1979). A Plexiglas cell was constructed by Case Gielen of the Chemistry Department machine shop (University of Guelph) by gluing each panel with methylene chloride. Internal dimensions consisted of 3.0 x 3.6 x 4.7 cm and a total capacity of 50.76 cm^3. A 1.0 ml Spectra/Por® Float-A-Lyzer® G2 was attached inside the cell in similar fashion and a 1.0 mm diameter hole was drilled through both the Float-A-Lyzer® and Plexiglas cell. A portion of a 10.0 ml syringe tip (0.5 ml) was next cut and attached to the bottom of the cell so that flow was possible if the Float-A-Lyzer® compartment was filled. A 26 gauge Luer-lok™ needle was then used as a means of controlling the cell's flow rate through restriction. A titanium wire was wrapped in a helical fashion around the Float-A-Lyzer® to serve as the cathode. A graphite rod or Ti/RuO_2 plate of (d = 4.0 mm) was used as the anode, and was inserted inside of the Float-A-Lyzer®. The cathodic compartment was filled before each experiment with 50 ml fresh 25 mM sodium sulfate. A peristaltic pump was used to provide influent of acetaminophen or cyclophosphamide solutions to the anodic compartment. Effluent samples were collected over a period consisting of 15 drops for HPLC analysis prior to reaching steady state. During potentiostatic electrolyses the saturated calomel reference electrode was inserted into the cathodic compartment. For effluent toxicity experiments, electrolyses proceeded for 1 hour and a 1.0 ml aliquot was collected. Toxicity was assed via the protocols outlined previously (see Section 4.2.6).

Chapter Five: Results and Discussion

5.1 Introduction

The main concept discussed in this thesis is the electrochemical activation of a prodrug. This concept is best exemplified with a compound that does not show cytotoxic effects before it is electrochemically activated. In order to assess the feasibility of this concept, several means of analysis have first to be established:

A means of:

1. identifying compounds produced by electrolysis.
2. identifying the most favourable conditions for electrolysis.
3. determining cytotoxicity.
4. quantifying the effectiveness of prodrug electrolysis on cancer cells.

Sections 5.2-5.4 will contain results and discussion of experiments leading to the establishment of protocols of analysis and quantitation.

5.2 NAPQI Synthesis

In order to be able to identify primary products of acetaminophen electrolysis, N-acetyl-*p*-quinonimine (NAPQI) was synthesized by oxidizing acetaminophen with silver (I) oxide (see Section 4.2.4). To prevent hydrolysis of the quinonimine, this reaction was carried out in anhydrous chloroform, in which acetaminophen is poorly soluble. After 45 minutes of reaction time, shielded from light, the colourless chloroform mixture had turned an intense, but slightly opaque yellow. Flash chromatographic purification of this product, with anhydrous ethyl ether, eluted a faint yellow band of NAPQI. This yellow product was identified via HPLC as a peak with a distinct retention time compared to acetaminophen or benzoquinone (figure 15). Attempts at sublimation of NAPQI were unsuccessful, as it was prone to forming polymeric resins on the glassware when the ether was removed. Purified samples could be left in ether for up to 3 days, covered at $4^{o}C$, before decomposition could be detected by HPLC, signified by an increase in benzoquinone. Under the HPLC conditions employed (see Section 4.2.3),

acetaminophen, benzoquinone, and NAPQI have respective retention times of approximately 2.50, 4.00, and 5.00 minutes (figure 15). No standard curve was constructed for NAPQI due to its instability, and its synthesis serves as a qualitative identification measure for electrolyses.

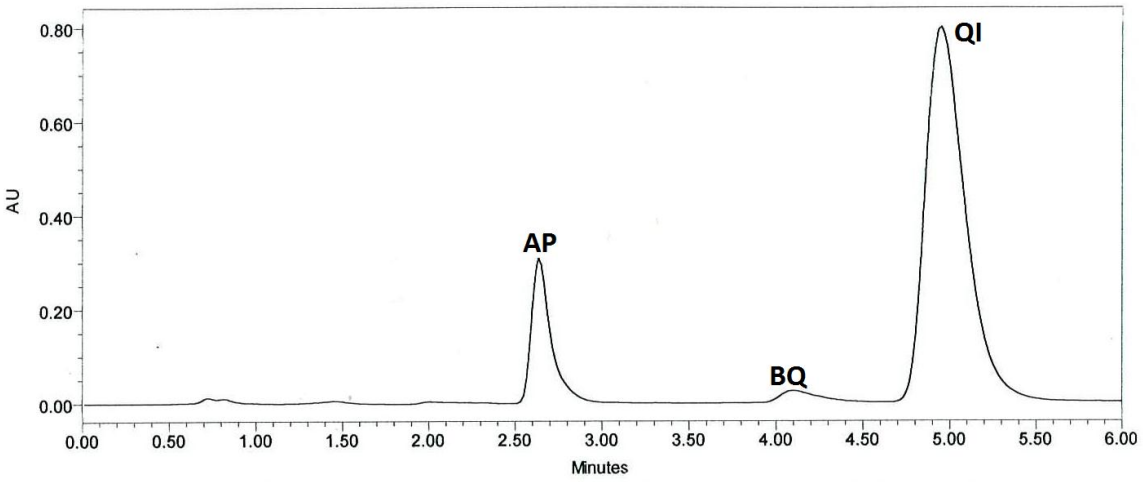

Figure 15. Reverse phase HPLC chromatogram of a mixture of purified acetaminophen, benzoquinone, and NAPQI in anhydrous ether. Acetaminophen (AP) and benzoquinone (BQ) were dissolved in a portion of ether containing purified NAPQI (QI). HPLC mobile phase was an isocratic mixture of 30:70 acetonitrile and water. Absorbance was read at 254 nm. Retention times were: AP: 2.50 min; BQ: 4.00 min; QI: 5.00 min.

5.3 Benzoquinone Calibration Curve

In order to quantify benzoquinone produced during electrolysis, a standard curve was constructed from solutions of a known concentration. Weighed amounts of BQ were dissolved in 25.0 ml of 25 mM Na_2SO_4, the conditions used during electrolysis. Concentrations of 0, 0.25, 0.5, 1.0, 2.5 and 5.0 mM were used. From the data, a line of $y= -2.08x10^6 x^2 + 1.94x10^7 x$ was obtained, with an $R^2 = 0.996$ (figure 16). By using Microsoft Excel to solve for x with experimentally obtained absorbance values (y), the experimental concentration of benzoquinone was obtained. Large concentrations were used so that electrolysed samples would not have to be corrected for dilution. The curvature of the graph (figure 16) is caused by a decrease in signal transmission.

Although detector saturation occurs above roughly 4 mM, electrolyses results remained under 2 mM concentrations.

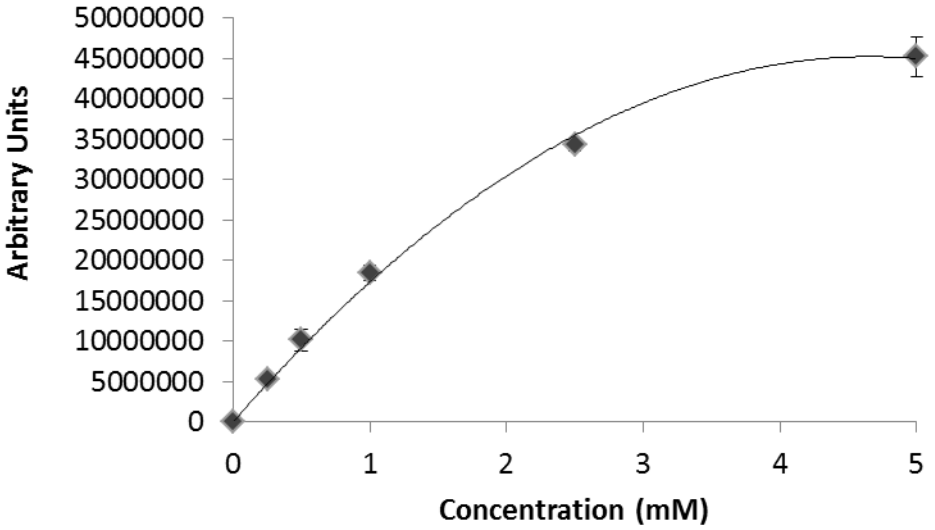

Figure 16. Benzoquinone calibration curve. Absorbance values were read at 254 nm by HPLC of 0.00, 0.25, 0.50, 1.00, 2.50 and 5.00 mM concentrations of benzoquinone. A trend line of $y= -2.08x10^{6}\ x^{2} + 1.94x10^{7}x$ was obtained with an $R^{2} = 0.996$. Results presented are averages of n = 3 data points.

5.4 Preliminary Experimentation

5.4.1 Electrolysis of Buffered Solutions

A series of amperostatic and potentiostatic electrolyses was conducted to determine buffer efficacy over the course of electrolysis. A divided batch cell was used with a titanium cathode and either a Ti/RuO_2 or graphite anode. A saturated calomel electrode served as a reference electrode for potentiostatic electrolyses. Sodium sulphate (25 mM) was dissolved in 50 ml of growth medium (phosphate buffered at pH 7.4). Acetaminophen was added to the growth medium to final concentrations of 1 or 5 mM, then separately electrolyzed for 30 minutes at both anodes. The pH of the solution dropped from 7.4 to approximately 6.0 during this time. This change in pH occurred at currents of 5, 10, and 20 mA (pH 6.8, 6.3, 5.5 respectively); a similar decrease in pH was

obtained potentiostatically at 1.0 V vs SCE at both anodes (Ti/RuO_2: 5.7, graphite: 6.8). The addition of 25 mM sodium sulfate as a supporting electrolyte did not affect pH. The red growth medium turned yellow due to the phenol red indicator in the medium by the end of the electrolyses, and a black deposit could be seen on the submerged part of the anode. This deposit was not water soluble, but was removable with acetone or ethanol; it was observed at both anodes and across all potentials. HPLC analysis revealed only trace amounts of benzoquinone or NAQPI throughout experiments. An acetaminophen-free sample of growth medium was then electrolyzed, and used to plate EMT-6 cells, which were incubated overnight (37 ^{O}C; 5% CO_2). Cells were grown in 100 µl of electrolyzed medium. This experiment examined the tolerance of the EMT-6 cells to acidic pH, as the anodic decomposition of water produces hydrogen ions ($2H_2O$ (l) → O_2 (g) + $4H^+$ (aq) + $4e^-$). As such, it was important to know, in a qualitative way, whether the cells could survive in electrolyzed medium. This information would later aid in the design of a quantitative assay (MTS assay). After 24 hours incubation time, plated cells were visually inspected, and appeared to be dead. These cells were spherical, retracted from their neighbours, and with a mottled appearance, suggesting apoptosis. The sterility of the electrolyzed growth medium suggests the intolerance of EMT-6 cells to low pH (pH 6.3). The use of a buffered electrolytic solution was then investigated.

Sodium citrate, monobasic sodium phosphate, and TRIS buffers were prepared at pH 7.4 and ionic strength of 100 mM, by adjusting pH with sodium hydroxide or sulfuric acid; commercially available phosphate-buffered saline (pH 7.4) was also used. One mM or five mM acetaminophen was prepared using the buffered solutions, and 50.0 ml was electrolyzed for 30 minutes; a supporting electrolyte of 25 mM sodium sulfate was added to citrate and tris buffers for conductivity. Once again, electrolysis took place at 1.0 V vs SCE; 5, 10, and 20 mA; and, at both Ti/RuO_2 and graphite anodes. In addition to producing anodic polymerization, electrolysis of the buffered solutions resulted in a decrease in pH in all cases; final pH of solutions ranged from 3.0-6.3. These values are lower than those produced in the previous experiment, suggesting that the growth medium has a larger buffer capacity, due to the greater concentration of the

constituents (~250 mM). Citrate (108 µM) and TRIS (116 µM) buffers were the only solutions which managed to produce significant benzoquinone yields. This occurred at 20 mA, using 5 mM acetaminophen, and a graphite anode. Several different oxidation products could be observed between buffers, but only phosphate-containing solutions changed colour. These gradually progressed from colourless, to yellow, to brown. The brown colouration produced in phosphate experiments was replicated chemically by doping a sample of buffer with benzoquinone; within 1 hour, the faint yellow solution became brown. HPLC analysis revealed only trace amounts of benzoquinone remaining after incubation in phosphate buffer. The use of buffers in a divided cell is recommended against because of the poor yield of oxidation products, anodic polymerization, and significant changes in pH.

5.4.2 MTS Assay Calibration

Incorporating results from the buffered solution experiments, an MTS-based colorimetric assay was developed to quantify cell viability. Initial work was set out to characterize the optimal conditions of the MTS reagent with respect to the chosen EMT-6 cell line. This involved conducting experiments looking at the response of the assay to the following parameters: plated cell density and MTS reagent incubation time (at 37°C; 5% CO_2). EMT-6 cells were plated at densities of 2500, 5000, 10000, and 15000 cells per 100 µl. After 24 hours for cells to reach confluency, they were treated with 2 ng/ml transforming growth factor beta (TFG-β) as a positive control for reduced cell growth. After 24 hours of incubation with TGF-β, 20 µl of MTS reagent were added to the cells, and incubated for either 1, 2, or 4 hours. Absorbance change of the MTS reagent was read at 490 nm (see Section 4.2.6). Untreated controls showed an increase in absorbance that correlated with increasing density (figure 17A, pg. 50); as MTS reagent exposure time increased, so too did absorbance values (figure 17A). The same behaviour was seen in TGF-β treated cells, except that absorbance values were significantly lower than the control group (figure 17B). Based on the absorbance value that detected the best resolution between TGF-β treated versus control cells, all subsequent cell viability

assays involved a plated cell density of 5,000 cells per 100 µl, and an MTS reagent incubation time of 2 hours. These conditions were chosen so that control group absorbances would approximate about a value of 1.0 to avoid saturation of the absorbance signal. Sample aliquots of 50 µl were chosen for use in the MTS assay which, when combined with 100 µl growth medium, represented a sample dilution of 1:3; this dilution was corrected for in all subsequent mentioning of the assay. The large sample aliquot was used so as to avoid the need for higher concentrations of toxicant in electrolyzed solutions; i.e., a 10 µl aliquot requires a higher concentration of toxicant when diluted in 100 µl, a feat which may have not been technically possible. Additionally, larger dilution factors were not used so as to maintain the integrity of the growth medium. Because the sample is diluted when performing the assay, electrolyzed solutions were required to produce higher toxicant concentrations than the LC_{99}. For this specific assay protocol, lethality is not directly measured and the LC value is herein refered to properly as an inhibitory concentration (IC). Electrolyses were required to produce three times the toxicant IC_{99} in order to be considered effective; this dilution effect is also considered to apply to a tumour: the volume of effluent will be diluted by a volume of interstitial fluid proportional to the volume of the tumour. In other words, any effluent injected into a tumour will be diluted by at least a factor of 0.5. The requirement for higher concentrations of toxicant means longer electrolysis times and/or higher currents, this is because prodrug oxidation is dependent on the amount of charge passed through the cell as a function of time (Amperes = Coulombs/second). In this work, the electrolytic conditions were required to produce a minimum of three times the IC_{99} of a toxicant in order to account for this dilution.

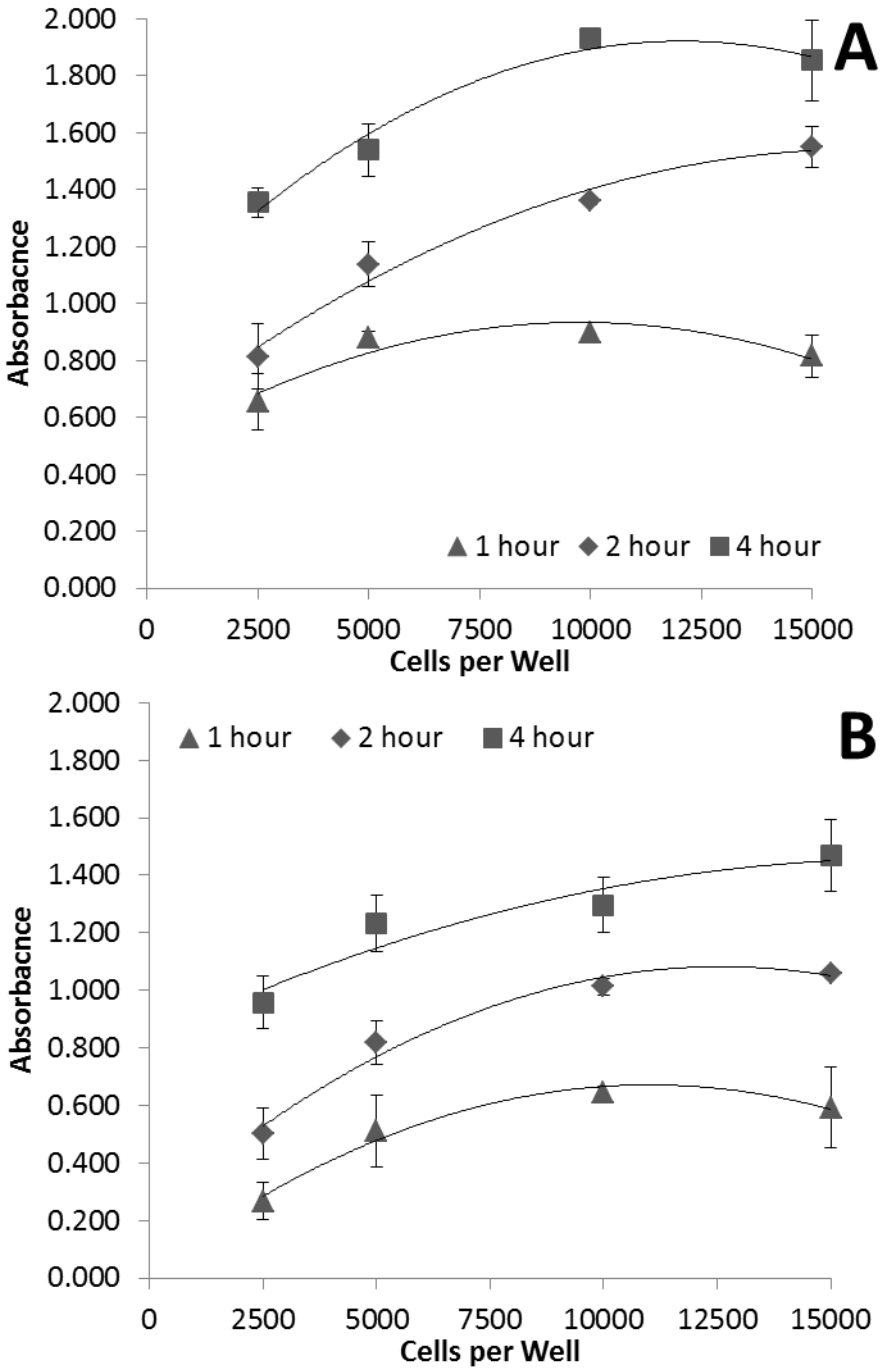

Figure 17. Effect of cell density on MTS response. EMT-6 cells plated at 2500, 5000, 10000, 15000 cells per well in 100 µl SAM and incubated for 24 hours with 2 ng/ml transforming growth factor beta (TFG-β). Solutions were then exposed to the MTS reagent for 1, 2, or 4 hours before absorbance was read at 490 nm. Data are blank corrected for growth medium and MTS reagent. Panel A: Control, panel B: TFG-β. Data are an average of n = 3 ± standard deviation.

A 24 hour treatment (incubation) time was used in toxicity experiments to estimate the effectiveness of a treatment. This length of time was used in toxicity experiments to ensure cells were treated under a subconfluent state, when they are more likely to respond to DNA damaging agents that target dividing cells (e.g., CP). The incubation time was chosen because it is approximately the same length of time required for the EMT-6 line to reach confluency. Since cancer cells, in general, have near-infinite replicative capacity, observing toxicity too soon runs the risk of a false positive for treatment. For example, after 2 hours of toxicant exposure at a given concentration, results from an MTS assay reveal a 75% decrease in cell viability. The fate of the remaining 25% viable cells is unknown, and the question left unanswered is whether or not these remaining cells are in the process of dying or if they are resistant to the treatment. If these cells have survived the toxicant exposure, the treatment did not work and the cancer will grow back over time. By assessing toxicity after the confluency time, this uncertainty in response is reduced. Any surviving cells will have begun to repopulate the environment (culture dish or organ) and a long-term measure of treatment effectiveness can be obtained.

5.4.3 Chemical Reactivity of the MTS Reagent

Because the MTS assay measures the production of a reducing agent (NAD(P)H), an experiment was conducted to investigate the chemical reactivity of the MTS reagent against chosen model compounds: acetaminophen, benzoquinone, and cyclophosphamide – two of which are capable of redox cycling (see Section 3.1). Under cell-free conditions of the MTS assay, only benzoquinone produced a significant increase in absorbance compared with controls. Absorbance values began to increase exponentially at approximately 85 µM benzoquinone (figure 18). When this experiment was repeated with mQ water instead of growth medium, the absorbance increase of the MTS reagent did not occur (not shown). This shows that BQ does not directly interact with the MTS assay, and that absorbance changes are due to BQ interaction with components of the growth medium. One explanation of the increase in absorbance is

that over the 24 hour incubation period, BQ oxidized components (e.g., glutathione) in the medium to form hydroquinone (HQ), which then acted to reduce the MTS reagent. Additional controls were required because of this absorbance increase during the toxicity testing of benzoquinone (i.e., BQ in cell-free assay medium).

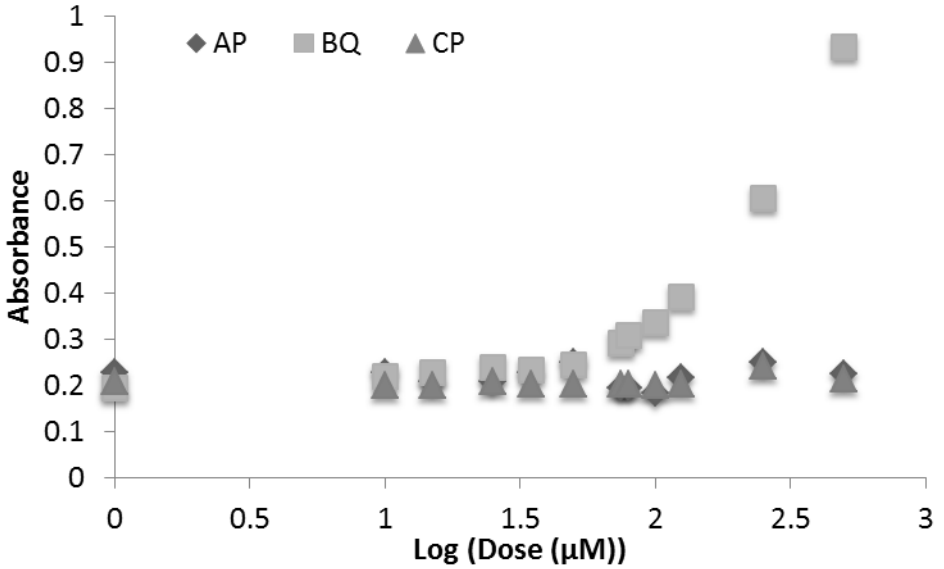

Figure 18. Chemical reaction of model compounds with MTS reagent in cell-free growth medium. 50.0 µl aliquots of treatment were incubated in 100 µl of growth medium for 24 hours at 37 ^{o}C. 20.0 µl of MTS reagent was then added and incubated for an additional 2 hours; absorbance read at 490 nm. AP: acetaminophen, BQ: benzoquinone, CP: cyclophosphamide. Average of n = 3 data points.

5.4.4 Model Compound Dose-Response Curves

A dose-response curve was constructed for cyclophosphamide across a concentration range of 10 to 500 µM. Cyclophosphamide oxidation products, such as 4-OH-CP or the phosphoramide mustard, were not available for toxicity testing. Cyclophosphamide produced no significant toxicity at these concentrations (R^2 = 0.006; figure 19). The dose range used was selected based on work done by Paci *et al.* (2001), where they report the LC_{50} of cyclophosphamide (200 µM) and the LC_{50} of the 4-OH-CP (10-20 µM) against carcinoma KB cells. No toxicity was observed over this dose range in EMT-6 cells, implying that EMT-6 lacks the CYP enzymes for bioactivation of CP. It has

been shown that cultured EMT-6 metastases display inter-tissue variability in response to cyclophosphamide treatment (Holden *et al.*, 1997). Metastases grown *in vitro* from different tissues had shown a 2-3 log range of sensitivity differences to cyclophosphamide. It is no surprise then that there would be significant variability between cancer cell lines to the same drug, if there is such variance of the cell line within the same animal.

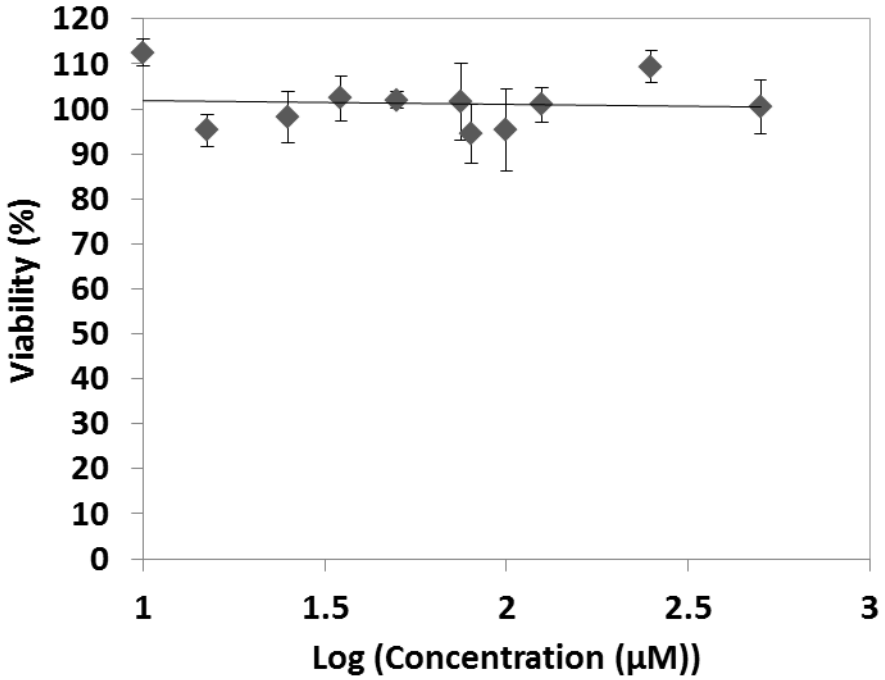

Figure 19. Dose-response curve of EMT-6 cells treated with cyclophosphamide. EMT-6 cells were plated at a concentration of 5000 cells/100 µl. Confluent cells were incubated for 24 hours in growth medium containing 10, 15, 25, 35, 50, 75, 80, 100, 125, 250, and 500 µM cyclophosphamide. Data shown as a percent viability relative to untreated controls. Blank corrections for treatment, growth medium, and MTS have been accounted for. Data are average of n = 3 ± standard deviation of repetitions; R^2 = 0.006.

Concentrations of acetaminophen ranging from 10 to 500 µM were used to construct a dose-response curve similarly to cyclophosphamide. After 24 hours of incubation, MTS assay revealed that there was no decrease in cell viability relative to controls (R^2 = 0.073; figure 20). Visual inspection of the cells revealed that they were spindle-shaped and confluent. Due to the instability of NAPQI, no dose-response curve

could be made for this substance. The stability of benzoquinone, however, was more amenable to toxicity testing.

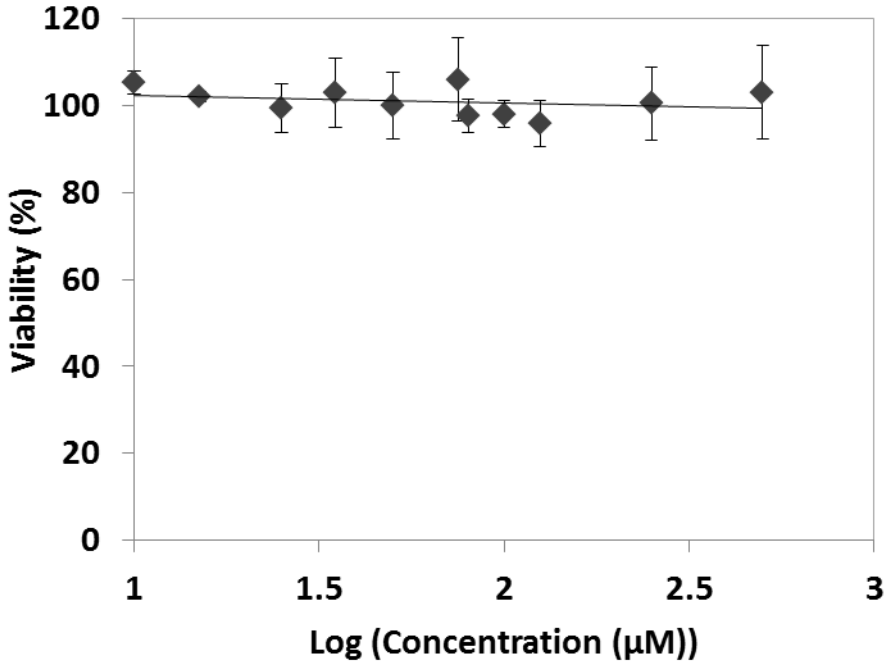

Figure 20. Dose-response curve of EMT-6 cells treated with acetaminophen. EMT-6 cells were plated at a concentration of 5000 cells/100 µl. Confluent cells were incubated for 24 hours in growth medium containing 10, 15, 25, 35, 50, 75, 80, 100, 125, 250, and 500 µM acetaminophen. Data shown as a percent viability relative to untreated controls. Blank corrections for treatment, growth medium, and MTS have been accounted for. Data are average of n = 3 ± standard deviation of repetitions; $R^2 = 0.073$.

Across a concentration range of 10 to 500 µM, benzoquinone produced a significant decrease in cell viability (figure 21). Cells which were once spindle-shaped and confluent became round in shape and retracted from their neighbours, post treatment. Construction of a probit curve produced IC_{50} and IC_{99} values of 26 and 138 µM benzoquinone, respectively (figure 21 insert). While the IC_{99} of BQ is 138 µM, the 1/3 dilution of the MTS assay requires electrolyses to produce three times that amount to be toxic (414 µM). This thesis will refer to 138 µM as the IC_{99}, unless otherwise noted. This decision was made on the basis that, in more general terms, the dilution factor will

change based on tumor volume and assay parameters, but the IC_{99} will remain the same for each compound.

These values were determined by solving for x from the probit equation of y = -3.935x + 10.575, and taking the anti-log. Concentrations of 250 and 500 µM benzoquinone were not included in the probit curve, but are shown on the probit graph to make note of the limit of resolution of the MTS assay. Because the probit curve is a logarithmic function, a more sensitive assay would be required to obtain corresponding probit values smaller than a 97% response. The probit function is meant as statistical enhancement of the IC_{50} confidence interval, not the IC_{99}, as sought in the case of the thesis. For proof-of-concept, this resolution limit of the MTS assay is acceptable for these preliminary experiments.

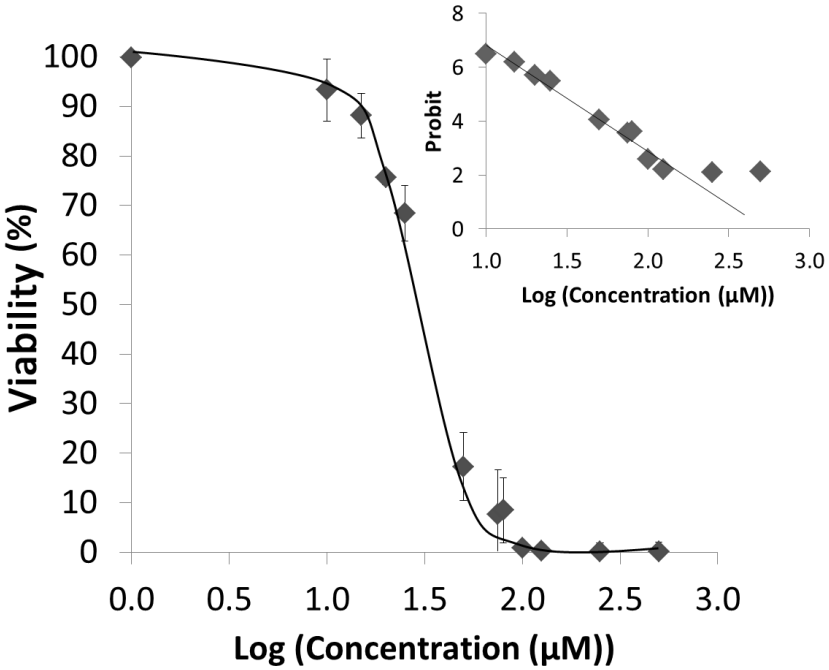

Figure 21. Dose-response curve of EMT-6 cells treated with benzoquinone. EMT-6 cells were plated at a concentration of 5000 cells/100 µl. Confluent cells were incubated for 24 hours in growth medium containing 10, 15, 20, 25, 50, 75, 80, 100, 125, 250, and 500 µM benzoquinone. Data shown as a percent viability relative to untreated controls. Blank corrections for treatment, growth medium, and MTS have been accounted for. Data are average of n = 3 ± standard deviation of repetitions.

5.5 Electrolysis of Cyclophosphamide

Cyclophosphamide was initially chosen as a model compound because it is currently in widespread clinical used as a chemotherapeutic, and is oxidatively bioactivated. Linear sweep voltammetry was performed on CP using Ti/RuO_2 and graphite microelectrodes, but no oxidation peak for cyclophosphamide could be observed within the range of water stability at either anode. Paci *et al.,* (2001) had managed to obtain a voltammetric peak for CP in acetonitrile on glassy carbon at 2.0 V vs SCE; however, this is beyond the potential for water oxidation at graphite. Paci *et al*. had also electrochemically produced 4-MeO-CP at graphite in methanol, but did not perform any electrolyses in aqueous conditions. To address this, amperostatic electrolyses of 50.0 ml of 0.5 mM CP solutions were carried out in 25 mM Na_2SO_4 at constant current (5 mA and 20 mA), with Ti/RuO_2 and graphite anodes; the experiments were followed by HPLC for up to 2 h.

In order to follow CP oxidation by HPLC with an optical detector, a derivatization step was needed to visualize products of oxidation. While cyclophosphamide absorbs in the 190-210 nm range directly, its absorbance is poor, and is outside the usable wavelength range for solutions. Electrolyses often can produce many oxidation products with similar retention times; these can obscure the compound of interest's chromatogram peak. Since the toxicologically active compound, phosphoramide mustard (see Section 3.1), elicits toxicity by reacting with nucleophiles, the basic idea was to capture any reactive species produced through oxidation (mustards), with the nucleophilic chromophore, diethyldithiocarbamate (DDTC). The DDTC-PM adduct absorbs maximally at 275 nm (Cummings *et al.*, 1991); DDTC itself does not absorb at this wavelength, nor does CP. When unelectrolyzed cyclophosphamide was subjected to the derivatization process (see Section 4.2.1), no reaction occurred; i.e., no products were seen chromatographically. It was concluded that any products of derivatization observed had been produced through the electrochemical oxidation of cyclophosphamide.

Electrolyzed samples of cyclophosphamide were prepared amperostatically at 5 and 20 mA, in a divided batch cell, at both Ti/RuO_2 and graphite anodes. The 50.0 ml electrolyzed solution contained 0.5 mM cyclophosphamide and 25 mM Na_2SO_4. Samples were taken every 30 min to coincide with the length of derivatization. Water oxidation (i.e., bubbles) was observed at Ti/RuO_2 at 5 and 20 mA; there were no bubbles observed at graphite at these currents. The chromatograms consistently showed a grouping of peaks assumed to be a collection of mono- and di-DDTC-PM adducts, evident by the multiple shoulders in the chromatogram (figures 22-25, pg. 57-60). Of the derivatized oxidation products observed, the largest peak had a retention time of 21 minutes. This peak formed consistently after 30 minutes of electrolysis time at both Ti/RuO_2 and graphite anodes, at both 5 and 20 mA (figures 22-25, pg. 57-60). The peak's intensity remained relatively constant over the course of the electrolyses. Unfortunately, there was no feasible means of identifying the suspected PM-DDTC products. Mass spectrum analysis had been attempted, but product identification proved more difficult than deemed worthwhile, and investigation was halted. As identification of these products was a secondary goal of the thesis, not knowing the identity of these compounds was considered acceptable. Therefore, HPLC analysis is purely qualitative to the aqueous oxidation of cyclophosphamide.

The use of cyclophosphamide exemplifies a particular challenge for working with reactive intermediates and a possible limitation to this thesis's context. An easily quantifiable, or stable toxicant cannot always be afforded (as with acetaminophen's benzoquinone); as such, it is effluent toxicity that is the real measure of electrolysis success. It is to this end that the qualitative evidence of cyclophosphamide electrooxidation is sufficient to test the toxicity of the electrolyzed solution. The lack of product identification made it difficult to understand how electrolysis affected cyclophosphamide; for this reason, acetaminophen will be used to characterize electrolyses. The acetaminophen system is well defined electrochemically and is directly amenable to HPLC quantitation.

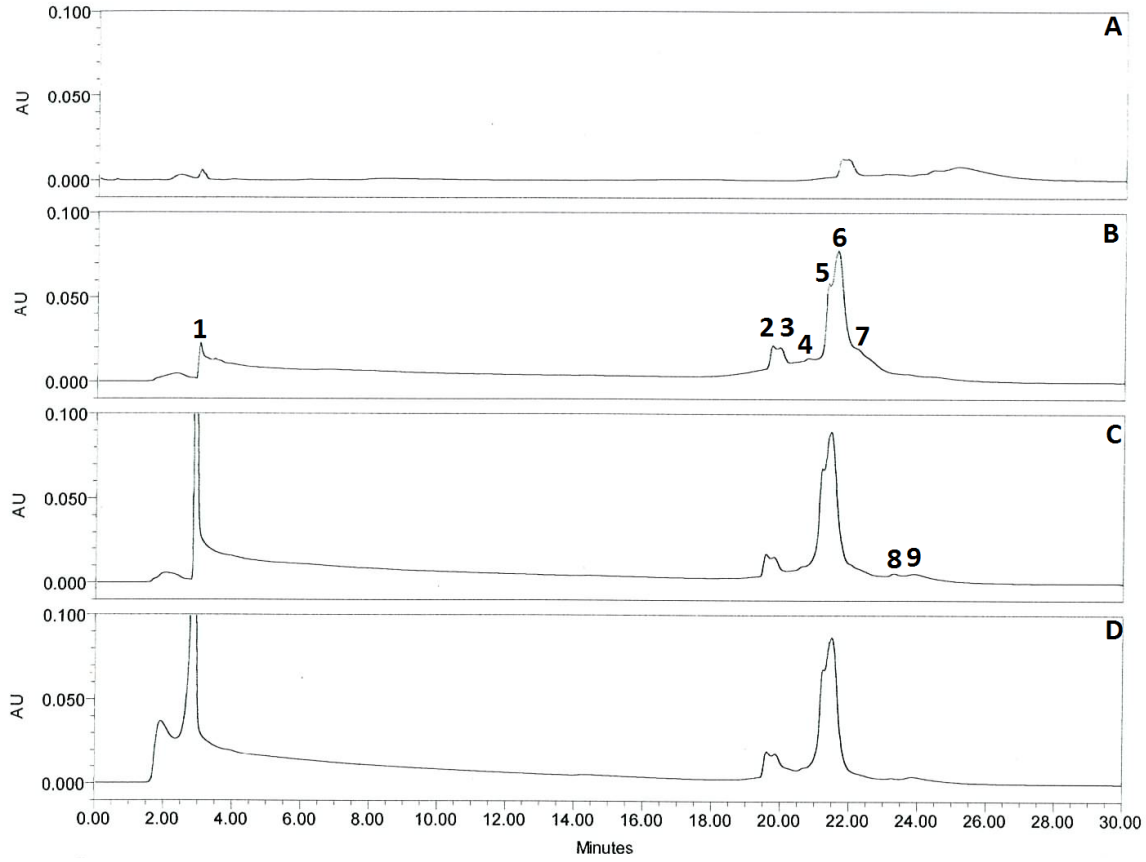

Figure 22. Reversed phase HPLC chromatograms of 0.5 mM cyclophosphamide electrolyzed at 5 mA with a Ti/RuO_2 anode. Absorbance read at 275 nm. A: t=0; B: t=30; C: t=60 ; D: t=90. Supporting electrolyte: 25 mM Na_2SO_4. Recurring peaks between electrolyses have been labelled but have not been chemically identified.

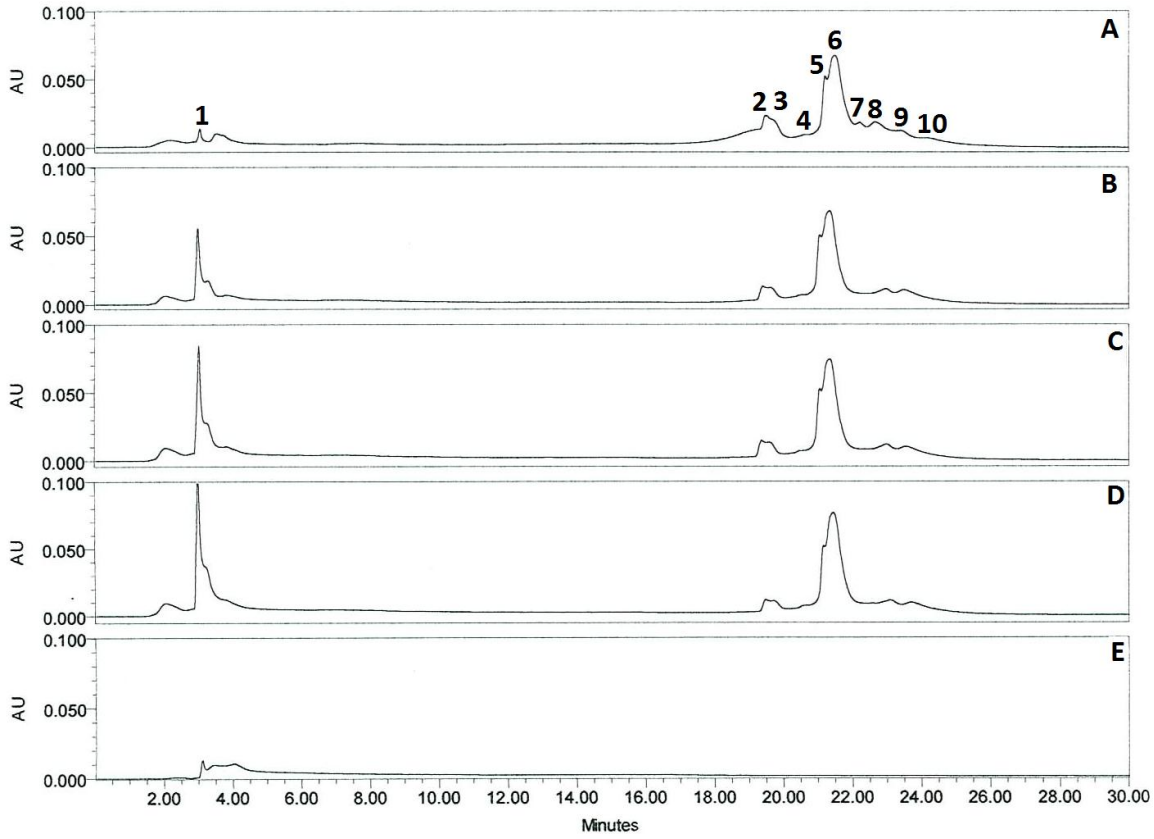

Figure 23. Reversed phase HPLC chromatograms of 0.5 mM cyclophosphamide electrolyzed at 5 mA with a graphite anode. Absorbance read at 275 nm. A: t=30; B: t=60; C: t=90 ; D: t=120 ; E: t=0. Supporting electrolyte: 25 mM Na_2SO_4. Recurring peaks between electrolyses have been labelled but have not been chemically identified.

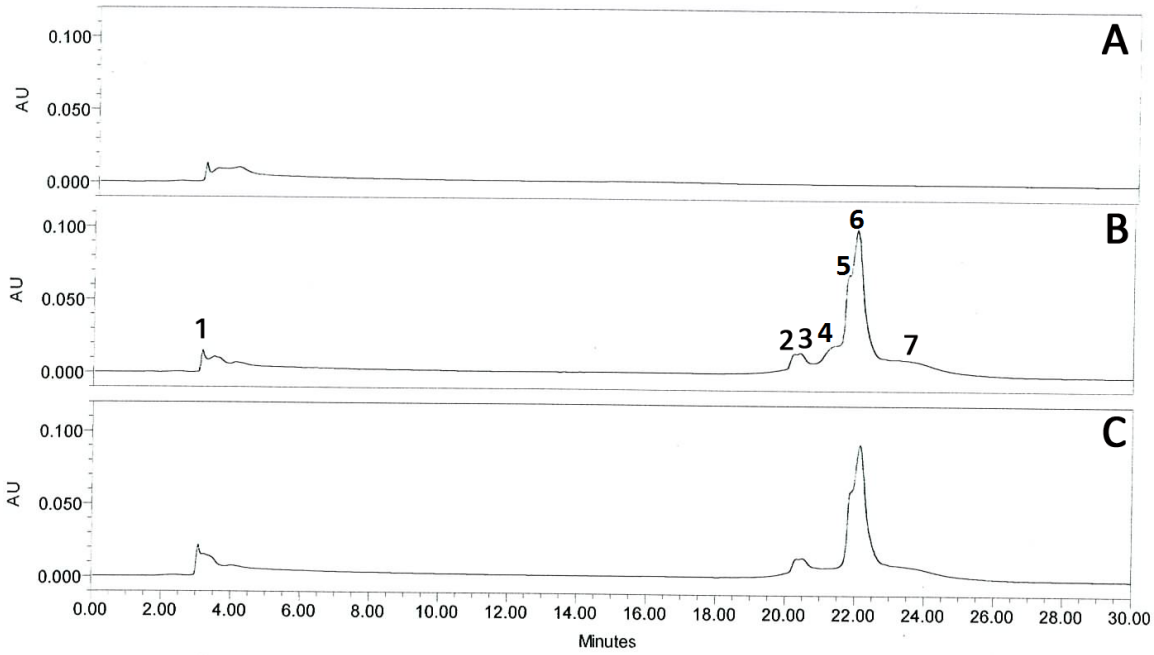

Figure 24. Reversed phase HPLC chromatograms of 0.5 mM cyclophosphamide electrolyzed at 20 mA with a Ti/RuO_2 anode. Absorbance read at 275 nm. A: t = 0; B: t = 60; C: t = 90. Supporting electrolyte: 25 mM Na_2SO_4. Recurring peaks between electrolyses have been labelled but have not been chemically identified.

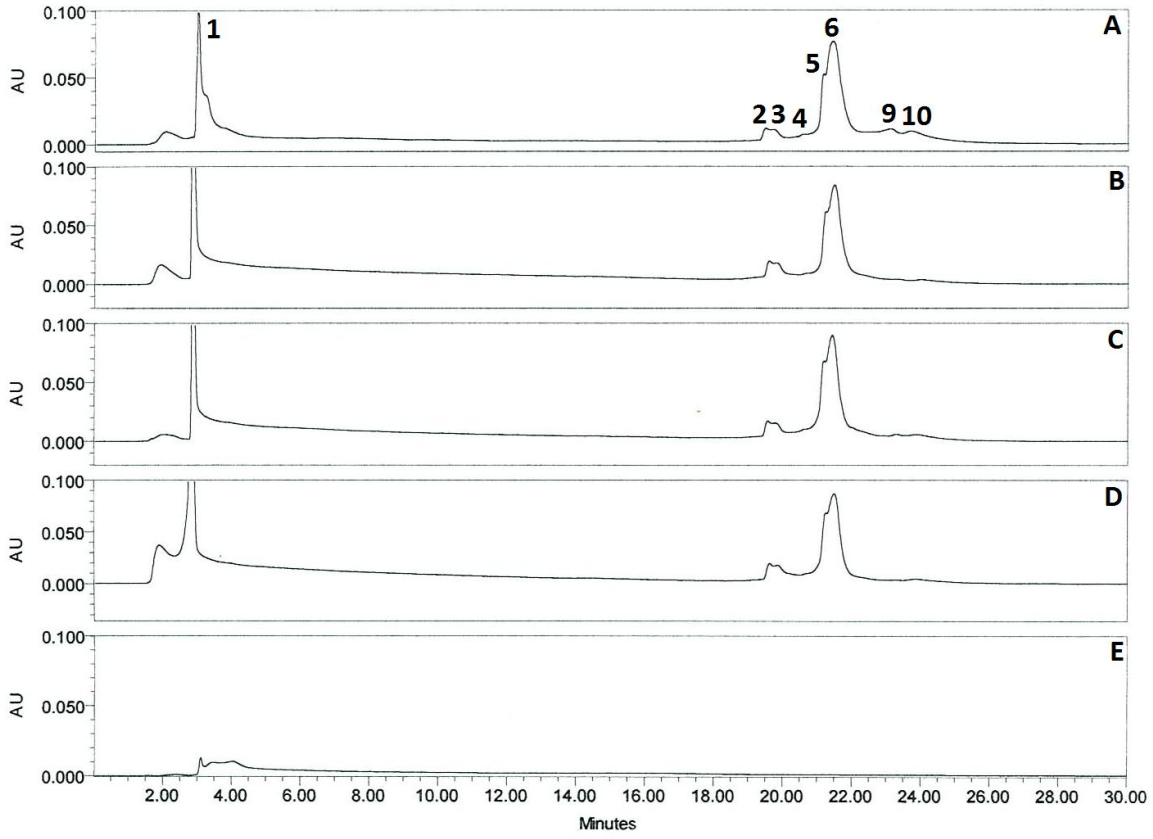

Figure 25. Reversed phase HPLC chromatograms of 0.5 mM cyclophosphamide electrolyzed at 20 mA with a graphite anode. A: t=30; B: t=60; C: t=90 ; D: t=120; E: t=0. Supporting electrolyte: 25 mM Na_2SO_4. Recurring peaks between electrolyses have been labelled but have not been chemically identified.

5.6 Electrolysis of Acetaminophen

5.6.1 *Potentiostatic Electrolyses*

Linear sweep voltammetry was performed on 1 mM acetaminophen using Ti/RuO_2 and graphite microelectrodes, with 25 mM Na_2SO_4 as a supporting electrolyte. No oxidation peak was observed within the range of water stability at Ti/RuO_2 (figure 26A). Oxidation peaks could not be observed due to the extremely low over potential of water at Ti/RuO_2, as denoted by the rapid increase in current (mA). Bubble formation at the electrode's surface was observed experimentally, confirming water oxidation. In figure 27B a pencil lead graphite microelectrode shows a clear oxidation peak of acetaminophen at approximately 0.9 V vs. a saturated calomel reference electrode (SCE). Note that the current is in µA; no bubbles were observed. This is the oxidation peak of acetaminophen to NAPQI and is indicative of a direct electron transfer oxidation. Cyclic voltammetry at physiologic pH show a reversible peak corresponding to the reduction of NAPQI back to acetaminophen (Nematollahi *et al.*, 2009). From these results, subsequent potentiostatic electrolyses were carried out at 1.0 V vs SCE for both electrodes.

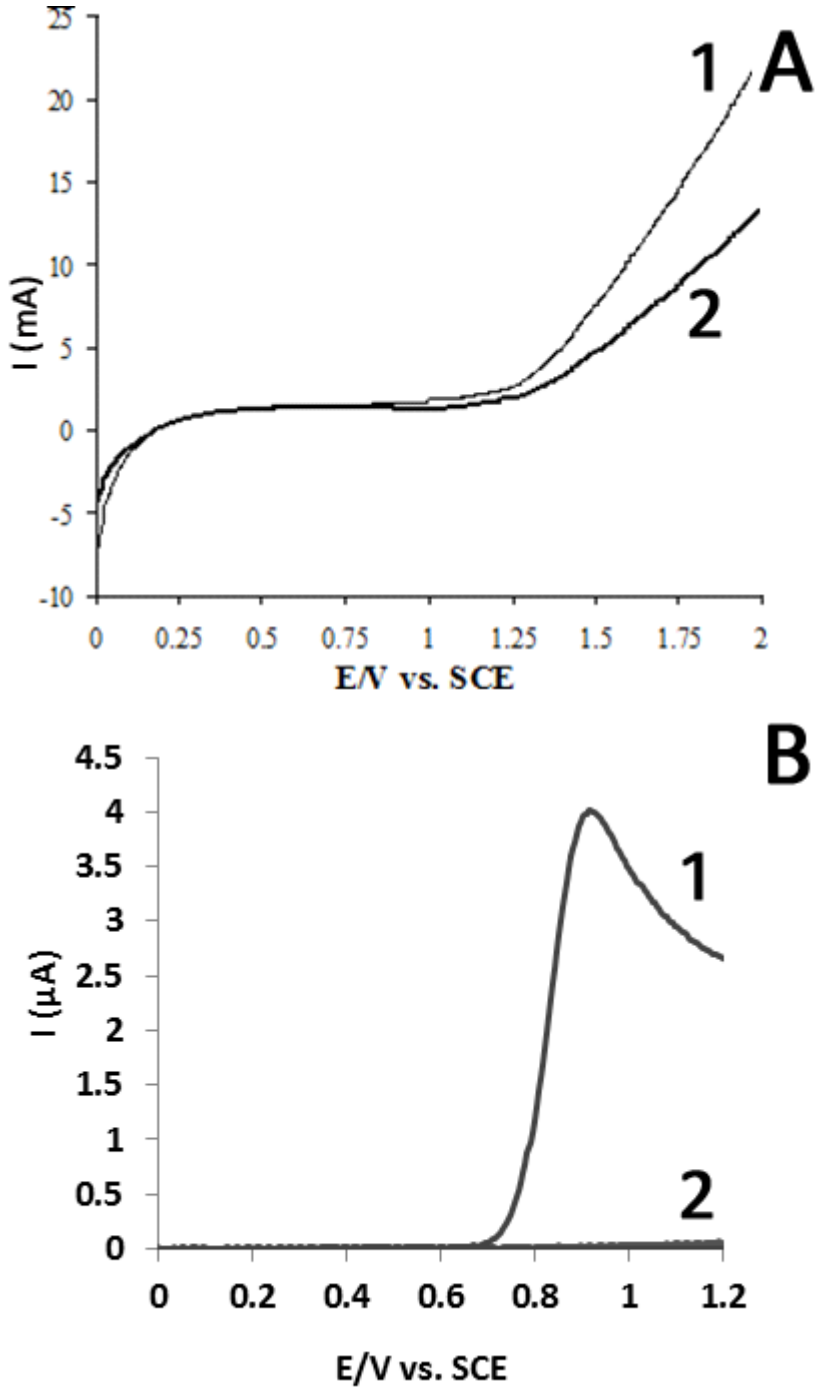

Figure 26. Linear sweep voltammograms for 1 mM acetaminophen at Ti/RuO_2 and graphite anodes vs. SCE. Sweep rate 50 mV/s; supporting electrolyte 25 mM Na_2SO_4. Panel A: Ti/RuO_2: 1 – AP, 2 – Solvent; scan from 0.0 – 2.0 V. Panel B: Graphite: 1 – AP, 2 – Solvent; scan from 0.0 - 1.2 V. Note: scale magnitudes.

Potentiostatic oxidation of 1.0 mM acetaminophen (AP) was conducted in a divided batch cell with 25 mM Na_2SO_4 as supporting electrolyte. A divided cell was used with a titanium cathode and a SCE. After one hour electrolysis at Ti/RuO_2, 607 µM AP was consumed, 270 µM BQ were produced, and the BQ IC_{99} concentration of 138 µM was met at 35 minutes (figure 27, pg. 64). At graphite; 564 µM AP was consumed after 1 hour; 350 µM BQ were produced; and it took 25 minutes to reach the BQ IC_{99} (figure 27, pg. 64). Both electrolyses failed to produce the 414 µM concentration required for MTS assay toxicity. Significant oxygen evolution was observed during electrolyses at Ti/RuO_2 but not at graphite. During potentiostatic electrolyses the amount of current flowing (i.e., substrate oxidation) is proportional to the concentration of substrate at the anode surface, which in turn, is dependent on mass transport of the substrate from the bulk of solution. In other words, as acetaminophen is consumed the rate of oxidation will decrease proportionally. Since both experiments used equal concentrations of acetaminophen, the rates of oxidation of acetaminophen at graphite and Ti/RuO_2 were the same.

Either type of anode used is suitable from a prodrug oxidation standpoint. However, the lag in benzoquinone production at Ti/RuO_2 (figure 27B, pg. 64) suggests that other products of acetaminophen oxidation are being formed. In other words, oxygen transfer oxidation reactions appear to be less selective than direct electron transfer oxidation reactions. Due to the high overpotential of water oxidation at graphite, amperostatic conditions will be used to observe oxygen transfer reactions at this anode. The increase in current however will cause an increase in oxygen evolution and a decrease in oxidation efficiency.

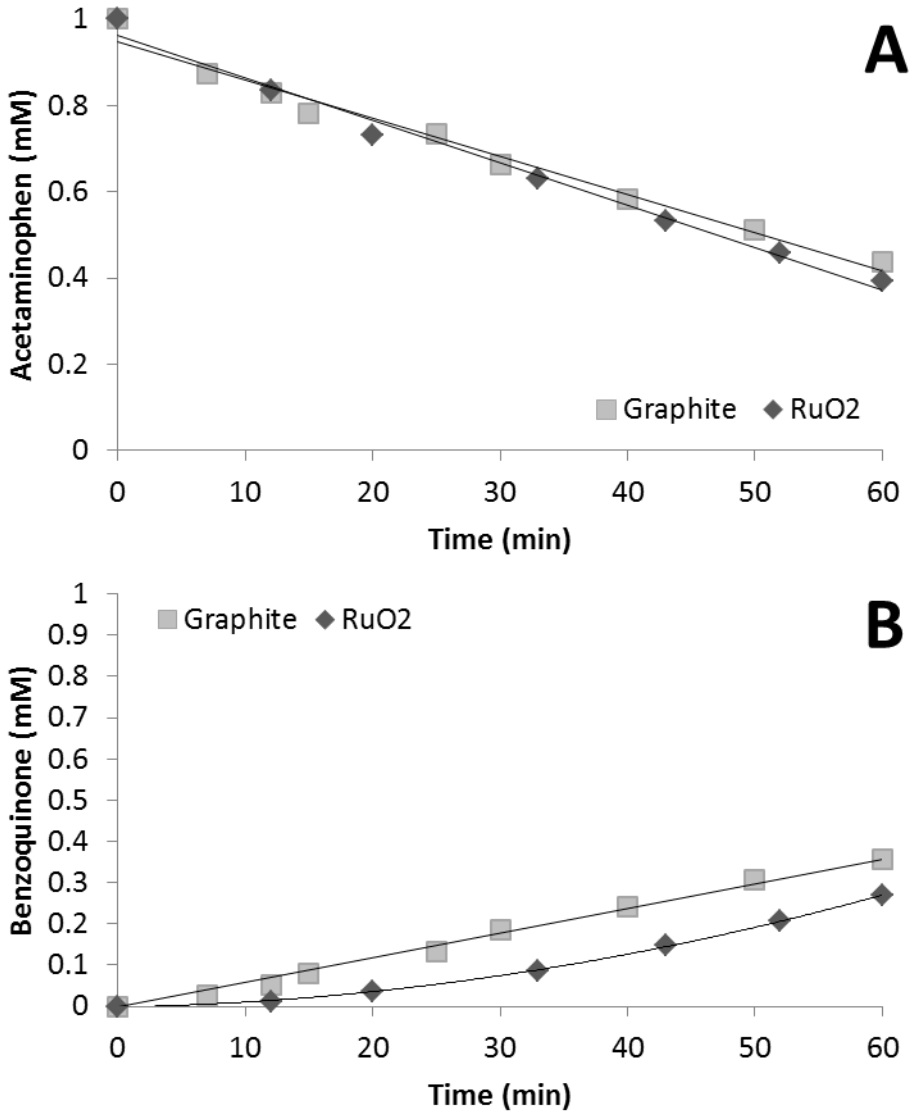

Figure 27. Potentiostatic electrolysis of 1 mM acetaminophen at 1.0 V vs SCE. Panel A: oxidation of acetaminophen; panel B: formation of benzoquinone. Divided batch cell volume: 50 ml. Supporting electrolyte: 25 mM Na_2SO_4. After 60 minutes 270 and 350 µM of benzoquinone were produced Ti/RuO_2 and graphite, respectively. R^2 values for panel A: graphite: 0.980; Ti/RuO_2: 0.988. R^2 values for panel B: graphite: 0.991; Ti/RuO_2: 0.944.

5.6.2 Amperostatic Electrolysis

The amperostatic oxidation of 1 mM acetaminophen was investigated using currents of 20, 40, and 80 mA with a Ti/RuO_2 anode. All three currents were capable of exceeding the BQ IC_{99} within the hour long electrolysis; this concentration (138 µM) was reached by 33 minutes at 20 mA and by 15 and 18 minutes at 40 and 80 mA, respectively (figure 28A, pg. 66). In terms of total BQ produced, 265, 364, and 431 µM were obtained as current increased from 20 to 80 mA (figure 28B, pg. 66); however, only the 80 mA electrolysis would be expected to be IC_{99} lethal to cells. Copious amounts of bubbles were produced at the Ti/RuO_2 anode. Similar to the potentiostatic experiment, a constant loss of acetaminophen can be observed independently of current (i.e., mass transport control). The relative efficiency of benzoquinone production improved over potentiostatic conditions, as more benzoquinone was produced per unit of acetaminophen oxidized. A lag in the production of benzoquinone was observed at 20 mA, similar to the previous experiment at Ti/RuO_2, but the rate became linear at 40 and 80 mA. Once again, mass transport controlled kinetics can be observed at this anode with respect to acetaminophen oxidation. Benzoquinone production, too, is mass transport controlled, since the hydrolysis of NAPQI is a chemical reaction. Overall, amperostatic electrolysis results were not a great improvement over potentiostatic electrolysis at Ti/RuO_2. This is in agreement with mass transport controlled kinetics, which are independent of applied current.

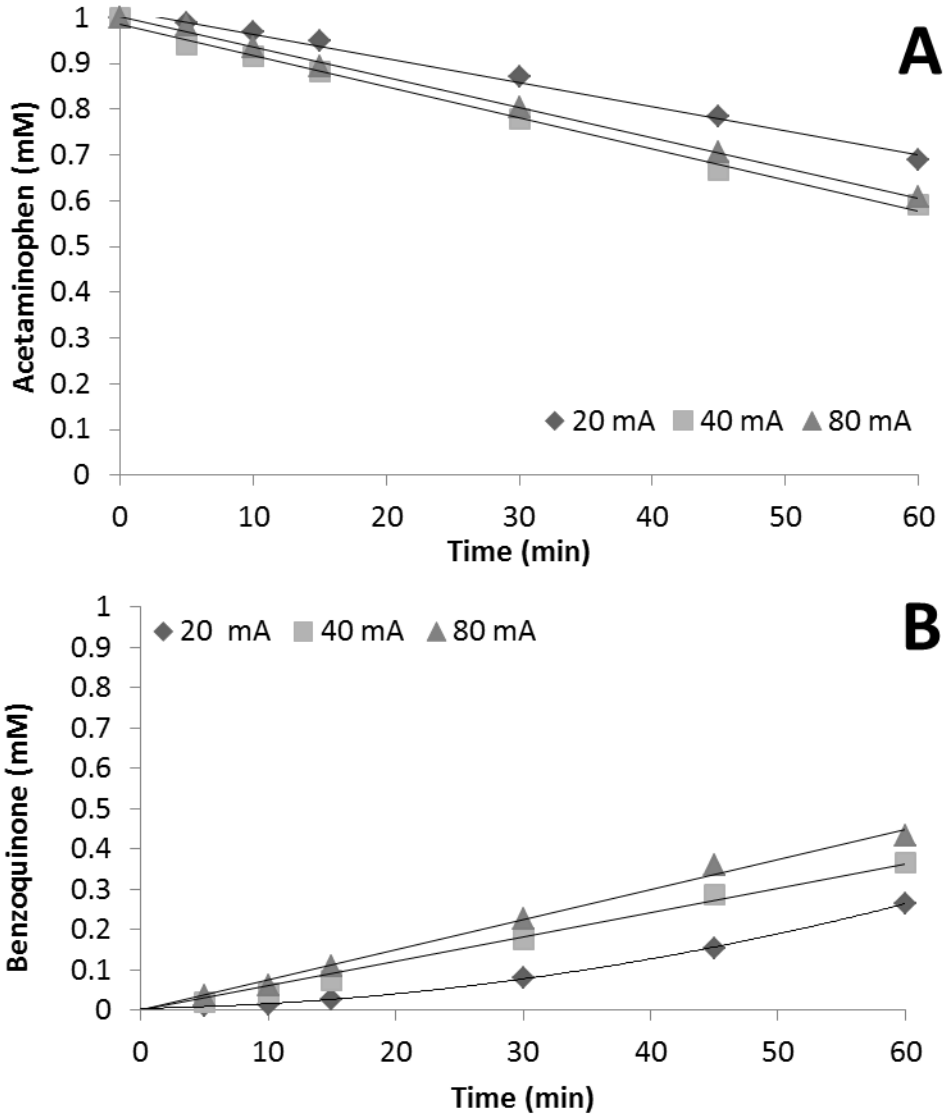

Figure 28. Loss of acetaminophen (A) and benzoquinone production (B) during a divided batch cell amperostatic electrolysis of 1 mM acetaminophen at a Ti/RuO_2 anode. Divided batch cell volume: 50 ml. Supporting electrolyte: 25 mM Na_2SO_4. Panel A: $R^2_{20} = 0.992$; $R^2_{40} = 0.998$; $R^2_{80} = 0.995$. Panel B: $R^2_{20} = 0.915$; $R^2_{40} = 0.990$; $R^2_{80} = 0.992$. Curves on graph are intended to highlight each dataset and were not involved in R^2 analysis.

The previous amperostatic experiment was repeated at a graphite anode. In this experiment, the BQ IC_{99} was exceeded by 15 min at all currents (figure 29B). Minor amounts of oxygen production could be observed at 20 mA as small bubbles, and bubble formation increased proportionately with current. The highest concentration of BQ produced by each current was 430, 394, and 323 µM at 20, 40, and 80 mA, respectively; only 20 mA would be lethal in the MTS assay. These results are similar to those seen amperostatically at Ti/RuO_2, but there was a 10 min improvement in reaching the IC_{99} over potentiostatic graphite. The overall rate of acetaminophen oxidation was similar to the potentiostatic experiment at graphite (i.e., mass transport controlled). The decrease in the overall amount of benzoquinone as current increases is suggestive of benzoquinone decomposition at higher currents (Boudreau *et al.*, 2010 B). While benzoquinone production has been greater at graphite than at Ti/RuO_2, overall formation rates are still unacceptable (see Section 5.4.4). Conditions which can produce high concentrations of toxicant are sought not only for convenience, but are considered beneficial, as the larger amount of toxicant produced is required to offset any dilution that may occur *in vitro* or *in vivo*. Using conditions which can achieve a high concentration (> IC_{99}) in a short time frame is a benefit from a technological standpoint as excessive amounts of time would not be required to 'prime' the toxicity of the effluent. The electrolysis must be efficient with respect to both toxicant yield and length of time required.

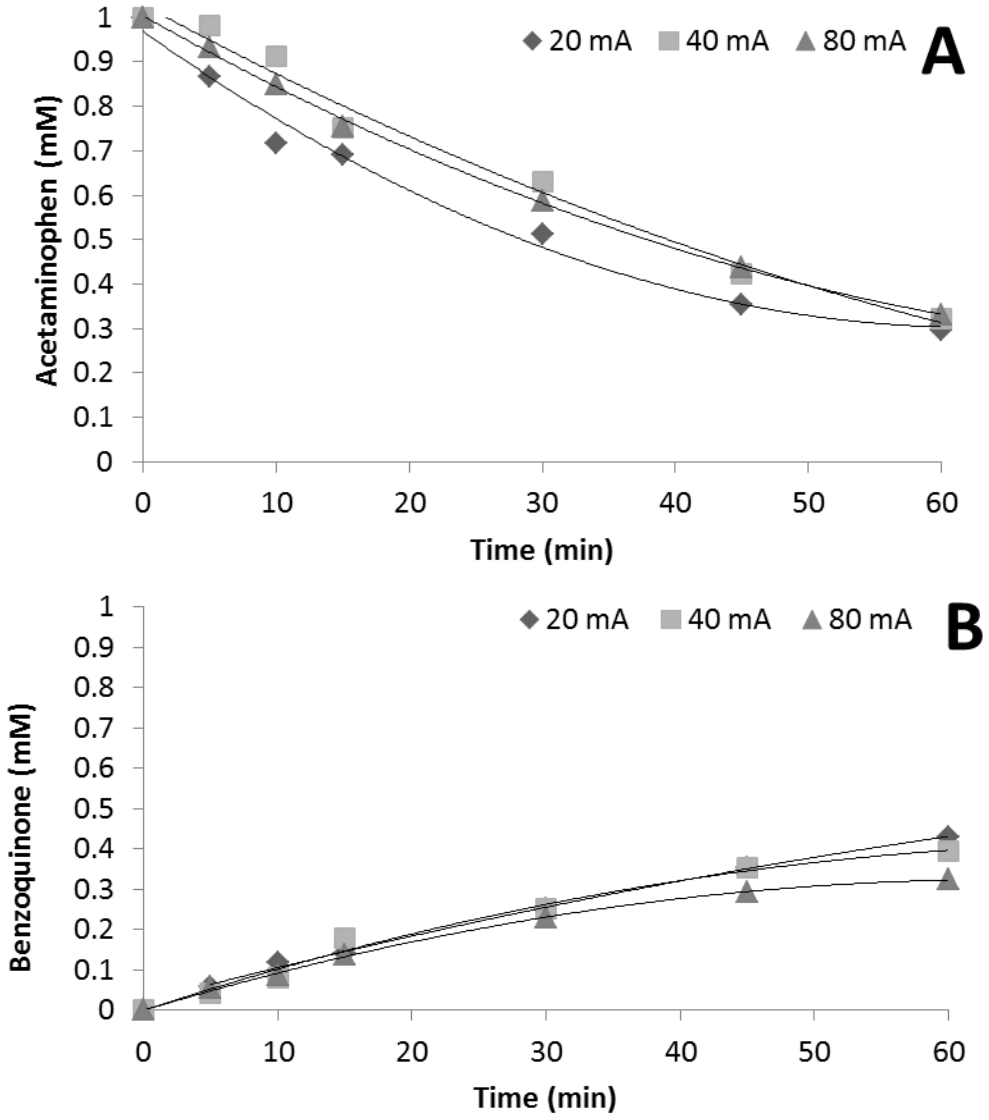

Figure 29. Loss of acetaminophen (A) and benzoquinone production (B) during a divided batch cell amperostatic electrolysis of 1 mM acetaminophen at a graphite anode. Divided batch cell volume: 50 ml. Supporting electrolyte: 25 mM Na_2SO_4. Panel A: R^2_{20} = 0.934; R^2_{40} = 0.976; R^2_{80} = 0.982. Panel B: R^2_{20} = 0.960; R^2_{40} = 0.943; R^2_{80} = 0.918. Curves on graph are intended to highlight each dataset and were not involved in R^2 analysis.

Next, the starting concentration of acetaminophen was increased to 5 mM in an attempt to improve both rate of benzoquinone formation and the overall amount produced. No improvement in the yield of BQ was observed when the starting concentration of AP was increased from 1 mM to 5 mM, using a Ti/RuO_2 anode under amperostatic conditions (Table 1, pg. 70). The rate of BQ formation increased with the applied current (figure 30A, pg. 71). When starting concentrations of acetaminophen were increased to 5 mM at graphite, a dramatic increase in the rate of production as well as the total amount of benzoquinone was obtained (figure 30B, pg. 71). By 5 minutes electrolysis time the BQ IC_{99} had been produced at currents of 20, 40, and 80 mA. Highest concentrations of BQ produced at each current were 1630, 1550, and 1270 µM, respective to 20, 40, and 80 mA; well in excess of the 414 µM required by the MTS assay. As one can see, there is a decrease in the production of benzoquinone as current increases, which is once again attributed to its decomposition.

In general, a decrease in current efficiency can be attributed to the parasitic evolution of oxygen at higher currents. While all electrolyses were able to exceed the IC_{99} of 138 µM, only by increasing the starting concentration of acetaminophen were experiments able to reach the concentration of 414 µM required to off-set assay dilution (table 1; see Section 5.4.4). From the amperostatic results, in terms of current efficiency and benzoquinone yielded, table 1 shows a clear preference for graphite at 5 mM acetaminophen and the lowest practical current.

Table 1. Amperostatic efficiency as a measure of benzoquinone yield after 60 min electrolysis

Anode	AP (mM)	Current (mA)	IC_{99} Time (min)*	BQ_{max} (µM)[§]	BQ_{max} Yield (%)[¤]	BQ Current Efficiency (%)
Graphite	1	20	57	430	43.0	10.4
		40	> 60	349	34.9	6.9
		80	> 60	323	32.3	2.7
	5	20	11.5	1630	32.6	23.1
		40	13.5	1550	31.0	11.3
		80	13.5	1270	25.4	5.9
RuO_2	1	20	> 60	265	26.5	1.4
		40	> 60	364	36.4	2.0
		80	56	431	43.1	1.5
	5	20	> 60	330	6.6	2.1
		40	> 60	303	6.1	2.9
		80	> 60	330	6.6	1.9

*: electrolysis time required to reach diluted IC_{99} (414 µM)

[§]: during 60 minutes electrolysis time

[¤]: BQ concentration as a function of AP lost after 60 min

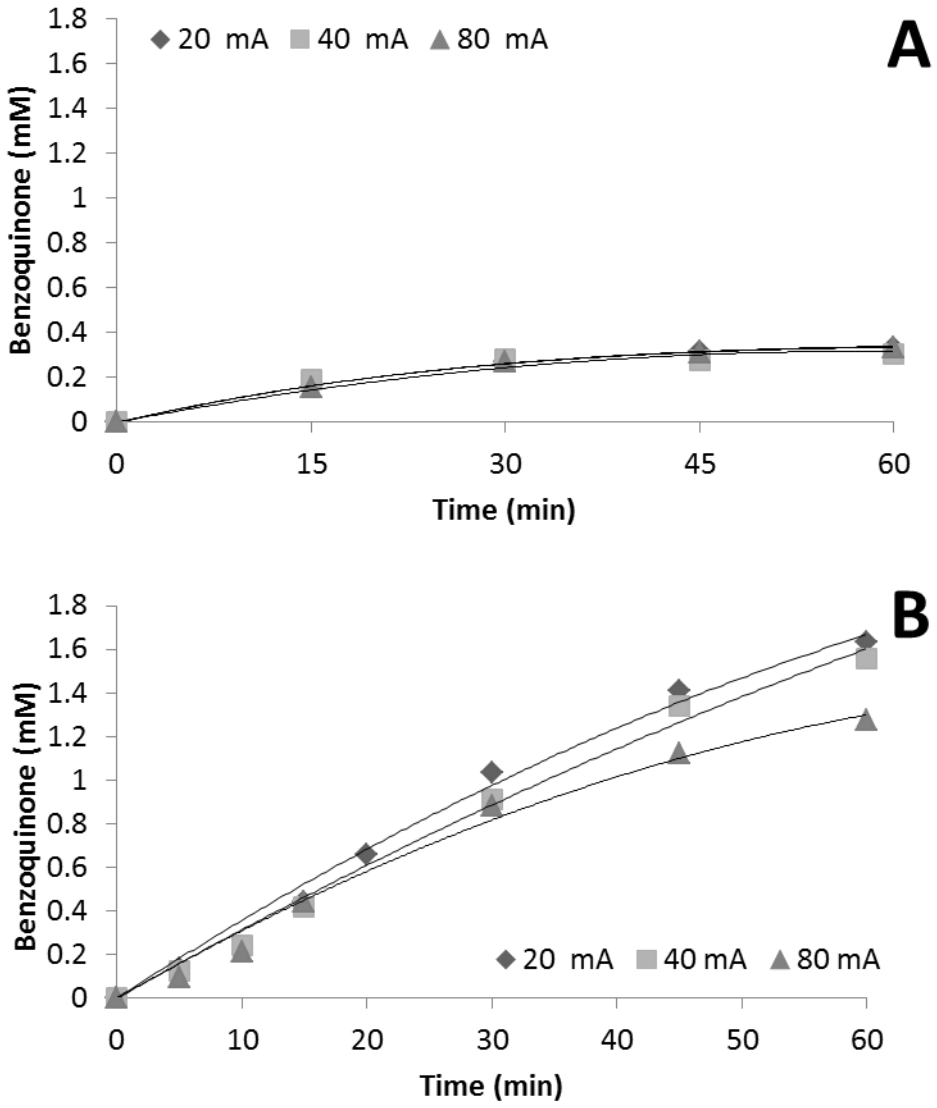

Figure 30. Benzoquinone production during divided batch cell amperostatic electrolysis of 5 mM acetaminophen at Ti/RuO_2 and graphite anodes. Divided batch cell volume: 50 ml. Supporting electrolyte: 25 mM Na_2SO_4. Panel A: Ti/RuO_2; panel B: graphite. Curves on graph are intended to highlight each dataset.

5.6.3 The Absence of NAPQI

In Section 3.2, NAPQI was a focus of discussion regarding acetaminophen toxicity. However, neither potentiostatic nor amperostatic electrolysis produced NAPQI above trace amounts (µM). These observations point to concerns on the relative rates of NAPQI formation and hydrolysis, an allusion to the pitfalls of using reactive toxicants that are simply too reactive (see Sections 1.4 and 3.2). NAPQI decomposition follows half-order kinetics at physiologic pH and has a half-life in solution of approximately 11 min (Dahlin *et al.*, 1982). Additionally, the rate of decomposition increases at mM NAPQI concentrations; in the presence of acetaminophen; and in acidic solutions – the very conditions that are used in this thesis (Miner and Kissinger, 1979). It would seem as no surprise then, that NAPQI was not seen in high yields during electrolysis. The formation and toxicity of benzoquinone, however, allows for toxicological analysis of acetaminophen electrolysate.

5.7 Toxicity of Electrolyzed Solutions

To assess toxicity of the batch cell solutions, 1 mM and 5 mM concentrations of acetaminophen or cyclophosphamide were electrolyzed. The most efficient amperostatic conditions were chosen for toxicity testing (20 mA at graphite). The use of a Ti/RuO_2 anode, along with potentiostatic conditions, was excluded from this experiment because of poor performance (table 1). Samples (2.0 ml) were collected after 15 and 30 minutes of electrolysis time. Confluent cells plated at a density of 5000 cells/100 µl growth medium were treated with 50 µl electrolysate; 150 µl total volume. After 24 hours exposure time (at 37 °C, 5% CO_2), 20 µl MTS reagent was added to the cells and incubated for 2 hours; absorbance was read at 490 nm. Treatments and assay were performed in triplicate. A solution of electrolyzed 25 mM sodium sulfate served as a control for electrolysis and showed no significant toxicity relative to naive controls (50 µl mQ water; figure 31). Microscopic inspection of cells verified non-toxic responses, as spindle-shaped and confluent cells were observed.

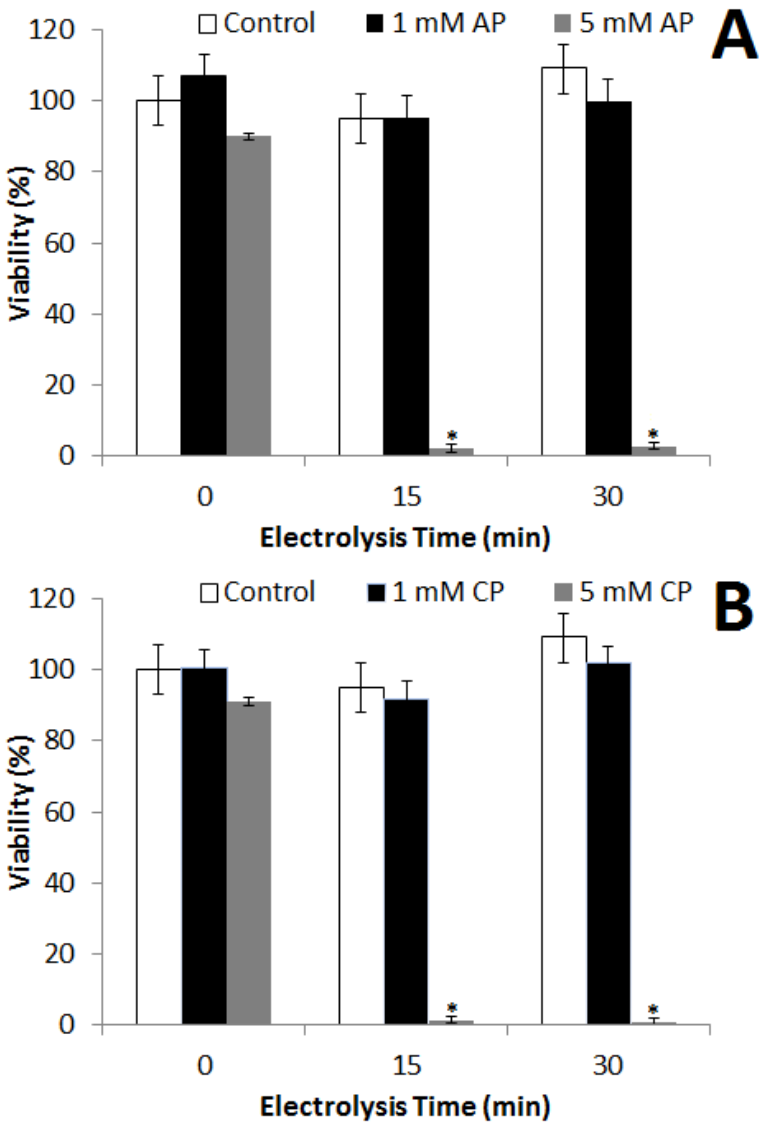

Figure 31. Response of EMT-6 cells treated with electrolyzed solutions of acetaminophen (AP) and cyclophosphamide (CP). Solutions (1 and 5 mM) were electrolyzed at 20 mA, for 30 minutes, at a graphite anode. Electrolysis took place in a divided batch cell with a solution volume of 50.0 ml, and 25 mM Na_2SO_4 as supporting electrolyte. Control: 25 mM Na_2SO_4. Confluent cells, plated at a concentration of 5000 cell/100 µl, were then incubated for 24 hours with 50.0 µl electrolyzed solution. Cell viability was assessed with a 2 hour incubation of 20.0 µl MTS reagent. Absorbance was read at 490 nm. Percent viability is corrected relative to untreated cells (50.0 µl mQ water). *: $p < 0.01$ via student t-test.

One millimolar concentrations of acetaminophen or cyclophosphamide did not produce toxic electrolysates; cells were spindle-shaped and confluent under microscope, visually confirming a lack of lethality (figure 31). Sample dilution by a factor of 1:3 is believed to have caused this result; correcting for dilution gives a concentration of 300 µM starting prodrug administered. Since the 15 minute electrolyses are toxic, and the 414 µM is only reached at ~ 12 min (table 1), detoxification by GSH in the growth medium is considered to be unlikely, as otherwise, cell response would be expected to be greater, i.e., if detoxification occurs more cells would survive. Higher starting concentrations of prodrug (5 mM) were non-toxic to cells with respect to both acetaminophen and cyclophosphamide (figure 31); corrected for dilution, this gave a maximal concentration of 1.6 mM prodrug administered. Only electrolyzed solutions of 5 mM prodrug produced significant toxicity for both acetaminophen and cyclophosphamide, killing >97% of cells relative to untreated controls at both 15 and 30 minutes electrolysis time (figure 31). Visual inspection presented cells which were round in shape, speckled in complexion, and retracted from adjacent cells for both compounds. Despite the previously discussed analytical issues with cyclophosphamide, its electrochemical oxidation products are toxic. The hypothesis and concept of prodrug electrochemical toxication works for both acetaminophen and cyclophosphamide.

Figure 32 represents an attempt to set the results of these batch reactor toxicity experiments in the context of the probit curve produced in figure 21. Note that the figure is plotted as a function of corrected benzoquinone concentration. The toxicity of electrolyzed solutions of acetaminophen follows closely with benzoquinone toxicity. This suggests that there are no synergistic effects occurring between benzoquinone and acetaminophen in solution; i.e., one would expect to see a difference in the electrolyzed solution's toxicity from that of the probit curve. For example, if the electrolyzed acetaminophen solution was more potent than benzoquinone alone, this would be reflected as a data point appearing at lower concentrations than the probit curve at the same probit value. Similarly, if acetaminophen (or other oxidation products) were somehow detoxifying the electrochemically produced benzoquinone, the data point

would appear at a higher concentration than the probit curve at the same probit value. In this way, toxicity of electrolyzed solutions can be directly compared against the probit of a standard chemotherapeutic regime. Electrolyzed solutions which are more potent than chemical counterparts (e.g., electrolyzed vs. unelectrolyzed cyclophosphamide) can be further developed as treatments for cancer, allowing one to screen compounds for which electrolytic activation provides an advantage.

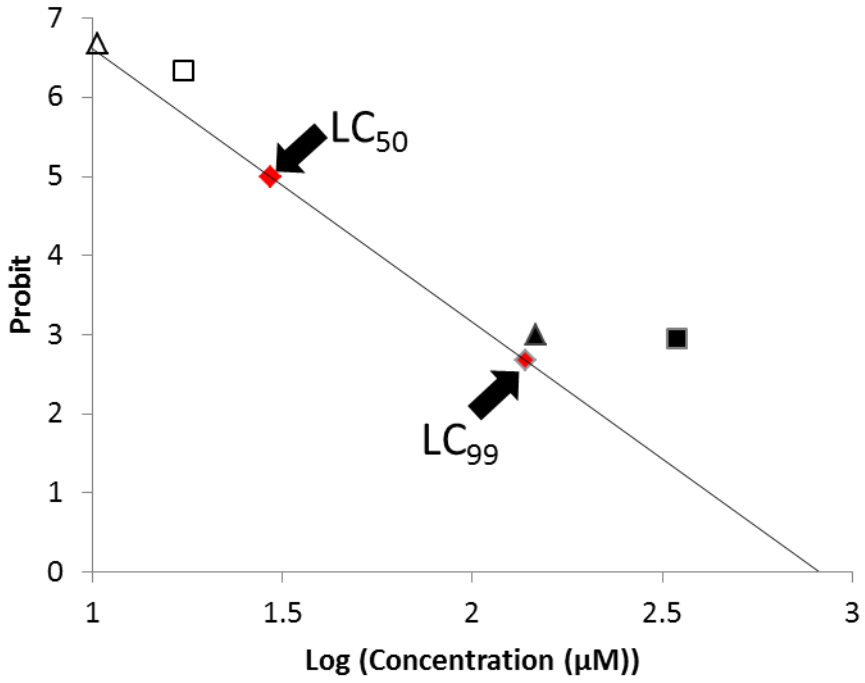

Figure 32. Comparison of electrolyzed solutions of acetaminophen with benzoquinone's chemical toxicity. Benzoquinone concentrations obtained from experiments described in figure 31 are superimposed over a modified figure 21 insert. For comparison, benzoquinone's IC_{50} and IC_{99} are highlighted on the chart with arrows. The line represents the probit equation from figure 21: y = -3.935x + 10.575. Open shapes: starting concentration of 1 mM acetaminophen; filled shapes: starting concentration of 5 mM acetaminophen. Triangles: 15 min electrolysis time; squares: 30 min electrolysis time. Data presented are benzoquinone concentrations after administration of effluent to EMT-6 cells and have been corrected for assay dilution.

From figure 32, the initial 1 mM acetaminophen concentration did not produce enough benzoquinone to reach the IC_{50} after 30 minutes of electrolysis time (empty symbols). The 5 mM concentration of acetaminophen produced levels of benzoquinone which were on par with the IC_{99} after 15 minutes (solid symbols). At high acetaminophen concentration (5 mM) and long electrolysis time (30 min), the linearity of the model no longer fits; as seen in figure 21. This deviation is due to the diminished resolution of the MTS assay and the sigmoidal nature of the probit function at high responses. There is good toxicological agreement between the chemical and electrochemically-produced benzoquinone.

5.8 Flow Cell Design and Construction

The foregoing experiments suggest that electrochemical toxication for treating cancer is at least a viable concept during batch electrolyses. However, a flow system is more compatible with the delivery of effluent to a tumor than a batch cell; a batch cell's electrolysate has no direct access to a patient and would require a transfer step from batch cell to tumor. On the other hand, effluent from a flow cell can be delivered to a target site while remaining within the electrolytic system. In other words, a flow system decreases the possibility that active oxidation products will be destroyed by reaction between formation and injection. For prodrugs which produce short lived toxicants, oxidation can be kept close to the tumour in terms of both residency time and physical distance. A flow cell was constructed to help simulate a piece of medical technology in which one can continuously deliver the activated toxicant to a tumour.

The flow cell design used in this thesis is a modified version from Miner and Kissinger (1979; figure 33, 34). The original design was divided with a piece of Vycor® glass; a porous, inert material ideally suited to electrochemical purposes. Unfortunately, due to a combination of rarity and cost, the material was not obtained. Other porous materials were considered, such as ceramics and plastics, but ultimately a reusable dialysis device was chosen. The 0.5 kDa Spectra/Por Float-A-Lyzer G2 dialysis device is a self-contained esterified cellulose membrane. The plastic base was well suited for

providing membrane rigidity as well as serving as an attachment point to the rest of the cell. A 1.0 ml capacity model was chosen to serve as the size of the anodic chamber. A 2.0 mm diameter hole was drilled into the center of the base to allow effluent flow, and the device was then set into a Plexiglas cube (50 cm^3). The cathodic chamber (cube) was non-circulating; there were no conductivity issues arising from exhausted catholyte because of the large volume compared with the anolyte. A titanium wire was used as the cathode and had been wrapped, in a helical fashion, around the separating membrane; this was done to minimize resistance during electrolysis. To control flow rate, a portion of a Luer-lok syringe was fastened to the bottom of the Plexiglas cell, in line with the previously drilled hole. This served as a convenience measure for exchanging needle tips.

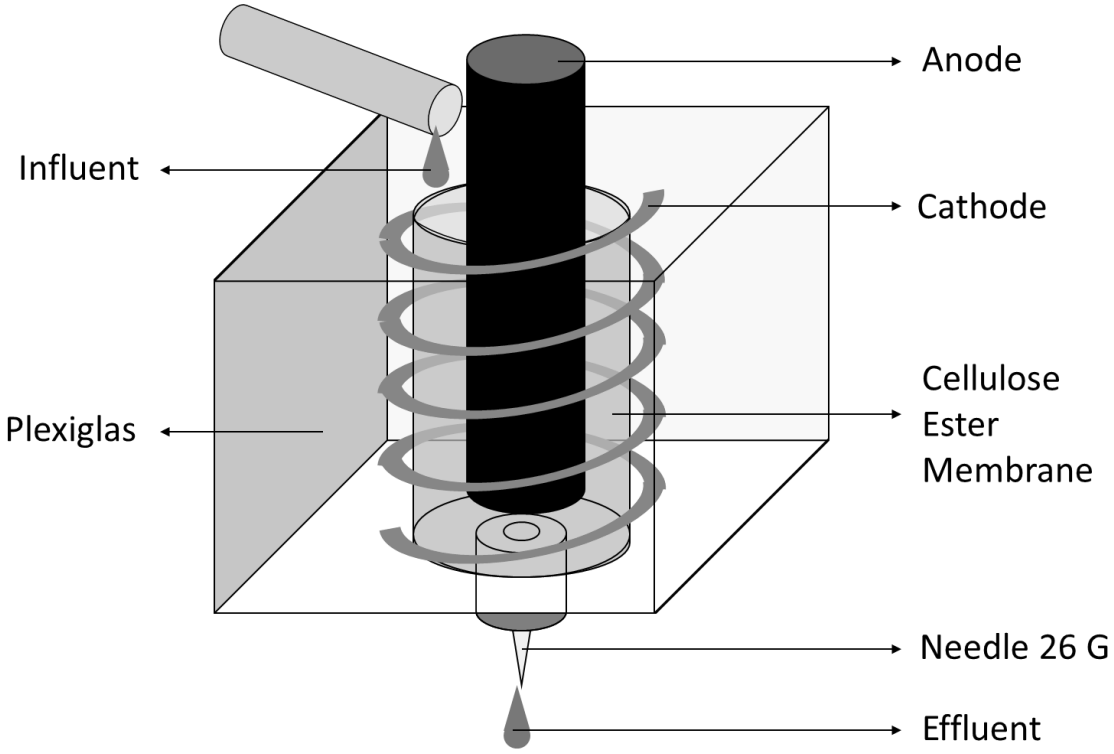

Figure 33. Flow cell diagram. Dimensions: 3.0 x 3.6 x 4.7 cm; total volume: 50.76 cm^3; anode chamber volume: 1.0 ml. Effluent droplet size: 5.5 ± 0.2 µl.

Needle tips were chosen to control flow rate as they would produce uniformly sized drops of effluent, based on their diameter. A 26 gauge needle, which controlled

flow rate of the finished cell, consistently produced 5.5 ± 0.2 mg droplets of effluent (5.5 ± 0.2 µl). Other sized needles were initially used, but proved to be ineffective. With larger bores, the flow rate was too fast to maintain cell volume; with smaller bores, restriction was too great to overcome gravity (i.e., no flow). Flow rate was measured during each experiment by collecting 5.0 ml of effluent in a volumetric flask and averaging with respect to time. Flow rate was found to be affected by current and anode between experiments (see Section 5.10).

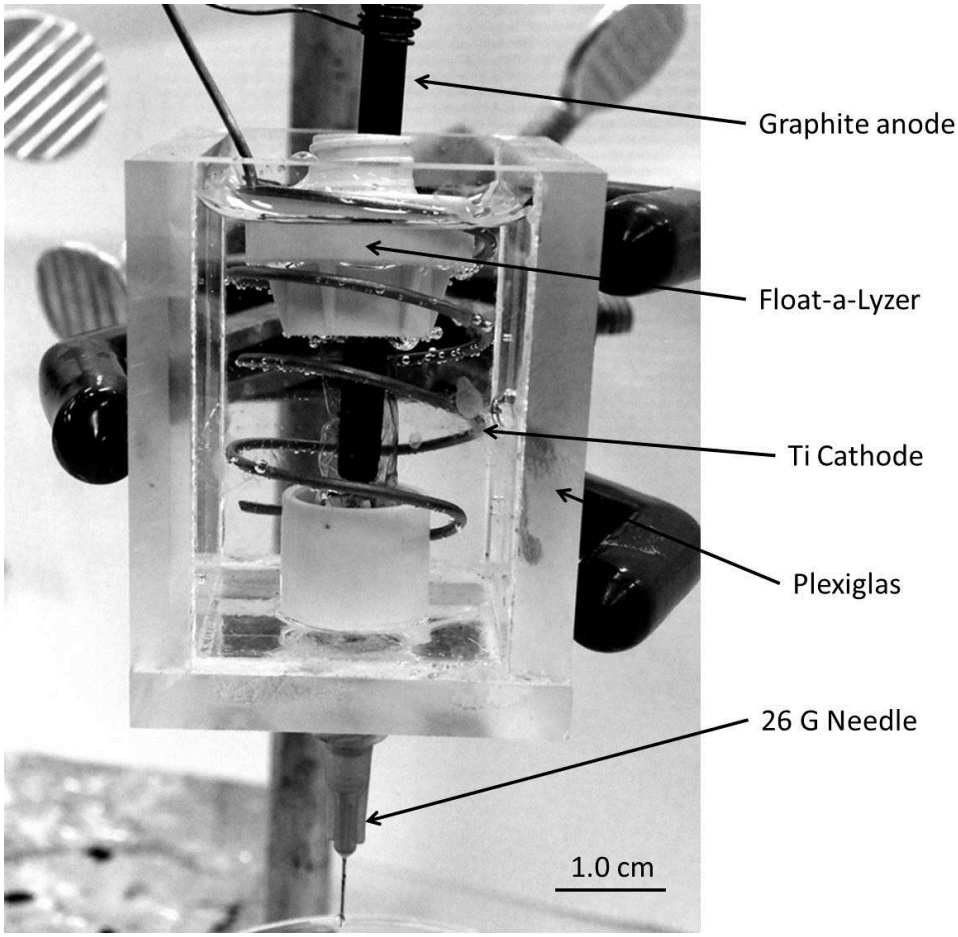

Figure 34. Photograph of constructed flow cell.

Rather than being driven by a peristaltic pump, the constructed cell's flow rate was gravity driven and restriction controlled. This was done as a convenience to anode changing and cleaning between experiments as the cell was not enclosed. The diameter of the anodic chamber was 1.0 cm, which limited anode size to 0.4 cm in diameter; any

larger and the solution did not flow. Larger anodes took up too much cell volume, decreasing the space that could be occupied by solvent. Since the cell's flow is gravity driven, a minimum water pressure of ~18 mg/mm^2 was needed to push effluent out of the needle and produce flow.

Anodes used in the flow cell were 0.40 cm in diameter and were fabricated from either graphite or Ti/RuO_2. Submerged anodic surface area was calculated to be 4.7 cm^2 for the graphite rod, and 3.2 cm^2 for the Ti/RuO_2 plate. For a comparison with batch cell electrodes see table 2. The cellulose-ester dividing membrane performed well during the course of initial electrolyses; there was no deterioration or leaking. Effluent pH values ranged from 3.0 to 3.5, similar to batch cell results.

Table 2. Electrode surface areas and current densities used for flow and batch systems

Anode	Cell	Submerged Surface Area (cm^2)	Current (mA)	Current Density (mA/cm^2)
Graphite	Batch	20.0	20.0	1.0
	Flow	4.7	5.0	1.1
Ti/RuO_2	Batch	5.3	20.0	3.8
	Flow	3.2	5.0	1.6

5.9 Toxicity of Flow Cell Effluent

Flow cell effluent toxicity was assessed using amperostatic conditions. Concentrations of 1 and 5 mM acetaminophen or cyclophosphamide were electrolysed for one hour at 5 mA with a graphite anode (Ti/RuO_2 absence discussed below). This was to ensure that steady state concentrations of effluent had been reached and that the cell was performing adequately. Once again, 25 mM sodium sulfate electrolyzed under the same conditions served as a control (effluent pH: 3.5). No toxicity was observed due to acidic pH; the growth medium had sufficient buffering capacity. The flow rate of the cell was measured at 230 µl/min; residency time was calculated at 4.35 minutes. 1.0 ml samples of steady state effluent were collected and cells were exposed to 50 µl effluent for 24 hours (see Section 4.2.6). As with the batch electrolyses, effluents containing 1 mM of either prodrug did not significantly affect cell viability; though, the 1 mM solution

of cyclophosphamide did produce a non-significant decrease (figure 35). The higher (5 mM) concentration of acetaminophen produced similar effluent cytotoxicity to the batch cell (97% reduction of cell viability; figure 35). While the 5 mM cyclophosphamide solution did produce significant cytotoxicity, there remained 12% of cells that were viable after 24 hours. Visual inspection confirmed small colonies of spindle-shaped, adherent EMT-6 cells, possibly representing cell subpopulations of treatment-resistant cells. These results suggest that cyclophosphamide activation in the flow cell is not as effective as in the batch reactor. Similar to the batch cell, acetaminophen and cyclophosphamide precursors can be used to generate toxicologically significant effluents in a flow cell.

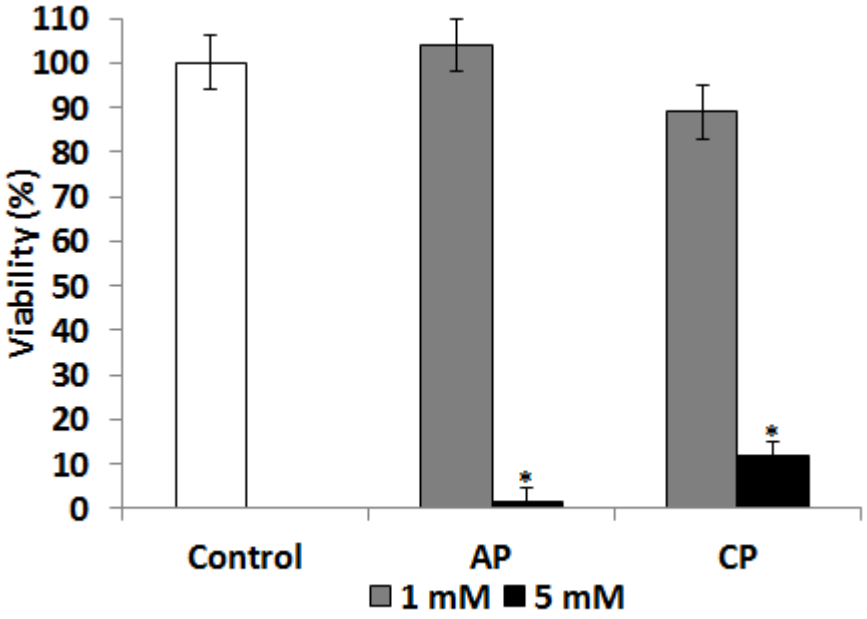

Figure 35. EMT-6 cell viability 24 hours after exposure to 50 µl electrolyzed flow cell effluent. 1 mM and 5 mM concentrations of acetaminophen (AP) or cyclophosphamide (CP) were electrolyzed at 5 mA, for 60 minutes, at a graphite anode (d = 0.40 cm). Electrolysis took place in a divided flow cell and 25 mM Na_2SO_4 as supporting electrolyte. Control: 25 mM Na_2SO_4. Confluent cells, plated at a concentration of 5000 cell/100 µl, were then incubated for 24 hours with 50.0 µl electrolyzed solution. Cell viability was assessed after 2 hour incubation with 20.0 µl MTS reagent. Absorbance was read at 490 nm. Percent viability is corrected relative to untreated cells (50.0 µl mQ water). *: $p < 0.05$.

5.10 Limitations of the Constructed Flow Cell

The design of the flow cell proved successful from a toxicological standpoint; however, performance-related issues appeared upon further experimentation. It was found that current density was a major factor in determining flow rate. Initial kinetic experiments conducted at 10-20 mA, prior to toxicity testing, saw erratic rates of flow and substrate oxidation. This erratic behaviour was attributed to formation of oxygen bubbles at high current densities. Recall that at graphite in the batch cell, it was possible

to avoid O_2 production, but due to high current densities, it was not possible to avoid bubble formation in this cell. Essentially, during the electrolysis, bubbles would become lodged in certain locations within the cell, causing backflow. Underneath the anode, and between the dividing membrane and the anode, were two locations prone to bubble stagnation. After time, these trapped bubbles would grow sufficiently large to dislodge themselves, floating to the chamber surface (figure 36, pg. 83). This liberated anode surface for oxidation and restored original flow rate. This process would repeat several times during electrolyses and prevented the formation of a steady state effluent. With a current of 10 mA, the cell would stop functioning after approximately 40 minutes of electrolysis time. However, by decreasing the current to 5 mA, bubble formation was decreased significantly enough to prevent this effect from happening for at least 6 hours. Because of the low overpotential for water oxidation at Ti/RuO_2 anodes, this described process was accelerated to such an extent that the anode was deemed unusable in this cell.

In addition to issues of oxygen evolution, higher current densities caused the graphite anode to decompose. Anode degradation became increasingly accelerated as currents were increased from 10 mA to 20 mA, a phenomenon previously investigated by Rueffer *et al.* (2011). Reuffer *et al.* (2011) report significant mass loss (>1.1 g C) of graphite anodes in the presence of sulfate ion, compared with sodium hydroxide, chloride, and bromide electrolytes. In short, accumulated anode particulate clogged the bore of the needle and caused the anodic compartment to overflow. It was determined that a maximal current of 10 mA could be applied to this cell without significant anode degradation occurring. The small graphite anode used in the flow cell essentially limited applied currents to a maximum of 5 mA. On a positive note, a current of 5 mA was all that was needed to produce toxic effluents of both acetaminophen and cyclophosphamide.

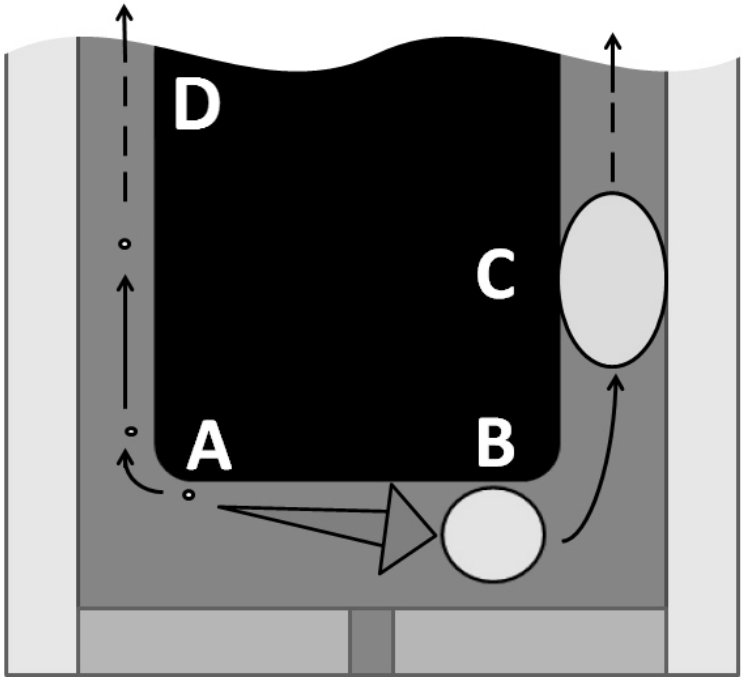

Figure 36. Generation of erratic flow by anodic oxygen production. A-D: small oxygen bubbles produced at the anode surface rise to the top of the chamber in an unimpeded manner. A-B: small oxygen bubbles produced at the bottom face of the anode become trapped and accumulate in size. B-C: sufficiently large bubbles which formed underneath the anode (A-B) become liberated and float to the surface. Occasionally these liberated bubbles will be very large and will become wedged between the dividing membrane and the anode's surface. Wedged bubbles decrease surface area and alter oxidation rate and solvent flow.

Chapter Six: Conclusions

The aim of this thesis was to provide a proof-of-concept for an electrochemical system that is capable of producing cytotoxic concentrations of a toxicant from non-toxic precursors; and, to show that said compounds can be used therapeutically against cancer cell lines.

The electrochemical oxidation of both acetaminophen and cyclophosphamide produced electrolyzed solutions that were cytotoxic against EMT-6 cells at the IC_{99} level (after dilution with growth medium). Both graphite and Ti/RuO_2 anodes were capable of producing toxicant species from cyclophosphamide and acetaminophen; the presence of a high overpotential for water oxidation at graphite made it the superior anode. The low overpotential for water oxidation at Ti/RuO_2 prohibited use in the flow reactor. In terms of toxicant yield and rate of formation, graphite was the preferred anode with respect to acetaminophen electrolyses. From what could be discerned from cyclophosphamide electrolyses, both graphite and Ti/RuO_2 anodes performed equally in terms of rate of formation and yield of presumed toxicant. Amperostatic electrolyses conducted in batch and flow systems were capable of producing equivalent toxicity with respect to acetaminophen and cyclophosphamide. Overall, current-controlled amperostatic electrolyses at graphite, where the substrate had a high starting concentration, were the most favourable conditions for substrate activation and cytotoxicity.

The use of cyclophosphamide and acetaminophen as model compounds was appropriate for this thesis, despite certain short comings associated with these agents. Both cyclophosphamide and acetaminophen were chosen as model substrates because they are oxidatively activated *in vivo* to cytotoxic compounds, yet elicit decreases in cell viability by invoking different mechanisms of cytotoxicity. These compounds are considered successful because only their electrolyzed solutions produced toxicity in EMT-6 cells. Quantitative and qualitative identification of cyclophosphamide oxidation products proved to be an area of severe analytical difficulty, however, identification of

these products was secondary to the goals of the thesis and do not exclude further study of this compound within the context of the thesis. In terms of acetaminophen, the stability and potency of benzoquinone contributed to its toxicity; not the primary oxidation product NAPQI, as originally thought. Although NAPQI is responsible for acetaminophen toxicity *in vivo*, it contributes no role here other than to serve as an intermediate for benzoquinone formation. Contrary to the allusion in Section 1.2, the use of short-lived toxicants, such as NAPQI, does not appear as a viable subject area for further research; however, the use of non-DNA alkylating toxicants, such as benzoquinone, does. The production of toxicants, different from the classic DNA-damaging agents that target proliferating cells, appears to be a promising avenue for further research into localized cancer treatments.

Discounting the generation and use of short-lived toxicants as a treatment option, a serious question is raised, 'What benefit, if any, does electrochemical activation have over pre-existing localized techniques;' considering, chemically stable toxicants can be injected into a tumour without the need for electrochemical activation? To this end, one would argue, that the arguments raised in the introduction section regarding localized and activated compound therapies (e.g., photodynamic therapy) still apply to toxicants produced through oxidative P450 bioactivation, i.e., the electrochemical activation of prodrugs might be a novel and useful method of causing toxicity in tumour cells which usually lack the P450 enzymes to generate the toxicants themselves. This thesis provides a unique method of activating compounds which current treatment methods do not take advantage. As seen through experimentation, no effect was observed between acetaminophen or cyclophosphamide and EMT-6 cell viability. Decreases in cell viability were only observed once electrolyzed solutions were administered; these results indicate that intra-tumour injection of these drugs would be ineffective *in vivo*, as EMT-6 lacks the enzymes to activate said compounds. By mimicking P450 activation, electrooxidation can be used to activate compounds in tissues where the enzymes are absent. The site specific approach of drug administration allows the use of toxicants whose mechanism of action does not involve cellular

replication (e.g., benzoquinone). Further investigation into cancer survival when cells are treated with non-mitotic versus mitotic toxicants is required.

Regarding the general feasibility and applicability of this thesis at the clinical level, one potential advantage of this method over existing ones is the cost. It is feasible and inexpensive to design a flow cell to generate toxicants in a clinical setting, whereby the drug can be immediately administered directly into the tumor of a patient. This can be particularly useful for the treatment of early stage tumors were minimally invasive approaches are desired and have a higher probability of success.

As this thesis's concept is still in preliminary stages of research, defining the depth of its applicability is more important than knowing its breadth. Knowing, through experimentation, whether or not the ideas contained within this thesis provide extended survivability *in vivo* (depth of subject) is the true proof-of-concept. Growing tumors *in vivo* introduces several complicating variables that could never be achieved as a whole *in vitro*; factors such as intratumor blood flow, angiogenesis, immunosurveillance and immune response, signalling relationships between interstitial growth factors, homeostasis, etc., etc.. An *in vitro* model is simply not dynamic enough to simultaneously address all of these factors. Progression of localized electrochemical activation, in general, into a true cancer treatment, will require the use of animal models. The preliminary results contained in this document have identified an area of research which has not yet been addressed in the medical or scientific communities. This thesis has been shown successful as a proof-of-concept.

"It's a big part of writing a thesis, being able to communicate and understand things; being able to communicate *that* you understand things."

- *Jordache Boudreau*

References

Canadian Cancer Society's Steering Committee on Cancer Statistics (Canadian Cancer Society). (2011). *Canadian Cancer Statistics 2011*. Toronto, ON: Canadian Cancer Society.

Al-Hajj M, Benito-Hernandez A, Morrison SJ, Clarke MF. (2003). Prospective identification of tumorigenic breast cancer cells. *Proceedings of the National Academy of Sciences*. **100**: 3983-3988.

Alothman AZ, Buhkari N, Wabaidur SM, Haider S. (2010). Simultaneous electrochemical determination of dopamine and acetaminophen using multiwall carbon nanotubes modified glassy carbon electrode. *Sensors and Actuators B: Chemical*. **146**: 314-320.

National Cancer Institute. PDQ® Colon Cancer Treatment. Bethesda, MD: National Cancer Institute. Date last modified: 27/03/2012. Available at: <http://cancer.gov/cancertopics/pdq/treatment/colon/HealthProfessional>. Date last Accessed: 02/04/2012.

Andersson DA, Gentry C, Alenmyr L, Killander D, Lewis SE, Adnersson A, Bucher B, Galzi JL, Sterner O, Bevan S, Hogestatt ED, Zygmunt PM. (2011). TRPA1 mediates spinal antinociception induced by ancetaminophen and the cannabinoid delta-9-tetrahydrocannabiorcol. *Nature Communications*. **2**: 1-11.

Anundi I, Lahteenmaki T, Rundgren M, Moldeus P, Lindros KO. (1993). Zonation of acetaminophen metabolism and cytochrome P450 2E1-mediated toxicity studies in isolated periportal and perivenous hepatocytes. *Biochemical Pharmacology*. **45**: 1251-1259.

Bao L, Xiong R, Wei G. (2010). Electrochemical polymerization of phenol on 304 stainless steel anodes and subsequent coating structure analysis. *Electrochimica Acta*. **55**: 4030-4038.

Baumann A, Lohmann W, Schubert B, Oberarcher H, Karst U. (2009). Metabolic studies of tetrazepam based on electrochemical simulation in comparision to *in vivo* and *in vitro* methods. *Journal of Chromatography A*. **1216**: 3192-3198.

BC Cancer Agency Breast Tumour Group. (2001). BCCA Protocol summary for adjuvant therapy for breast cancer using cyclophosphamide, doxorubicin and fluorouracil (BRAJCAF). Vancouver: BC Cancer Agency.

Beltramo M, Steall Nm Calignano A, Lin SY, Makriyannis A, Piomelli D. (1997). Functional role of high-affinity anandamide transport, as revealed by selective inhibition. *Science*. **277**: 1094-1097.

Berridge MV, Tan AS. (1993). Characterization of the cellular reduction of 3-(4,5-dimethylthiazol-2-yl)-2,5-diphenyltetrazolium bromide (MTT): Subcellular localization, substrate dependence, and involvement of mitochondrial electron transport in MTT reduction. *Archives of Biochemistry and Biophysics.* **303**, 474–82.

Bertolini A, Ferrari A, Ottani A, Guerzoni S, Tacchi R, Leone S. (2007). Paracetamol: new vistas of an old drug. *CNS Drug Reviews*. **12**: 250-275.

Bohnenstengel F, Hofmann U, Eichelbaum M, Kroemer HK. (1996). Characterization of the cytochrome P450 involved in side-chain oxidation of cyclophosphamide in humans. *European Journal of Clinical Pharmacology.* **51**: 297-301.

Bond GR. (2009). Acetaminophen protein adducts: a review. *Clinical Toxicology*. **47**: 2-7.

Borner K, Kisro J, Bruggemann SK, Hagenah W, Peters SO, Wagner T. (2000). Metabolism of ifosfamide to chloroacetaldehyde contributes to antitumor activity *in vivo*. *Drug Metabolism and Disposition* **28**: 573-576.

Boudreau J, Bejan D, Li S, Bunce NJ (2010 A). Competition between electrochemical advanced oxidation and electrochemical hypochlorination of sulfamethoxazole at a boron-doped diamond anode. *Industrial Engineering and Chemistry Research.* **49**: 2537-2542.

Boudreau J, Bejan D, Bunce NJ. (2010 B). Competition between electrochemical advanced oxidation and electrochemical hypochlorination of acetaminophen at boron-doped diamond and ruthenium dioxide based anodes. *Canadian Journal of Chemistry.* **88**: 418-425.

Bracey MH, Hanson MA, Masuda KR, Stevens RC, Cravatt BF. (2002). Structural adaptations in a membrane enzyme that terminates endocannabinoid signalling. *Science*. **298**: 1793-1796.

Brade WP, Herdrich K, Varini M. (1985). Ifosfamide- pharmacology, safety and therapeutic potential. *Cancer Treatment Reviews.* **12**: 47.

Brock N. (1989). Oxazaphosphorine cytostatics: Past-present-future. *Cancer Research* **49**: 1-7.

Brock N. (1998). The history of oxazaphosphorine cytostatics. *Cancer*. **78**: 542-547.

Chang TKH, Weber GF, Crespi CL, Waxman DJ. (1993). Differential activation of cyclophosphamide and ifosphamide by cytochromes P450 2B and 3A in human liver microsomes. *Cancer Research.* **53**: 5629–5637.

Chang TKH, Yu L, Maurel P, Waxman DJ. (1997). Enhanced cyclophosphamide and ifosfamide activation in primary human hepatocyte cultures: Response to cytochrome P450 inducers and autoinduction by oxazaphosphorines. *Cancer Research.* **57**: 1946-1954.

Chatterjee D, Liu CJT, Northey D, Teicher BA. (1995). Molecular characterization of the in vivo alkylating agent resistant murine EMT-6 mammary carcinoma tumors. *Cancer Chemotherapy and Pharmacology*. **35**: 423-431.

Cummings J, MacLellan A, Smyth JF. (1991). Determination of reactive nitrogen mustard anticancer drugs in plasma by high-performance liquid chromatography using derivatization. *Anaytical Chemistry.* **63**: 1514-1519.

Dahlin DC, Miwa GT, Lu AYH, Nelson SD. (1984). N-Acetyl-p-benzoquinone imine: A cytochrome P-450-mediated oxidation product of acetaminophen. *Proceedings of the National Academy of Sciences.* **81**: 1327-1331.

DeBerardinis RJ, Lum JJ, Hatzivassiliou G, Thompson CB. (2008). The biology of cancer: metabolic reprogramming fuels cell growth and proliferation. *Cell Metabolism*. **7**: 11-20

Devane WA, Hanus L, Breuer A, Pertwee RG, Stevenson LA, Griffin G, Gibson D, Mandelbaum A, Etinger A, Mechoulam R. (1992). Isolation and structure of a brain constituent that binds to the cannabinoid receptor. *Science*. **258**: 1946–1949.

Ding X, Kaminsky LS. (2003). Human extrahepatic cytochrome P450: function in xenobiotic metabolism and tissue-selective chemical toxicity in the respiratory and gastrointestinal tracts. *Annual Reviews in Pharmacoogy and Toxicology*. **43**: 149-173.

Dunst J, Stadler P, Becker A, Lautenschlager C, Pelz T, Hansgen G, Molls M, Kuhnt T. (2003). Tumour volume and tumor hypoxia in head and neck cancers: The amount of the hypoxic volume is important. *Strahlentherapie und Onkologie.* **179**: 521-526.

Eggermont AMM, de Witt JHW, ten Hagen TLM. (2001). Current uses of isolated limb perfusion in the clinic and a model system for new strategies. *Lancet Oncology*. **4**: 429-437.

Fegley D, Kathuria S, Mercier R, Li C, Goutopoulos A, Makriyannis A, Piomelli D. (2004). Anandamide transport is independent of fatty-acid amide hydrolase activity and is blocked by the hydrolysis-resistant inhibitor AM1172. *Proceedings of the National Academy of Sciences*. **101**: 8765-8761.

Fierro S, Nagel T, Baltruschat H, Comninellis C. (2007). Investigation of the oxygen evolution reaction on Ti/IrO_2 electrodes using isotope labeling and on-line mass spectrometry. *Electrochemistry Communications*. **9**: 1969-1974.

Gavva NR, Treanor JJS, Garami A, Fang L, Surapaneni S, Akrami A, Alvarez F, Bak A, Darling M, Gore A, Jang GR, Kesslak JP, Ni L, Norman MH, Palluconi G, Rose MJ, Salfi M, Tan E, Romanovsky AA, Banfield C, Davar G. (2008). Parmacological blockade of the vanilloid receptor TRPV1 elicits marked hyperthermia in humans. *Pain*. **136**: 202-210.

Ghavam Baigi M, Brault L, Neguesque A, Beley M, El Hilali R, Gauzere F, Bagrel D. (2007). Apoptosis/necrosis switch in two different cancer cell lines: Influence of benzoquinone- and hydrogen peroxide-induced oxidative stress intensity, and glutathione. *Toxicology in vitro*. **22**: 1547-1554.

Ghoreishi SM, Behpour M, Sadeghzadeh S, Golestaneh M. (2011). Electrochemical determination of acetaminophen in different pharmaceutical forms with gold nanoparticles carbon paste electrode. *Acta Chimica Slovenica*. **58**: 69-74.

Giraud B, Herbert G, Deroussent A, Veal GJ, Vassal G, Paci A. (2010). Oxazaphosphorines: new therapeutic strategies for an old class of drugs. *Expert Opinions On Drug Metabolism and Toxicology.* **6**: 919-938.

Gregus Z, Madhu C, Klassen CD. (1988). Species variation in toxication and detoxication of acetaminophen in vivo: a comparative study of biliary and urinary excretion of acetaminophen metabolites. *Journal of Pharmacology and Experimental Therapeutics.* **244**: 91-99.

Hemminki K. (1985). Binding of metabolites of cyclophosphamide to DNA in a rat liver microsomal system and *in vivo* mice. *Cancer Research.* **45**: 4237-4243.

Hillard EA, Caxio de Abreu F, Melo Ferreria DC, Jaouen G, Goulart MOF, Amatore C. 2008. Electrochemical parameters and techniques in drug development, with an emphasis on quinones and related compounds. *Chemical Communications*. **23**: 2612-2628.

Hinz B, Cheremina O, Brune K. (2008). Acetaminophen is a selective cyclooxygenase-2 inhibitor in man. *Journal of the Federation of American Societies for Experimental Biology*. **22**: 383-390.

Hogestatt ED, Jonsson BAG, Ermund A, Andersson DA, Bjork H, Alexander JP, Cravatt BF, Basbaum AI, Zygmunt PM. (2005). Conversion of acetaminophen to the bioactive N-acylphenolamine AM404 via fatty acid amide hydrolase-dependent arachidonic acid conjugation in the nervous system. *The Journal of Biological Chemistry*. **280**: 31405-31412.

Holden SA, Emi Y, Kakeji Y, Northy D, Teicher BA. (1997). Host distribution and response to antitumor alkylating agents for EMT-6 tumour cells from subcutaneous tumor implants. *Cancer Chemotherapy and Pharmacology*. **40**: 87-93.

Hubert JJ. (1992). Bioassay 3rd ed. Kendall/Hunt Publishing Company. Dubuque, Iowa. ISBN: 0840368496.

Huitema ADR, Mathot RAA, Tibben MM, Rodenhuis S, Beijnen JH. (2001). A mechanism-based pharmacokinetic model for the cytochrome P450 drug-drug interaction between cyclophosphamide and thioTEPA and the autoinduction of cyclophosphamide. *Journal of Pharmacokinetics and Pharmacodynamics.* **28**: 211-230.

Huitema ADR, Tibben MM, Kerbusch T, Jantien Kettenes-van den Bosch J, Rodenhuis S, Beijnen JH. (2000). Simple and selective determination of the cyclophosphamide metabolite phosphoramide mustard in human plasma using high-performance liquid chromatography. *Journal of Chromatography B*. **745**: 345-355.

Hwang J, Adamson C, Butler D, Janero DR, Makriyannis A, Bahr BA. (2009). Enhancement of endocannabinoid signaling by fatty acid amide hydrolase inhibition: A neuroprotective therapeutic modality. *Life Sciences.* **86**: 615-623.

Jurva U, Holmen A, Gronberg G, Masimirembwa C, Weidolf L. (2008). Electrochemical generation of electrophilic drug metabolites: characterization of amodiaquine, quinoneimine and cysteinyl conjugates by MS, IR, and NMR. *Chemical Research in Toxicology*. **21**: 928-935.

Jurva U, Wikstrom HV, Weidolf L, Bruins AP. (2003). Comparison between electrochemistry/mass spectrometry and cytochrome P450 catalyzed oxidation reactions. *Rapid Communications in Mass Spectrometry.* **17**: 800-810.

Kapalka A, Foti G, Comninellis C. (2007). Investigations of electrochemical oxygen transfer reaction on boron-doped diamond electrodes. *Electrochimica Acta.* **53**: 1945-1961.

Kensler TT, Behme RJ, Brooke D. (1978). High-performance liquid chromatographic analysis of cyclophosphamide. *Journal of Pharaceutical Sciences.* **68**: 172-174.

Kerbusch T, Herben VMM, Jeuken MJJ, Ouwerkerk J, Keizer HJ, Beijnen JH. (2001). Distribution of ifosfamide and metabolites between plasma and erythrocytes**.** *Biopharmaceutics and Drug Disposition***. 22:** 99-108**.**

Langley SEM, Laing R. (2002). Prostate brachytherapy has come of age: a review of the technique and results. *British Journal of Urology International*. **89**: 241-249.

Larson AM, Polson RJ, Fontana RJ, Lalani E, Hynan LS, Reisch JS, Schiodt FV, Ostapowicz G, Shakil AO, Lee WM. (2005). Acetaminophen-indiced actue liver failure: results of a United States multicenter, prospective study. *Hepatology*. **42**: 1364-1372.

Lester D, Greenber LA. (1947). The metabolic fate of acetanilide and other aniline derivative; major metabolites of acetanilide appearing in the blood. *Journal of Pharmacology and Experimental Therapeutics*. **90**: 68-75.

Lin MT. (1978). Effects of intravenous and intraventricular prostaglandin E1 on thermoregulatory responses in rabbits. *Journal of Pharmacology and Experimental Therapeutics.* **204**: 39-45.

Lindner U, Weersink WMA, Haider MA, Gertner MR, Davidson SRH, Atri M, Wilson BC, Fenster A, Trachtenberg J. (2009). Image guided photothermal focal therapy for localized prostate cancer: phase I trial. *Journal of Urology*. **182**: 1371-1377.

Lohmann W, Karst U. (2008). Biomimetic modeling of oxidative drug metabolism. *Analytical and Bioanalytical Chemistry.* **391**: 79-96.

Lohmann W, Karst U. (2006). Simulation of the detoxification of paracetamol using on-line electrochemistry/liquid chromatography/mass spectrometry. *Analytical and Bioanalytical Chemistry*. **386**: 1701-1708.

Lohr M, Bago ZT, Bergmeister H, Ceijna M, Freund M, Gelbmann W, Gunzburg WH, Jesnowski R, Hain J, Hauenstein K, Henninger W, Hoffmeyer A, Karle P, Kroger JC, Kundt G, Liebe S, Losert U, Muller P, Probst A, Puschel K, Renner M, Renz R, Saller R, Salmons B, Schuh M, Schwendenwein I, von Rombs K, Wagner T, Walter I. (1998). Cell therapy using microencapsulated 293 cells transfected with a gene construct expressing CYP 2B1, an ifosfamide converting enzyme, instilled intra-arterially in patients with advanced

stage pancreatic carcinoma: a phase I/II study. *Journal of Molecular Medicine.* **77**: 393-398.

Madsen KG, Olsen J, Skonberg C, Hansen SH, Jurva U. (2007). Development and evaluation of an electrochemical method for studying phase-I metabolites: Correlation to *in vitro* drug metabolism. *Chemical Research in Toxicology*. **20**: 821-831.

Madsen KG, Skonberg C, Jurva U, Cornett C, Hansen SH, Johansen TN, Olsen J. (2008). Bioactivation of diclofenac *in vitro* and *in vivo*: Correlation to electrochemical studies. *Chemical Research in Toxicology*. **21**: 1107-1119.

Manjunatha R, Nagaraju DH, Suresh GS, Melo JS, D'Souza SF, Venkatesha TV. (2011). Electrochemical detection of acetaminophen on the functionalized MWCNTs modified electrode using layer-by-layer technique. *Electrochimica Acta*. **56**: 6619-6627.

Marnett LJ. (1999). Lipid peroxidation-DNA damage by malondialdehyde. *Mutation Research*. **424**: 83-95.

McNeal JE, Bostwick DG, Kindrachuk RA, Redwine EA, Freiha FS, Stamey TA. (1986). Pattern of progression in prostate cancer. *The Lancet*. **327**: 60-63.

Meunier B, De Visser SP, Shaik S. (2004). Mechanism of oxidation reactions catalyzed by cytochrome p450 enzymes. *Chemical Reviews*. **104**: 3974-3980.

Michaud PA, Panizza M, Ouattara L, Diaco T, Foti G, Comninelllis C. (2003). Electrochemical oxidation of water on synthetic boron-doped diamond thin film anodes. *Journal of Applied Electrochemistry*. **33**: 151-154.

Miner JD, Kissinger PT. (1979). Evidence for the involvement of N-Acetyl-*p*-benzoquinone imine in acetaminophen metabolism. *Biochemical Pharmacology.* **28**: 3285-3290.

Monks TJ, Jones DC. (2002). The metabolism and toxicity of quinones, quinonimines, quinone methides, and quinone-thioethers. *Current Drug Metabolism*. **3**: 425-438.

Mossman T. (1983). Rapid colorimetric assay for cellular growth and survival: application to proliferation and cytotoxicity assays. *Journal of Immunological Methods*. **65**: 55-63.

Neamtollahi D, Shayani-Jam H, Alimoradi M, Niroomand S. (2009). Electrochemical oxidation of acetaminophen in aqueous solutions: Kinetic evaluation of hydrolysis, hydroxylation and dimerization processed. *Electrochimica Acta*. **54**: 7407-7415.

Nouri-Nigjeh E, Permentier HP, Bischoff R, Bruins AP. (2011). Electrochemical oxidation by square-wave potential pulses in the imitation of oxidative drug metabolism. *Analytical Chemistry*. **83**: 5519-5525.

O'Conner AE, Gallagher WM, Byrne AT. (2009). Porphyrin and nonporphyrin photosensitizers in oncology: preclinical and clinical advances in photodynamic therapy. *Photochemistry and Photobiology*. 85: 1053-1074.

Ono K, Shrieve DC. (1987). Effect of glutathione depletion by L-buthionine sulfoximine on the cytoxicity of cyclophosphamide in a single and fractionated doses to EMT-6/SF mouse tumors and bone marrow. *Journal of the National Cancer Institute*. **79**: 811-815.

Ottani A, Leone S, Sndrini M, Ferrari, Bertolini A. (2006). The analgesic activity of paracetamol is prevented by the blockade of cannabinoid CB1 receptors. *European Journal of Pharmacology*. **531**: 280-281.

Owens RB, Smith HS, Hackett AJ. (1974). Epithelial cell cultures form normal glandular tissue of mice. *Journal of the National Cancer Institute*. **53**: 261-269.

Paci A, Martens T, Royer J. (2001). Anodic oxidation of ifosfamide and cyclophosphamide: a biomimetic metabolism model of the oxazaphosphorinane anticancer drugs. *Bioorganic and Medical Chemistry Letters.* **11**: 1347-1349.

Paci A, Rieutord A, Brion F, Prognon P. (2001). Separation Methods of alkylating anti-neoplastic compounds. *Journal of Chromatography B*. **746**: 255-287.

Pine SR, Ryan BM, Varticovski L, Robles AI, Harris CC. (2010). Microenvironmental modulation of asymmetric cell division in human lung cancer cells. *Proceedings of the National Academy of Sciences*. **107**: 2195-2200.

Polcaro AM, Vacca A, Masica M, Ferrara F. (2008). Product and by-product formation in electrolysis of dulute chloride solutions. *Journal of Applied Electrochemistry*. **38**: 979-984.

Promega. (2009). CellTiter 96® AQ_{ueous} one solution cell proliferation assay technical bulletin. Part: #TB245. United States of America.

Pulen A, Boucher Y, Ramanujan S, McKee TD, Gohongi T, di Tomaso E, Brown EB, Izumi Y, Campbell RB, Berk DA, Jain RK. (2001). Role of tumor-host interactions in interstitial diffusion of macromolecules: cranial verssu subcutaneous tumors. *Proceedings of the National Academy of Sciences*. **98**: 4628-4633.

Rawls SM, Ding Z, Cowan A. (2006). Role of TRPV1 and cannabinoid CB1 receptors in AM404-evoked hypothermia in rats. *Pharmacology, Biochemistry and Behaviour*. **83**: 508-516.

Raz O, Haider MA, Davidson SRH, Lindner U, Hlasny E, Weersink R, Gertner MR, Kurcharcyzk W, McCluskey SA, Trachtenberg J. (2010). Real-time magnetic resonance imaging-guided focal laser therapy in patients with low-risk prostate cancer. *European Urology*. **58**: 173-177.

Razmi H, Habibi E. (2010). Amperometric detection of cacetaminophen by an electrochemical sensor based of cobalt oxide nanoparticles in a flow injection system. *Electrochimica Acta*. **55**: 8731-8737.

Rockwell S. (1977). *In vivo-in vitro* tumor systems: new models for studying the response of tumors to therapy. *Laboratory Animal Science.* **27**: 831-851.

Rockwell SC, Kallman RF, Fajardo LF. (1972). Characteristics of a serially transplanted mouse mammary tumor and its tissue-culture-adaptive derivative. *Journal of the National Cancer Institute*. **49**: 735-749.

Rueffer M, Bejan D, Bunce NJ. (2011). Graphite: An active or an inactive anode? *Electrochimica Acta*. **56**: 2246-2253.

Samel S, Keese M, Lux A, Jenowski R, Prosst R, Saller R, Hafner, Sturm J, Post S, Lohr M. (2006). Peritoneal cancer treatment with CYP2B1 transfected, microencapsulated cells and ifosfamide. *Gene Therapy*. **13**: 65-73.

Schmidt LE, Dalhoff K, Poulsen H. (2002). Acute versus chronic alcohol consumption in acetaminophen-induced hepatotoxicity. *Hepatology*. **35**: 876-882.

Shapiro CL, Recht A. (2001). Side effects of adjuvant treatment of breast cancer. *New England Journal of Medicine*. **344**: 1997-2008.

Shono T, Toda T, Oshino N. (1982). Electron transfer from nitrogen in microsomal oxidation of amine and amide. Simulation of microsomal oxidation by anodic oxidation. *Journal of the American Chemical Society*. **104**: 2639–2641.

Sladek NE. (1973). Bioassay and relative cytotoxic potency of cyclophosphamide metabolites generated *in vitro* and *in vivo*. *Cancer Research*. **33**: 1150-1158.

Siddiqui K, Chopra R, Vedula S, Sugar L, Haider M, Boyes A, Musquear M, Bronskill M, Klotz L. (2010). WRI-guided transurethral ultrasound therapy of the prostate gland using realtime thermal mapping: initial studies. *Urology*. **76**: 1506-1511.

Struck RF, Kirk MC, Witt MH, Russell Laster W. (1974). Isolation and mass spectral identification of blood metabolites of cyclophosphamide: evidence for phosphoramide mustard as the biologically active metabolite. *Biomedical Mass Spectrometry.* **2**: 46-52**.**

Twentyman PR. (1977). Sensitivity to cytotoxic agents of the EMT-6 tumor in vivo: tumor volume versus in vitro plating: Cyclophosphamide. *British Journal of Cancer*. **35**: 208-217.

Vaccarino AL, Paul D, Mukherjee PK, Rodruiguez de Turco EB, Marcheselli VL, Xu L, Trudell ML, Minguez JM, Matia MP, Sunkel C, Alvarez-Builla J, Bazan NG. (2007). Synthesis and in vivo evaluation of non-hepatotoxic acetaminophen analogues. *Bioorganic and Medicinal Chemistry*. **15**: 2206-2215.

Veldeman L, Madani I, Hulstaert F. (2008). Evidence behind use of intensity-modulated radiotherapy: A systematic review of comparative clinical studies. *Lancet Oncology*. **9**: 367–375. Erratum in: *Lancet Oncology.* 2008. **9**: 513.

Videtic GMM, Stephans K, Reddy C, Gajdis S, Kolar M, Clouser E, Djemil T. (2010). Intensity modulated radiotherapy-based stereotactic body radiotherapy for medically inoperable early-stage lung cancer: excellent local control. *International Journal of Radiation Oncology, Biology and Physics*. **77**: 344-349.

Vrouenraets MB, Visser GWM, Snow GB, van Dongen GAMS. (2008). Basic principles, applications in oncology and improved selectivity of photodynamic therapy. *Anticancer Research*. **23**: 505–522.

Wang JJH, Chan KK. (1995). Analysis of ifosfamide, 4-hydroxyifosfamide, N2-dechloroethylifosfamide, N3-dechloroethylifosfamide and phosphoramide mustard in plasma by gas chromatography-mass spectrometry. *Journal of Chromatography B*. **674**: 205-217.

Watson E, Dea P, Chan KK. (1985). Kinetics of phosphoramide mustard hydrolysis in aqueous solution. *Journal of Pharmaceutical Science.* **74**: 1283-1292.

Whitehead RE, Ferrer JV, Javitch JA, Justice JB. (2001). Reaction of oxidized dopamine with endogenous cysteine residues in the human dopamine transporter. *Journal of Neurochemistry*. **76**: 1242-1251.

Xie HJ, Yasar U, Lundgren S, Griskevicius L, Terelius Y, Hassan M, Rane A. (2003). Role of polymorphic human CYP2B6 in cyclophosphamide bioactivation. *Pharmacogenomics Journal.* **3**: 53-61.

Yap TA, Carden CP, Attard G, de Bono JS. (2008). Targeting CYP17: established and novel approaches in prostate cancer. *Current Opinion in Pharmacology*. **8**: 449-457.

Yin H, Xu L, Porter NA. (2011). Free radical lipid peroxidation: mechanisms and analysis. *Chemical Reviews*. **111**: 5944-5972.

Zhang J, Tian Q, Zhou SF. (2006). Clinical pharmacology of cyclophosphamide and ifosfamide. *Current Drug Therapy*. **1**: 55-84.

Zon G, Ludeman SM, Egan W. (1977). High resolution nuclear magnetic resonance investigations of the chemical stability of cyclophosphamide and related phosphoramidic compounds. *Journal of the American Chemical Society.* **99**: 5785-5795.